SONOPHOTOCATALYTIC DEGRADATION OF PARACETAMOL IN THE PRESENCE OF IRON-DOPED TITANIUM DIOXIDE

YAP HUI CHENG

MASTER OF ENGINEERING SCIENCE

LEE KONG CHIAN
FACULTY OF ENGINEERING & SCIENCE
UNIVERSITI TUNKU ABDUL RAHMAN
DECEMBER 2018

SONOPHOTOCATALYTIC DEGRADATION OF PARACETAMOL IN THE PRESENCE OF IRON-DOPED TITANIUM DIOXIDE

By

YAP HUI CHENG

A dissertation submitted to the Department of Chemical Engineering,
Lee Kong Chian Faculty of Engineering & Science,
Universiti Tunku Abdul Rahman,
in partial fulfillment of the requirements for the degree of
Master of Engineering Science
December 2018

ABSTRACT

SONOPHOTOCATALYTIC DEGRADATION OF PARACETAMOL IN THE PRESENCE OF IRON-DOPED TITANIUM DIOXIDE

Yap Hui Cheng

In recent years, growing consideration has been given to the presence of emerging pollutants (EPs) in water sources. EPs such as paracetamol possess characteristics of bioaccumulative, persistent and highly soluble in water. However, conventional treatment methods such as physical adsorption, chlorination and activated sludge may ineffective to remove and degrade the paracetamol. Therefore, in this study, sonophotocatalytic degradation has been proposed as an advance hybrid method to accelerate the process of paracetamol degradation. Titanium dioxide (TiO_2) and iron-doped TiO_2 (Fe-doped TiO_2) particles were synthesised by sol-gel method using tetrabutyl orthotitanate and iron (III) nonahydrate as titanium and iron sources, respectively. Various Fe dopant concentrations (1, 3, 5 and 10 wt%) and calcination temperatures (200, 400, 600 and 800 °C) of Fe-doped TiO_2 were prepared. Characterisations of samples were performed using FESEM-EDX, XRD, XPS and nitrogen adsorption-desorption analysis to examine the surface morphology, elemental composition, phase structure, chemical states and surface analysis. 3% Fe-doped TiO_2-600 catalyst showed the highest catalytic activity due to the presence of Fe dopant in optimum amount and mixed anatase-rutile phase. The effect of operating parameters such as energy

sources (ultrasonic, ultraviolet and combined irradiations), initial paracetamol concentrations (5 – 25 mg/L), catalyst dosages (0.5 – 2.0 g/L), solution pH (pH 3 – 11) and H_2O_2 amounts (0.1 – 10 mM) were investigated to determine the optimum conditions. Sonophotocatalytic degradation of paracetamol had achieved 100 % after 30 minutes when the sonicator power of 296 W, frequency of 50 kHz, UV wavelength of 302 nm, 5 mg/L of paracetamol, 1 g/L 3% Fe-doped TiO_2-600, solution pH of 5 and 0.5 mM H_2O_2 were applied. Catalyst reusability study revealed that the spent 3% Fe-doped TiO_2-600 exhibited insignificant reduction (approximately 17 %) in catalytic activity after four consecutive cycles. The sonophotocatalytic degradation of paracetamol was fitted well into pseudo first-order kinetic reaction. It achieved the highest pseudo first-order rate constant and synergy index of 0.0142 min^{-1} and 1.09, respectively. This proved that sonophotocatalytic degradation in the presence of Fe-doped TiO_2 could potentially apply to degrade and remove pharmaceutical compounds.

ACKNOWLEDGEMENT

I have putting a lot of efforts in this research study. However, it would not been possible without the inspiration, support and guidance of many parties. I would like to take this opportunity to express my gratitude to all of them.

I would like to thanks to my research supervisor Dr Pang Yean Ling and co-supervisor Dr Steven Lim for their invaluable advice, guidance and enormous patience throughout the development of the research.

In addition, I would like to express my sincere thanks to my family members and my friends who have been constant source of inspiration and support to me during the research period.

APPROVAL SHEET

This dissertation entitled "**SONOPHOTOCATALYTIC DEGRADATION OF PARACETAMOL IN THE PRESENCE OF IRON-DOPED TITANIUM DIOXIDE**" was prepared by YAP HUI CHENG and submitted as partial fulfillment of the requirements for the degree of Master of Engineering Science at Universiti Tunku Abdul Rahman.

Approved by:

_____

(Dr. Pang Yean Ling)
Date: 31 Dec 2018
Supervisor
Department of Chemical Engineering
Lee Kong Chian Faculty of Engineering & Science
Universiti Tunku Abdul Rahman

_____

(Dr. Steven Lim)
Date: 31 Dec 2018
Co-supervisor
Department of Chemical Engineering
Lee Kong Chian Faculty of Engineering & Science
Universiti Tunku Abdul Rahman

LEE KONG CHIAN FACULTY OF ENGINEERING & SCIENCE

UNIVERSITI TUNKU ABDUL RAHMAN

Date: 31 Dec 2018

SUBMISSION OF DISSERTATION

It is hereby certified that **YAP HUI CHENG** (ID No: **16UEM06199**) has completed this dissertation entitled "SONOPHOTOCATALYTIC DEGRADATION OF PARACETAMOL IN THE PRESENCE OF IRON-DOPED TITANIUM DIOXIDE" under the supervision of DR PANG YEAN LING (Supervisor) from the Department of CHEMICAL ENGINEERING, Faculty of ENGINEERING & SCIENCE, and DR STEVEN LIM (Co-Supervisor) from the Department of CHEMICAL ENGINEERING, Faculty of ENGINEERING & SCIENCE.

I understand that University will upload softcopy of my dissertation in pdf format into UTAR Institutional Repository, which may be made accessible to UTAR community and public.

Yours truly,

_____

(*Yap Hui Cheng*)

*Delete whichever not applicable

DECLARATION

I hereby declare that the dissertation is based on my original work except for quotations and citations which have been duly acknowledged. I also declare that it has not been previously or concurrently submitted for any other degree at UTAR or other institutions.

Name YAP HUI CHENG .

Date 31 DEC 2018 .

TABLE OF CONTENTS

LIST OF TABLES

LIST OF FIGURES

LIST OF ABBREVIATIONS

A_A	peak intensity of anatase
A_B	peak intensity of brookite
A_R	peak intensity of rutile
C_0	initial concentration of paracetamol, mg/L
C_t	concentration of paracetamol at time *t*, mg/L
k	Scherrer constant (0.9)
k_0	pseudo zero-order rate constant, mg/L·min
k_1	pseudo first-order rate constant, min^{-1}
k_2	pseudo second-order rate constant, L/mg·min
K_A	coefficient of anatase
K_B	coefficient of brookite
t	reaction time, min
W_A	phase composition of anatase
W_B	phase composition of brookite
W_R	phase composition of rutile
β	full-width at half maximum
θ	Bragg angle of prominent peak
λ	wavelength of CuK_α radiation

AOPs	advanced oxidation processes
BET	Brunauer-Emmett-Teller
BJH	Barrett-Joyner-Halenda
COD	chemical oxygen demand
EC_{50}	effective concentration
EDX	energy dispersive X-ray spectroscopy
EPs	emerging pollutants
FESEM	field emission scanning electron microscopy
HPLC	high performance liquid chromatography

PAC	powdered activated carbon
pKa	acid strength
UF	ultrafiltration
UV	ultraviolet
WWTPs	wastewater treatment plants
XPS	X-ray photoelectron spectroscopy
XRD	X-ray diffraction
zpc	zero point charge

•OH	hydroxyl radical
$C_{16}H_{36}O_4Ti$	tetrabutyl orthotitanate
C_2H_5OH	ethanol
$C_8H_9NO_2$	paracetamol
CH_3OH	methanol
e^-	electron
Fe	iron
$Fe(NO_3)_3 \cdot 9H_2O$	iron (III) nitrate nonahydrate
Fe^{2+}	ferrous ion
Fe^{3+}	ferric ion
h^+	hole
H_2O_2	hydrogen peroxide
H_2SO_4	sulphuric acid
HCl	hydrochloric acid
NaOH	sodium hydroxide
PBDEs	polybrominated diphenyls ethers
PCBs	polychlorinated biphenyls
TiO_2	titanium dioxide

CHAPTER 1

INTRODUCTION

1.1 Water Pollution

Water is an essential component in human development and environmental sustainability. Access to clean water resource is important for eradication of poverty, reduction of child mortality and improvement of human health. According to a report by UNESCO (Vieno et al., 2017) , there was an increasing proportion of population which had gained access to clean water resources. Yet, approximately 748 million people in rural area were still lacking access to clean and safe drinking water. This might cause water-borne disease such as diarrhoea and subsequently led to fatality.

Over the last 50 years, the water usage was originally only one-third of current usage, which indicating that the water demand increases globally due to the rapid urbanisation and population growth. Water is used in agriculture, industry and households, whereby agricultural sector contributes to the highest water consumption with 70 % of the total global freshwater withdrawn from aquifers, lakes and rivers. On the other hand, there are two million tonnes of wastes discharged into water bodies daily worldwide (Geissen et al., 2015). In some of developing countries, sewage and industrial wastes are drained into water bodies without treatment (Vieno et al., 2017). It is expected that

agricultural sector and urban area constitute the largest amount of pollutant loading than that from industry area.

The large volume disposal of improper treated and untreated wastewater containing pollutants into aquifers, lakes and rivers has caused water pollution which becomes increasingly severe. By estimations, approximately 1500 km^3 of wastewater was generated per year globally (Geissen et al., 2015). Water pollution has increased the risk of water scarcity and water quality degradation in which directly affect to the human welfare, ecosystem function, economic growth and social development. In the year of 2030, it is expected that increasing stress on water resource will affect approximately 40 % of world population and this may place the people under the risk of diseases, hunger and poverty. Therefore, in order to sustain the clean access of water resource, attention needs to be focused on the wastewater treatment in managing the water issues.

1.2 Paracetamol as a Pollutant

Paracetamol, also known as acetaminophen is an analgesic and antipyretic drug used to treat pain and reduce fever. It is a commonly used medication available with or without a prescription. Generally, paracetamol is available in tablet form for orally administration in active dose of 300 – 500 mg (Khaled et al., 2018). In Baltic sea region, paracetamol is labelled as the most consumed medicine with the consumption achieved 520,000 kg per year (Vieno et al., 2017). Meanwhile, approximately 50 million people consumed paracetamol-containing products weekly in United States (Fan et al., 2017).

Paracetamol is commonly consumed by a wide range of population across life stages, including children, pregnant women and elderly. The increasing consumption of paracetamol can be easily detected in environment especially in water resources. It had been reported that the detection of paracetamol in the Tyne River was about 65 µg/L. It had also been detected in sludge and soil at concentration of 483 µg/kg and 81 µg/kg, respectively (Zur et al., 2018). Although the detected paracetamol concentration is relatively low, continuous unintended release may bring negative impacts to human and living organism. It has been reported that ingestion of paracetamol in small doses may be toxic in several situations, i.e. long term alcohol usage, co-ingestion with alcohol and prolonged fasting (Gupte, 2016). According to Zur et al. (2018), the effective concentration (EC_{50}) of paracetamol to microbial was 3435 mg/L, which was notably higher than the paracetamol detected in environment. However, the presence of paracetamol even at low concentration cannot be neglected, due to the ease of accumulation, poor biodegradability and high water solubility.

In several cases, paracetamol consumption can lead to haematological effects, increased the risk of wheezing and asthma in children and cause endocrine disruption in human adult testis. Besides, over dosage of paracetamol can also induce chronic renal disease and necrotic changes in lung. Fan et al. (2017) stated that prenatal paracetamol consumption could potentially increase the risk of asthma in children, especially prominent during the early stage of pregnancy period. Prenatal paracetamol may interrupt maternal immunity and reduce antioxidant level which consequently leads to impair maturation of foetal. Abedi et al. (2017) reported that paracetamol

consumption could reduce sperm motility and sperm count in mice due to damage in sperm DNA and alteration in structure of sperm chromatin. They also claimed that long term paracetamol consumption might cause insufficient sperm protamine in mice and subsequently affected the sperm fertility.

It had been reported that approximately 1 – 4 % of paracetamol was excreted from urine without getting metabolised (Fan et al., 2017). The unmetabolised paracetamol could induce inhibition in DNA synthesis (Zur et al., 2018). The remaining paracetamol was metabolised into metabolites such as paracetamol glucuronide and paracetamol sulfate in liver and subsequently passed through kidney before being excreted. Meanwhile, part of the paracetamol underwent oxidation process to produce stable and toxic metabolites such as hydroxylparacetamol and N-acetyl-p-benzoquinone imine (Fan et al., 2017; Zur et al., 2018). Zur et al. (2018) claimed that N-acetyl-p-benzoquinone imine may bring mutagenesis to lymphoma cells in mice and human body. Its toxicity could also lead to DNA damage and oxidation of membrane lipids.

1.3 Problem Statement

Increasing evidence has shown that EPs have been released into the environment due to their extensive usage. It had been reported that excessive amount of EPs in environment could bring hazards such as hormone disruption and genotoxicity (Sauve and Desrosiers, 2014). For instance, excessive amount of paracetamol could bring health hazards such as liver failure and gastrointestinal disease (Thi and Lee, 2017). In most of the

developing countries, conventional wastewater treatment is applied in handling the wastewater generated. Several methods involving the physical, biological and chemical treatments have been extensively employed in the conventional wastewater treatment plant (WWTP) in order to remove and/or degrade the pollutants before being released to the environment.

Physical treatments such as adsorption, coagulation and filtration are generally efficient for physical separation of suspended solid and aggregate. However, these methods are non-destructive as their mode of action only applied to transfer the pollutants from one phase to another phase and therefore, creating secondary pollutants. Besides, the adsorbent and membrane filter used require frequent regeneration and/or replacement. Meanwhile, coagulation may not be effective to treat all kinds of pollutants depending on the interaction between the coagulant and EPs to aggregate and settle down (Sheng et al., 2016). Biological treatment has been extensively employed in water treatment due to its relatively low operating cost and simplicity of operation. Nevertheless, biological treatment is not applicable to pollutants which are non-biodegradable. This treatment method is time consuming due to the slow growth rate of microbial and long period of biological mineralisation (Mansour et al., 2014).

The ineffectiveness of conventional treatment methods prompted the need to explore the possibility of advanced oxidation processes (AOPs), in order to remove the EPs such as paracetamol from wastewater effectively and efficiently. In recent year, AOPs have been reported as a potential method which can be employed in wastewater treatment due to its generation of highly reactive hydroxyl radicals (•OH) to degrade the organic pollutants non-

selectively. Among them, photocatalytic degradation is a popular method but it has limitation in treating wastewater with high turbidity, due to the low penetration of light in water medium. Therefore, sonophotocatalysis has been proposed to enhance degradation efficiency of paracetamol due to their synergistic effects such as simultaneous generation of reactive radical species and promote the mass transfer of EP towards the catalyst surface.

TiO_2 has been widely used as catalyst in wastewater treatment processes to enhance the degradation reaction. However, the relatively wide band gap energy and fast recombination of electron-hole pairs restrict its application in the industry. In order to narrow the wide band gap energy of TiO_2, doping with Fe has been considered to be one of the most promising approaches. However, limited knowledge has been demonstrated about the process behaviour of Fe-doped TiO_2 towards sonophotocatalytic degradation of paracetamol and therefore, further investigation has to be carried out. Lastly, the reaction kinetic for the sonophotocatalytic degradation of paracetamol in the presence of Fe-doped TiO_2 catalyst is also rarely reported and therefore, a reliable reaction kinetic order needs to be proposed.

1.4 Research Objectives

The aim of the research study is to investigate the sonophotocatalytic degradation of paracetamol in the presence of TiO_2 and Fe-doped TiO_2 catalysts. The objectives of this research include:

a) To synthesise and characterise TiO_2 and Fe-doped TiO_2 to accelerate the sonophotocatalytic degradation reaction of paracetamol.

b) To demonstrate the process behaviour of sonophotocatalytic degradation under various operating conditions.
c) To study the reaction kinetic order for sonophotocatalytic degradation of paracetamol.

1.5 Scope of Study

The scope of the present study includes the synthesis, characterisation and activity test of the synthesised TiO_2 and Fe-doped TiO_2 particles using sonophotocatalytic reaction. The Fe-doped TiO_2 particle was synthesised by sol-gel method using tetrabutyl orthotitanate and iron (III) nonahydrate as the titanium and iron sources, respectively. The particles were synthesised at various weight percentages of Fe dopant (0, 3, 5 and 10 wt% Fe) and calcination temperatures (200, 400, 600 and 800 °C). The synthesised particles were characterised using field emission scanning microscope, energy dispersive X-ray spectroscope, X-ray diffractometer, surface area analyser and X-ray photoelectron spectroscope to examine the surface morphology, elemental composition, crystal structure, crystallinity, surface area, porosity and chemical states of the synthesised particles.

Then, a series of experiments were conducted using the synthesised TiO_2 and Fe-doped TiO_2 particles to compare their catalytic activity on sonophotocatalytic degradation of paracetamol. The scope was extended to evaluate the effect of operating parameters in sonophotocatalytic degradation of paracetamol by using one-factor-at-a-time approach. The operating parameters include energy sources (ultrasound, ultraviolet and combined ultrasound and ultraviolet), initial concentration of paracetamol (5 – 25 mg/L),

catalyst dosage (0.5 – 2.0 g/L), solution pH (pH 3 – 11) and H_2O_2 addition (0.1 – 10 mM). The range of parameters were chosen based on the literature and preliminary study. The liquid samples were collected at a specified time interval within 2 hours reaction time and the residual concentration of the liquid samples were measured using high performance liquid chromatography (HPLC). Based on the results obtained, a suitable kinetic order on sonophotocatalytic degradation reaction of paracetamol was proposed.

1.6 Organisation of Thesis

The thesis is divided into five chapters. Chapter 1 gives brief introduction to the current water pollution issues and the emerging pollutants exist in environment. This section also highlights the environment problem faced and the objectives of this research study. The scope of study elaborates the research work conducted in order to achieve the objectives.

Chapter 2 presents the review on the conventional treatment method with their advantages and disadvantages. The recent works on AOPs, fundamental of ultrasonic and ultraviolet reaction systems are also studied. Next, a review on the modification and heat treatment to TiO_2 is also presented. This section also covered factors influencing the sonophotocatalytic degradation such as initial concentration, catalyst loading, solution pH and amount of H_2O_2 addition.

Chapter 3 comprises of chemicals, materials and experimental methodology. A list of materials and chemical reagents involved in the experimental work is provided, followed by the overall research flow chart.

The detailed procedures of catalyst preparation, characterisation methods, experimental setup and experimental conditions are stated in this chapter.

Chapter 4 presents the results and discussion in details. These include the characterisation of TiO_2 and Fe-doped TiO_2 particles, parameter studies on sonophotocatalytic degradation and reaction kinetic order of sonophotocatalytic degradation. Based on the results and discussion, the optimum condition for sonophotocatalytic degradation is determined.

Chapter 5 summarises the important findings obtained in this research study. Recommendations are provided to improve the present work and future direction of study.

CHAPTER 2

LITERATURE REVIEW

2.1 Emerging Pollutants

Emerging pollutants (EPs) are not new kind of pollutants but they are being released into the environment since they have been discovered in 1800s due to the rapid science and technology development (Miraji et al., 2016). The presence of EPs in environment has gained a lot of public attention as the advancement of analytical instrumentation allowed the detection of EPs even in trace concentration which may possess potential toxicity to human and aquatic organisms.

Generally, EPs can be defined as natural or synthetic substances that are not commonly regulated in routine monitoring programme but possess potential adverse effect to living organism when enter the environment (Meffe and de Bustamante, 2014). They could be categorised into more than 20 groups depending on their origin. Among the EPs, pharmaceuticals, personal care products, pesticides and chemicals for industrial and household usage are the most prominent (Miraji et al., 2016). These chemical products are produced to meet the needs of human, animals and plants.

EPs are bioaccumulative and persistent once they entered into aquatic environment. They are considered to be more polar, acidic and alkaline as compared to the natural chemicals in environment. Besides, hydrophobic

properties of EPs would tend to accumulate in the lipid-rich tissues and therefore being active throughout the food chain. To date, considering pharmaceuticals EP alone, there are more than 200 types of products have been detected in river waters, with concentration reaching 6.5 mg/L for antibiotic ciprofloxacin (Petrie et al., 2015). It is worth to mention that prolong exposure to EPs could also induce hormone interference in fishes, immune toxicity and microbiological resistance (Miraji et al., 2016; Murgolo et al., 2017).

EPs enter the environment through point sources and non-point sources (Tijani et al., 2016). Point sources refer to the EPs originated from a specific location, which include wastewater treatment plants effluent, wastewater released from households, industries, hospitals and manufacturing factories. It is expected that point sources release concentrated EPs to environment (Naidu et al., 2016). Meanwhile, non-point sources refer to the released of EPs from diffuse sources, whereby the original source is hard to predict. This may include leakage from sewage system, agriculture run-off and rain overflow in industrial area, where the concentration is much lower as compared to EPs from point sources (Naidu et al., 2016; Pal et al., 2014).

However, most of the EPs have been found to survive from the conventional treatment methods such as activated sludge. Subsequently, they contaminate the aquatic system and drinking water sources. Besides, there are limited information regarding potential risks of EPs as they tend to accumulate in soil, sediment and water system. Those EPs are more likely to appear as a complex mixture, which can bring unfavourable synergistic interactions. In addition, the legal and policy guidelines in managing the EPs are not well

established. Risk assessment of EPs is a huge task due to the large concentration difference of EPs in environment which is highly depended on the production rate, population size, daily usage, excretion rate and retention time of EPs in water sources (Kapelewska et al., 2018). Thus, more research studies on EPs should be carried out to fill the knowledge gaps.

2.1.1 Pharmaceutical Products

Pharmaceutical products are important in maintaining good health and welfare. The main purpose of pharmaceutical manufacturing is to cure and prevent diseases. Besides, they also have been extensively used in agriculture and aquaculture to prevent diseases and parasitic. At the same time, they also help to increase the production of crop and fishes (Sangion and Gramatica, 2016). Pharmaceuticals can be classified into several classes such as non-steroidal inflammatory drugs (i.e. paracetamol and ibuprofen), antibiotic (i.e. sulfamethoxazole), antiepileptic (i.e. carbamazepine), analgesic (i.e. tramadol) and beta blocker (i.e. propranolol) (Petrie et al., 2015).

The discharge of pharmaceutical compounds into the environment may reach mg/L level and this may cause undesirable effect to living organisms (Baccar et al., 2012; Cruz-Morato et al., 2014). There were approximately 203 pharmaceutical products across 41 countries had been identified in freshwater, with ciprofloxacin achieved the highest concentration at 6.5 mg/L (Hughes et al., 2013). Meanwhile, the concentration of ciprofloxacin in a drug manufacturing factory effluent could reach up to 31 mg/L (El-Shafey et al., 2012). It was also reported that sulfamethoxazole, an antibiotic was detected

in water source at 2000 ng/L (Zhang et al., 2017b). The release of residual sulfamethoxazole into environment may cause antimicrobial resistance, in which the bacteria gains resistance strains from the antibiotic compound (Ou et al., 2016). This may potentially threaten other living creatures as the available antibiotics will be less effective in treating these antibiotic-resistant pathogenic bacterias.

2.1.2 Personal Care Products

Personal care products are used to enhance the quality of daily life. Several examples of personal care products are cosmetics, body spray, toothpaste, deodorant and lotion (Chen et al., 2011; Miraji et al., 2016). These products involve the usage of antimicrobial (i.e. triclosan and chlorophene), fragrance (i.e. musk ketone, galaxolide), UV screen (i.e. benzophenone-3), preservatives (i.e. methyl paraben) and dye (i.e. 4-chloro-2-aminophenol) (Tijani et al., 2016; Pal et al., 2014; Ebele et al., 2017; Miraji et al., 2016). Unlike pharmaceutical compounds, personal care products are applied externally. Therefore, they are more likely to be discharged through daily activities such as bathing, swimming and washing.

According to a study conducted by Ebele et al. (2017), the lipophilic contaminants such as triclosan and its metabolite methyl-triclosan could enter into algae through its lipid content. The detected concentration of these contaminants in water and algae were 50 – 200 ng/L and 50 – 400 ng/L, respectively. Besides, triclosan had also been detected in urine and breast milk at concentrations of 19.9 ng/g and 9.3 ng/mL, respectively (Siddique et al.,

2016). During dermal application, the triclosan possibly entered into human body through skin penetration and therefore contributed to its presence in breast milk which subsequently implied potential adverse effect to infants.

On the other hand, 4-chloro-2-aminophenol, a light brown coloured solid is an intermediate used in production of hair dye. It is a highly toxic compound and the exposure through inhalation, ingestion and dermal contact may cause mortality (Barik and Gogate, 2016). The 4-chloro-2-aminophenol is also possibly present in the environment as an intermediate product formed during the degradation of 4-chloro-2-nitrophenol and 3-chloronitrobenzene (Arora et al., 2014).

2.1.3 Pesticides

Pesticides are commonly utilised in agricultural sector in order to protect the crops from pests and diseases (Meffe and de Bustamante, 2014; Pal et al., 2014). They can be classified into three categories: insecticides, fungicides and herbicides. Insecticides are applied to kill insects in agriculture, forestry, gardening and landscaping (El-Shahawi et al., 2010). The presence of fungi can cause the plant to mold or rot. Therefore, fungicides act as a protectant to control the growth of fungi in plant. Meanwhile, herbicides are used to kill unwanted plants and their application may be selective or non-selective. Selective herbicide can inhibit the growth of weeds without damage to crops while non-selective herbicide could destroy all the plants at selected area where herbicide is applied.

Pesticides are biologically active, high toxicity and commonly detected in groundwater (Naidu et al., 2016). According to Mosleh and Rahimi (2017), they reported that only approximately 0.1 % of pesticides used would reach the target pest. The remaining pesticides were released to the environment through rain wash and irrigation water. The neonicotinoids such as acetamiprid and imidacloprid are a new group of insecticides. Their mode of action focuses to the nicotinic acetycholine receptor and could be detrimental to central nervous system. These insecticides could potentially paralyse honey bees, bumblebees and solitary bees (Sauve and Desrosiers, 2014).

2.1.4 Flame Retardants

Polychlorinated biphenyls (PCBs) and polybrominated diphenyls ethers (PBDEs) are two synthetic chemicals being applied as flame retardant additives in the manufacturing of textile, electronic equipment, leather and plastics in order to reduce flammability and slow down combustion process (Miraji et al., 2016). These flame retardants are highly stable, persistent, bioaccumulative and able to undergo long-range transportation (Naidu et al., 2016). They are carcinogenic and expected to cause detrimental effects such as cancer, hormonal disruption and neurotoxicity. They had been detected in river water at concentration up to 165 ng/L (Miraji et al., 2016).

Besides, these lipophilic flame retardant additives tend to accumulate in lipid and therefore, it has been detected in the body of eels which has high lipid content (approximately 40 % of body weight) (Suhring et al., 2014). In Rhine, a river close to a highly industrialised area, the detected PBDEs

concentration reached 88.7 ng/g in eels (Suhring et al., 2013). According to Suhring et al. (2015), the PBDEs accumulated in eels create toxic potential during fertility phase. Based on their studies, at least 1 ng of these pollutants could transfer to egg and as a consequence, lowering the quality of egg which may affect the viability of offspring.

2.1.5 Plasticisers

Plasticisers are additives used to increase the products' flexibility (Sauve and Desrosiers, 2014). Among the plasticisers, bisphenol A is the most popular and one of the well-known endocrine disruptors. It is a common chemical compound used in the production of polycarbonate plastic products (Heo et al., 2012). Bisphenol A had been detected in industrial effluent and leachate from landfill with the concentration as high as 17.2 mg/L (Bilgin Simsek, 2017). Meanwhile, it had also been found in seafood (213.1 ng/g) and freshwater fish (224 ng/g) (Vandermeersch et al., 2015). The presence of bisphenol A had been proven to bring adverse effects such as low sperm count, decreased sperm quality and induces reproductive cancer. Besides, Siddique et al. (2016) reported that fetal exposure of 0.025 – 0.25 µg/kg body weight/day to bisphenol A could result in morphological alterations in both stroma and epithelium of the developing mammary gland, which might lead to neoplasia later in adulthood.

2.2 Conventional Methods to Remove Pharmaceutical Compounds

Pharmaceutical compounds represent a major group of EPs. The consumption of pharmaceutical products is growing tremendously due to rapid population growth, aging and medical coverage expansions. As a consequence, pharmaceutical products contribute to the increase number of detected EPs in environment. Pharmaceutical products could be released as residual and/or metabolites through excretion in urine or faeces after therapeutic treatment. Improper disposal of unconsumed pharmaceutical products could contribute to the presence of pharmaceuticals in environment.

Generally, wastewater containing EPs such as paracetamol was subjected to treatment by WWTPs which employed two stages of treatment processes: primary and secondary treatment. Primary treatment involves the physical separation of suspended solid by physical methods i.e. adsorption. This treatment method may only effective to treat several EPs while the others remain in the water. Meanwhile, secondary treatment involves biological treatment which utilises microbial to remove and/or degrade the pollutants. Table 2.1 summarises several treatment methods which are commonly reported and their significant findings using conventional treatment processes.

Table 2.1: Several examples of conventional treatments applied for the removal of EPs

Treatment method	Targeted EPs	Significant findings	References
Sand filtration and graphene adsorption	• Caffeine • Carbamazepine • Diclofenac • Ibuprofen	• Sand filtration resulted in low removal efficiency (<10 %) for all pollutants. • Adsorption by graphene was able to achieve removal efficiency of more than 95 % for all pollutants within 62 days. • The treated wastewater resulted in 50 % immobilisation of *Ceriodaphnia dubia*, proved that adsorption by graphene might be unable to reduce the toxicity level.	(Rizzo et al., 2015)
Adsorption-membrane filtration	• Norfloxacin • Ofloxacin	• The removal efficiency for norfloxacin and ofloxacin were 93 % and 88 % respectively. • Increasing the applied pressure only increase the permeate flux but did not affect the removal efficiency.	(Sharma et al., 2017)
Coagulation, powdered activated carbon (PAC) and ultrafiltration (UF)	16 pharmaceuticals products (carbamazepine, ibuprofen, naproxen)	• The removal efficiency for coagulation (10 ppm), PAC (50 ppm) and UF were 7 %, 50 % and 29 %, respectively. • The coupled operation such as PAC-UF and coagulation-UF improved the removal efficiency and achieved 70 % and 33 %, respectively.	(Sheng et al., 2016)

Table 2.1: Continued

Chlorination	• Methylparaben • Ethylparaben • Propylparaben	• The removal efficiency for chlorination of methylparaben, ethylparaben and propylparaben at chlorine contrentration of 0.7 mg/L were 51 %, 44 % and 38 %, respectively. • Chlorinated products such as methyl 3-chloro-4-hydroxybenzoate, ethyl 3-chloro-4-hydroxybenzoate and propyl 3-chloro-4-hydroxybenzoate were detected.	(Chen et al., 2018)
Biodegradation using fungal reactor	• Ciprofloxacin • Carbamazepine • Iopromide	• The removal efficiency of ciprofloxacin and iopromide were 99 % and 34 %, respectively by using *Trametes versicolor* fungal bioreactor. • An increament in concentration of carbamazepine (0.16 µg/L) was observed.	(Cruz-Morato et al., 2014)
Biodegradation	• Chlorpyrifos	• Biodegradation using Stenotrophomonas species G1 was able to remove 42.6 % of 50 mg/L chlorpyrifos in 20 hours of incubation at 37 °C.	(Deng et al., 2015)
Biodegradation using activated sludge	• Ibuprofen • Gemfibrozil • Ofloxacin	• The biodegradation of gemfibrozil, ofloxacin and ibuprofen by using activated sludge were approximately 70 %, 25 % and 100 %, respectively after 10 - 35 days.	(Boix et al., 2016)

Among the physical methods, adsorption is the most popular techniques to accumulate the pollutants onto the adsorbent surface through either physical or chemical interaction. Activated carbon typically possesses characteristics of high porosity and large surface area which could act as an absorbent that adsorbs the pollutants onto its porous network surface and subsequently being removed from wastewater (Altmann et al., 2014; Rodriguez-Narvaez et al., 2017). However, the adsorption using commercial activated carbon is costly due to its difficulty in regeneration (Sophia A and Lima, 2018). Therefore, recent studies focus on the low cost adsorbent produced from by-products or wastes with carbon rich materials generated from industrial and agricultural processes such as biochar (Yao et al., 2012). These materials were converted into biochar by pyrolysis heat treatment at temperature range of 300 – 1000 °C. Although large volume of feedstock (by-products or waste with carbon rich materials) is easily available, it may not be economical to convert the feedstock to biochar since it requires high energy input (Ahmed et al., 2017). Besides, the production of waste sludge during adsorption process may generate secondary waste and this limits its industry application.

Membrane filtration such as reverse osmosis, nanofiltration and ultrafiltration are commonly applied after coagulation. The coagulation process occurred when aluminium or iron based substances were added into the wastewater treatment system to facilitate the particle segregation of EPs and settled under gravity (Sheng et al., 2016). The filtration was then applied to remove the segregation by passing through a membrane filter. The performance of membrane filtration is governed by the nature of membrane

and the size of pollutants (Acero et al., 2009). Heo et al. (2012) reported that nanofiltration membrane was influenced by hydrophobic adsorption and steric hindrance whereas the rejection of polar trace organics was due to the electrostatic repulsion. This method is also favourable for the removal of acidic and negatively charged pollutants due to the electrostatic repulsion between membrane and EPs (Beier et al., 2010). However, this is an energy extensive process which requires driving force by pressure difference and the lifetime of membrane is relatively short due to the frequent clogging of pores by pollutants.

Biological treatment methods utilise microbial to degrade the targeted EPs into smaller molecules and bio-mineralised them into simple inorganic molecules such as water and carbon dioxide. This method involves low cost and mild condition applied during operation, provided that the target pollutants are readily to be bio-degraded or oxidised by the microbial. Nevertheless, the slow growth rate of microbial and long treatment period are the main challenging problems faced (Mansour et al., 2014). According to Rivera-Utrilla et al. (2013), approximately 30 – 75 % of anti-inflammatories and antibiotics were being removed from biological treatment. The removal efficiency was highly depended on the chemical and biological persistency of EPs, their physicochemical properties and applied operation conditions. Boix et al. (2016) reported that almost 100 % removal of ibuprofen was achieved by using biological degradation in the presence of activated sludge after 10 days. On the other hand, microbial degradation of paracetamol might produce toxic metabolites such as hydroxylparacetamol and N-acetyl-p-benzoquinone imine which were more stable than original compound (Zur et al., 2018). Marco-

Urrea et al. (2009) also reported that biological degradation using fungi could remove 10 mg/L ibuprofen after 3 hours of incubation. However, dihydroxy ibuprofen as the major metabolite was detected after the treatment process. Therefore, biological treatment was not recommended to be used for EPs removal.

In short, the conventional wastewater treatments are inadequate to remove these EPs since they may remain in the treated effluent and released into the surface water. The trace amount of EPs found in water sources and soil sediment has proven the ineffectiveness of conventional wastewater treatments in treating EPs. Therefore, emerging treatment method such as AOPs has been introduced due to the non-selectively reaction driven by •OH.

2.3 Advanced Oxidation Processes (AOPs)

In recent years, AOPs have gained much attention as they demonstrate great capabilities in treating organic pollutants in wastewater. AOPs utilise reactive radical species such as •OH which possess high oxidising power (2.8 V) to accelerate the degradation process (Rodriguez-Narvaez et al., 2017). Several examples of AOPs such as Fenton, photo-Fenton, photocatalysis, sono-chemical and ozonation are able to generate •OH. The amount of •OH available in the system is highly dependent on the type of reactions and experimental conditions i.e. solution temperature and solution pH.

2.3.1 Ultrasonic Irradiation

The occurrence of chemical reaction and effect of ultrasound in liquid mixture were first discovered by Richards and Loomis in year 1927 (Richards and Loomis, 1927). Ultrasound is a sound wave that has a frequency higher than human hearing ability. The ultrasound frequency is ranged from 18 kHz to 500 MHz with successive wavelength of 10 – 0.01 cm (Thompson and Doraiswamy, 1999). It has strong penetrability which is able to reach 20 – 30 cm depth from the energy source in liquid medium (Pang et al., 2011b).

The mechanism of ultrasound is derived from mechanical energy which penetrates through a liquid medium and subsequently produces acoustic cavitation. Acoustic cavitation is an important phenomenon which causes chemical and mechanical changes to accelerate the destruction of the pollutants in liquid medium (Adewu-Yi, 2005). The propagation of ultrasound waves occurs due to the pressure variation and forms compression-rarefaction cycles. Cavitation bubbles are created during rarefaction cycles when the magnitude of negative pressure is large enough to pull the water molecules apart. Consequently, nucleation sites are formed with trapped gases (Thompson and Doraiswamy, 1999). Meanwhile, the cavitation bubble grows gradually under the influence of positive pressure during the compression cycle. Eventually, the cavitation bubble will collapse when reaches its critical size (Mahvi, 2009; Pang et al., 2011a). In short, acoustic cavitation occurs in three stages i.e. nucleation, growth and violent collapse of gas- or vapor-filled microbubbles during ultrasonic wave-induced compression-rarefaction cycles in a liquid medium (Figure 2.1).

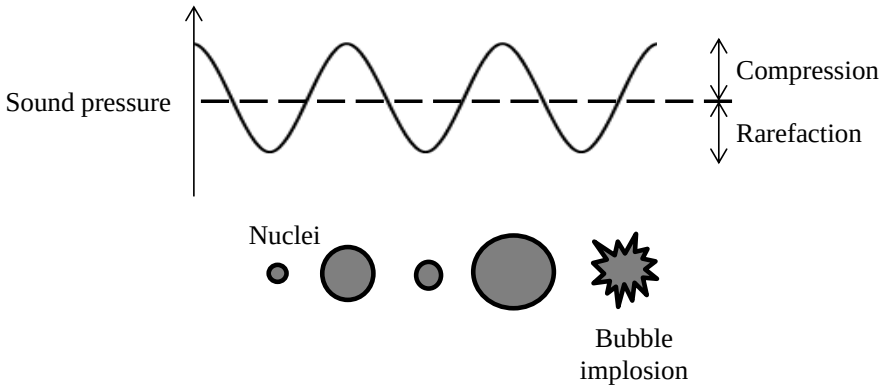

Figure 2.1: Cavitation bubble created during compression-rarefaction cycles (Mahvi, 2009)

Figure 2.2 shows three reaction zones in a sonochemical system: inside the cavitation bubble, interfacial region between cavitation bubble and bulk solution, and in the bulk solution (Thompson and Doraiswamy, 1999; Mahvi, 2009; Pang et al., 2011a; Eren, 2012). Localized hot spot (zone 1) is created when the cavitation bubble experiences a sudden collapse. Within this region, the temperature and pressure are extremely high and can reach up to 5000 K and 1000 atm, respectively (Eren, 2012; Hassani et al., 2016; Karaca et al., 2016). Such extreme temperature and pressure are able to promote the pyrolysis process to occur. Therefore, the water and dissolved oxygen molecules will experience thermal dissociation and being converted into reactive species such as •OH and •H as shown in Equations (2.1) – (2.5) (Pang et al., 2011a; Eren, 2012). The ultrasound could be denoted as symbol '))))'.

$$H_2O +))) \rightarrow \bullet OH + \bullet H \quad (2.1)$$

$$O_2 +))) \rightarrow 2\ \bullet O \quad (2.2)$$

$$\bullet OH + \bullet O \rightarrow \bullet OOH \quad (2.3)$$

$$\bullet O + H_2O \rightarrow 2\ \bullet OH \quad (2.4)$$

$$\bullet H + O_2 \rightarrow \bullet OOH \quad (2.5)$$

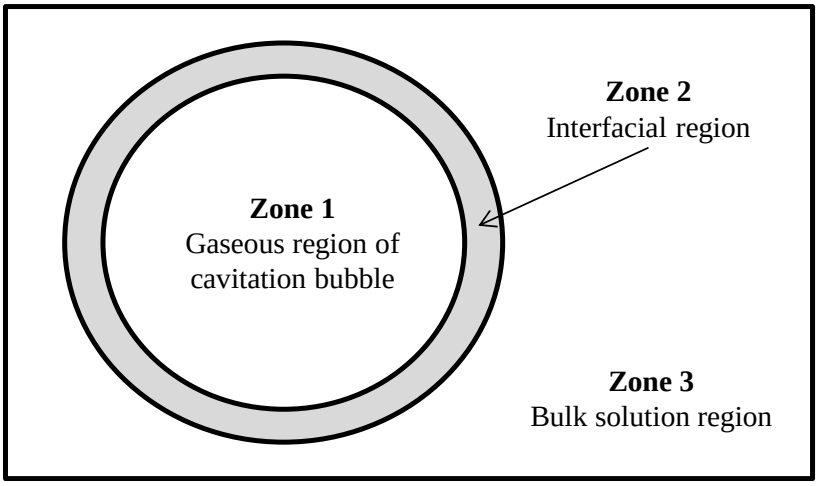

Figure 2.2: Three reaction zones in ultrasonically irradiated liquid medium (Thompson and Doraiswamy, 1999)

The second region is the interfacial region between gaseous phase cavitation bubble and liquid phase bulk solution (zone 2). In this region, the temperature is in the range of 1000 – 2000 K, which is lower than zone 1. The temperature gradient is due to the temperature difference between zone 1 and zone 2 to facilitate the diffusion of reactive radical species. Therefore, •OH mediated reaction is the dominating reaction and pyrolysis may occur in a lesser extent than zone 1. In this region, self-recombination of •OH and •OOH may occur and result in the formation of hydrogen peroxide (H_2O_2) (Equations (2.6) and (2.7)). The generated H_2O_2 can convert back into radical species by reaction with radicals that diffuse from zone 1 (Equations (2.8) and (2.9)) or by self-dissociation (Equation (2.6)). The degradation of hydrophobic and volatile pollutants is more likely to occur in zone 1 and 2.

$$2\ \bullet OH \leftrightarrow H_2O_2 \quad (2.6)$$

$$2\ \bullet OOH \rightarrow H_2O_2 + O_2 \quad (2.7)$$

$$\bullet H + H_2O_2 \rightarrow \bullet OH + H_2O \quad (2.8)$$

$$\bullet OH + H_2O_2 \rightarrow \bullet OOH + H_2O \quad (2.9)$$

The third region refers to the bulk solution (zone 3) at ambient temperature. Under ambient temperature, pyrolysis will not occur. Thus, the degradation process is dominated by •OH mediated reactions. Hydrophilic and non-volatile species are usually not easily degraded inside the cavitation bubbles. Therefore, the degradation process of these compounds most probably occurs at bulk solution through •OH mediated reaction (Pang et al., 2011a; Eren, 2012). Besides, the unreacted radicals may recombine and release to this region (Equations (2.10) – (2.13)).

$$\bullet OH + \bullet H \rightarrow H_2O \quad (2.10)$$

$$2\ \bullet OH \rightarrow H_2O + \bullet O \quad (2.11)$$

$$\bullet OOH + \bullet OH \rightarrow O_2 + H_2O \quad (2.12)$$

$$2\ \bullet H \rightarrow H_2 \quad (2.13)$$

Sonoluminescence is refers to light flash that produces during the implosion of cavitation bubbles and releases from the centre core of cavitation bubbles. It has wavelength of 200 – 500 nm, average photon energy of 6 eV and relatively short lifespan of 100 ps (Pang et al., 2010). The emission of light by sonoluminescence can act as energy source to trigger the sonocatalyst by providing sufficient energy to excite the electron (e^-) from the valence band to the conduction band, leaving equivalent amount of holes (h^+) at the valence band (Thompson and Doraiswamy, 1999). The conduction band e^- is responsible to reduce the dissolved oxygen while the valence band h^+ is able to oxidise the water molecules.

Figure 2.3 illustrates the schematic diagram of ultrasonic irradiation with and without the presence of catalyst. The turbulent microjet flow created during the implosion of cavitation bubbles can break down the sonocatalyst

into few small particles. This can increase the total surface area of sonocatalysts which act as weak points for nucleation of cavitation bubbles to occur (Karaca et al., 2016). As a consequence, it increases the number of cavitation bubbles and radical species created upon implosion of cavitation bubbles. By increasing the number of radicals created, it promotes the transfer of radicals from zone 1 to zone 3. Therefore, the accumulation of radicals in the bulk solution could enhance the degradation of hydrophilic and non-volatile pollutants (Wang et al., 2008).

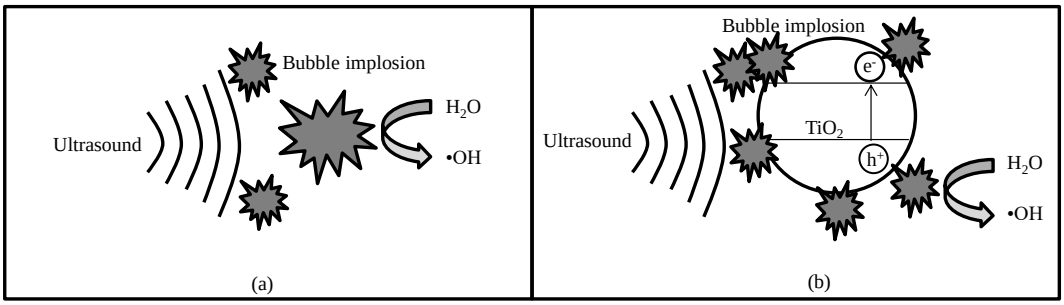

Figure 2.3: Schematic diagrams of (a) sonolysis and (b) sonophotocatalysis in the presence of TiO_2 (Adewu-Yi, 2005, Hassani et al., 2016)

2.3.2 Ultraviolet (UV) Irradiation

UV irradiation has also gained considerable attention in removal and degradation of EPs (Eskandarian et al., 2016; Ou et al., 2016). This treatment method involves the usage of UV light to transmit the light photons in order to produce photo-induced radicals and carry out a series of photochemical processes to degrade the targeted EPs (Burrows et al., 2002; Johnson et al., 2010). Typically, UV spectrum has wavelength range from 100 – 400 nm. It can be further classified into 3 classes: UV-A (315 – 380 nm), UV-B (280 – 315 nm) and UV-C (200 -280 nm) (Zoschke et al., 2014).

There are two types of UV irradiation, namely direct and indirect irradiations (Rubio-Clemente et al., 2014; Santos et al., 2016). Direct irradiation is a photosensitized degradation process whereby the light photons are being absorbed by EP to induce a series of photochemical reactions. As a consequence of being excited by light photons, the ground state of target EP (X) is converted to excited state (X*) (Equation (2.14)). Generally, target EP at excited state has higher potential energy than the one at ground state. Therefore, the excited state EP can return back to ground state by releasing the energy (Equation (2.15)). Besides, the excited state EP can be converted into intermediates by photochemical reaction as shown in Equation (2.16) (Santos et al., 2016). Further oxidation may lead to the degradation of EP into carbon dioxide and water as shown in Equation (2.17).

$$X + h\nu \rightarrow X^* \quad (2.14)$$

$$X^* \rightarrow X \quad (2.15)$$

$$X^* \rightarrow \text{Intermediates} \quad (2.16)$$

$$\text{Intermediates} \rightarrow \rightarrow \text{Photodegraded products} + CO_2 + H_2O \quad (2.17)$$

Meanwhile, the indirect irradiation carried out in the presence of UV sensitive materials such as humic acid and nitrate (Lester et al., 2013; Remucal, 2014; Norvill et al., 2016; Wang et al., 2017). In this process, the degradation occurs via •OH mediated reaction whereby the •OH is produced from UV sensitive materials (Wang et al., 2017). In short, the degradation efficiency of indirect irradiation is highly dependent on the absorption of light by UV sensitive material instead of EP itself (Remucal, 2014). Photooxidative degradation may also occur in the presence of oxygen and react with the intermediates (Yousif and Haddad, 2013).

Figure 2.4 illustrates the mechanism involved in the formation of e^- and h^+ with the aids of photocatalyst under UV irradiation. Photocatalysis is initiated by the light absorption of target pollutants and added photocatalyst (Rubio-Clemente et al., 2014). The energy carried by the light photons must be equal or larger than the band gap energy of photocatalyst in order to excite the e^- from valence band to conduction band (Leong et al., 2014). Upon excitation, the conduction band e^- and valence band h^+ are created (Equation (2.18)). Subsequently, the •OH radicals are produced by oxidation of water molecules via reaction (2.19). On the other hand, reaction (2.20) occurs when the dissolved oxygen is being reduced by conduction band e^-, forming superoxide radical ($\bullet O_2^-$) (Leong et al., 2014, Zangeneh et al., 2015). These radical species formed are responsible for the degradation of the target EPs (Equations (2.21) and (2.22)). Apart from this, the unreacted radicals can combine to form H_2O_2 (Equations (2.23) – (2.25)) (Fujishima and Rao, 1997; Chong et al., 2010).

$$\text{Catalyst} + h\nu \rightarrow h_{vb}^+ + e_{cb}^- \quad (2.18)$$

$$H_2O + h_{vb}^+ \rightarrow \bullet OH + H^+ \quad (2.19)$$

$$O_2 + e_{cb}^- \rightarrow \bullet O_2^- \quad (2.20)$$

$$\bullet OH + X \rightarrow \text{Photodegraded products} + CO_2 + H_2O \quad (2.21)$$

$$\bullet O_2^- + X \rightarrow \text{Photodegraded products} + CO_2 + H_2O \quad (2.22)$$

$$\bullet O_2^- + \bullet OH \rightarrow \bullet OOH \quad (2.23)$$

$$\bullet OOH + e_{cb}^- \rightarrow HOO^- \quad (2.24)$$

$$HOO^- + H^+ \rightarrow H_2O_2 \quad (2.25)$$

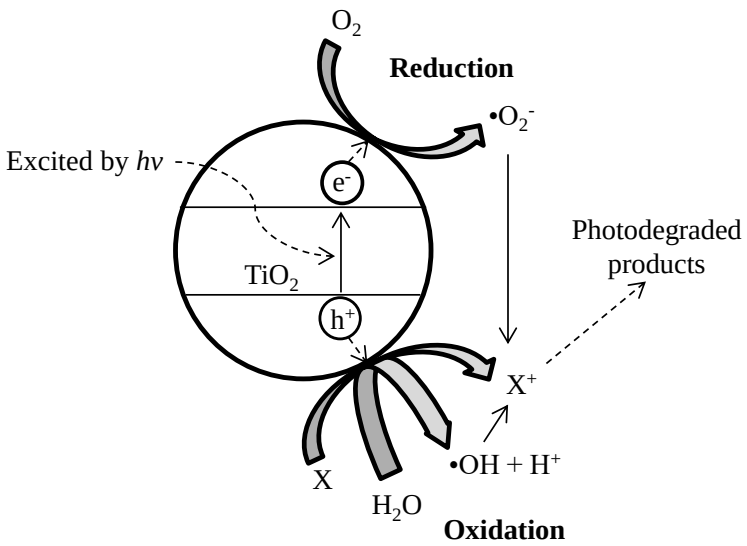

Figure 2.4: Formation of electron-hole pair and degradation of target pollutants by photocatalysis (Hassani et al., 2015)

2.3.3 Combination of Ultrasonic and UV Irradiation

In recent year, a lot of researches have focused on the individual application of ultrasonic and UV irradiations in wastewater treatment system. The creation of acoustic cavitation and photo-induced reaction are the main features of ultrasonic and UV irradiation, respectively. However, the individual treatment may not be effective in eliminating the recalcitrant EPs. For examples, sonolysis may not effective in treating the hydrophilic types of EPs since low concentration of •OH is available in bulk solution (Eren, 2012). On the other hand, effluent with high turbidity is not suitable to be treated via photolysis due to limited penetration of light in liquid medium (Norvill et al., 2016). Therefore, in order to overcome the shortcomings of both irradiations, combination of both irradiations with and without the presence of catalyst has become a novel and hybrid technique to enhance the degradation performance of EPs (Park et al., 2014).

The combination of ultrasonic and ultraviolet irradiation has been widely investigated in elimination of organic pollutants such as colouring dyes and phenolic compounds (Park et al., 2014). However, the studies of these combination applications on eliminating the EPs are limited. Although ultrasonic and ultraviolet irradiations produce energy wave from different sources, their combination can bring high synergistic effects such as continual production of •OH and eliminates mass transfer limitation which can enhance the degradation rate of target EPs.

In sonolytic process, •OH is being produced during the sudden collapse of cavitation bubble. It is found that •OH has short lifetime and can be easily recombined to produce H_2O_2. By applying hybrid technique of sonophotolytic process, the H_2O_2 produced can dissociate into •OH more easily when it is exposed to photolytic process than sonolytic process (Xu et al., 2013). This statement had also been proven by Na et al. (2012) in the degradation of diethyl phthalate by sonophotolytic process. They reported that the amount of H_2O_2 accumulated during sonolytic process was being consumed rapidly once underwent photolytic process. Consequently, the amount of H_2O_2 remained in low concentration under sonophotolytic process as the generation and consumption of H_2O_2 happened at the same time. Hence, larger amount of •OH was available to attack the target pollutants via •OH mediated reaction and resulting in enhancement of degradation efficiency.

Combined operation of sonolytic and photolytic processes in the presence of catalyst is known as sonophotocatalytic process. Catalyst deactivation is one of the major problems occurs during photocatalytic process. This is probably caused by fouling of pollutants on catalyst surface after a

long operation period. As a result, it reduces the availability of active sites on catalyst surface where the degradation process and generation of radical species take place. In order to resolve this problem, the application of sonolytic process is simultaneously applied. The ultrasound wave could clean the catalyst surface constantly which enables the elimination of undesired blockage phenomenon (Khokhawala and Gogate, 2010).

Limited mass transfer of target contaminants also restricts the performance of photocatalytic process (Adewu-Yi, 2005). With the aids of sonolytic process, the sudden collapses of cavitation bubbles will create hot spot zone and turbulent jet flow within the system. Under this condition, the solid particles will experience fragmentation into smaller size of particles. The smaller size particles can enhance the degradation reaction as it provides additional active sites for adsorption-degradation of target pollutant on catalyst surface as well as nucleation sites for cavitation bubbles to occur (Adewu-Yi, 2005; Joseph et al., 2009). Thus, it is anticipated that the sonophotocatalytic process will provide a superior performance of degradation efficiency for EPs.

2.3.4 Applications

Table 2.2 summarises the applications of sono-, photo- and sonophoto-degradation that had been carried out in recent years. Lim et al. (2014) investigated the effect of H_2O_2 concentration on the sonochemical degradation of phenol and bisphenol A. They found that the addition of H_2O_2 could enhance the degradation efficiency of both phenol and bisphenol A. H_2O_2 could promote the degradation of phenol in a larger extent as compared to that

in bisphenol A, probably related to their higher solubility in water. Phenol had higher probability of reacting with H_2O_2 and subsequently contributed to the increased degradation efficiency from 10 % to 50 %.

Adityosulindro et al. (2017) reported the degradation of ibuprofen by sonolytic and sono-Fenton reaction. In sonolytic process, the degradation of ibuprofen achieved was 50 % after 180 minutes. On the other hand, the sono-Fenton reaction in the presence of H_2O_2 could achieve 90 % and 100 % after 60 and 120 minutes, respectively. The addition of Fe^{2+} and H_2O_2 could generate additional •OH through Equations (2.26) – (2.28).

$$Fe^{2+} + H_2O_2 \rightarrow Fe^{3+} + OH^- + \bullet OH \quad (2.26)$$

$$Fe^{3+} + H_2O_2 \rightarrow Fe\text{-}OOH^{2+} + H^+ \quad (2.27)$$

$$Fe\text{-}OOH^{2+} \rightarrow Fe^{2+} + \bullet OOH \quad (2.28)$$

Taneja et al. (2018) carried out photolytic and photocatalytic degradation of brilliant green dye. They found that no degradation was observed during the photolytic process in the absence of catalyst. However, photocatalytic degradation in the presence of 0.5 g/L of cobalt tungsten oxide ($CoWO_4$) was able to achieve 94 % after 120 minutes. The possibility of combined irradiations for degradation of brilliant green dye was studied by Gole et al. (2017). In their study, various operations, i.e. ultrasound-assisted, UV-assisted and ultrasound-UV-assisted oxidation processes were being conducted. They reported that the combined operation achieved higher degradation efficiency (94.8 %) than ultrasound-assisted (81 %) and UV-assisted (72.3 %) oxidation processes due to the increased concentration of •OH available within the system.

Table 2.2: Applications of sono-, photo- and sonophoto-degradation in wastewater treatment

Target pollutants	Optimum conditions	Significant findings	References
Phenol Bisphenol A	• Ultrasonic reactor (40 W, 35 kHz) • [Phenol] = 0.044 mM • [Bisphenol A] = 0.044 mM • Treatment period = 60 minutes	• Sonolytic degradation of phenol and bisphenol A were able to achieve 12 % and 30 %, respectively. • Sonolytic degradation of phenol and bisphenol A in the presence of H_2O_2 were about 48 % and 47 %, respectively.	(Lim et al., 2014)
Ibuprofen	• Ultrasonic probe (20 kHz) • [Ibuprofen] = 20 mg/L • [H_2O_2] = 6.4 mM • [Fe^{2+}] = 0.134 mM • Treatment period = 180 minutes	• Sonolytic degradation of ibuprofen achieved 50 % removal in 180 minutes. • Sono-Fenton oxidation with the presence of H_2O_2 achieved 100 % after 120 minutes.	(Adityosulindro et al., 2017)
Ciprofloxacin	• Ultrasound bath (650 W, 35 kHz) • Volume = 100 mL • [Ciprofloxacin] = 10 mg/L • [TiO_2/montmorillonite] = 0.2 g/L • Treatment period = 2 hours	• Sonolytic degradation of ciprofloxacin was less than 10 %. • Sonocatalytic degradation efficiency of ciprofloxacin in the presence of TiO_2 and TiO_2/montmorillonite were 40 % and 60 %, respectively.	(Hassani et al., 2016)

Table 2.2: Continued

Ciprofloxacin	• Mercury lamp (254 nm) • Volume = 250 mL • [Ciprofloxacin] = 3 mg/L • [Ag/TiO_2] = 0.5 g/L • Treatment period = 180 minutes	• The optimal loading of Ag, Au and Cu on TiO_2 were 1.5, 1.5 and 1.0 wt%, respectively. • Photocatalytic degradation of ciprofloxacin in the presence of Ag/TiO_2 showed the best result as it achieved 100 % after 30 minutes.	(Duran-Alvarez et al., 2016)
Brilliant green dye	• Visible light source (85 W, 420 – 650 nm) • Volume: 100 mL • [Dye] = 10 mg/L • [$CoWO_4$] = 0.5 g/L • Treatment period = 120 minutes	• No degradation was observed under photolytic process. • Photocatalytic degradation of brilliant green dye in the presence of $CoWO_4$ was able to achieve 94 %.	(Taneja et al., 2018)
Thiobencarb	• Visible light tube (4 W, 400 – 700 nm) • [Thiobencarb] = 5 mg/L • [Molybdenum disulphide, MoS_2] = 1.0 g/L • Treatment period = 120 min	• Photocatalytic degradation efficiency of thiobencarb in the presence MoS_2 was 95 %.	(Huang et al., 2018)

Table 2.2: Continued

Diethyl phthalate	• UV-C lamp (40 W, 254 nm) • Ultrasound generator (65 W, 283 kHz) • Volume = 1 L • [Diethyl phthalate] = 45 µM • Treatment period = 120 minutes	• The sonolytic, photolytic and sonophotolytic degradation rate of diethyl phthalate were 7.2×10^{-3}/min, 2.9×10^{-3}/min and 1.7×10^{-2}/min, respectively.	(Na et al., 2012)
Brilliant green dye	• UV light (5 W, 240 V, 350 – 450 nm) • Ultrasonic bath (120 W, 20 kHz) • Volume = 3 L • [Dye] = 20.8 µM • [Zinc oxide, ZnO] = 2 g/L • Treatment period = 120 minutes	• Sonolytic, photolytic and sonophotolytic degradation of brilliant green dye were 35.6 %, 28.3 % and 60.3 %, respectively. • With the aids of ZnO, the sonocatalytic, photocatalytic and sonophotocatalytic degradation efficiencies were 81 %, 72.3 % and 95 %, respectively.	(Gole et al., 2017)
Abamectin	• LED light (465 – 470 nm) • Ultrasonic bath (25 kHz) • Reactant volume = 500 mL • [Abamectin] = 30 mg/L • [$Cu_2(OH)PO_4$-HKUST-1] = 0.4 g/L	• The sonolytic, photolytic, sonocatalytic, photocatalytic and sonophotocatalytic degradation of abamectin were 4.38 %, 10.20 %, 17.88 %, 57.46 % and 99.93 %, respectively.	(Mosleh and Rahimi, 2017)

Besides, Gole and Alhat (2017) investigated the amount of radicals produced during ultrasonic and ultraviolet irradiations. They concluded that the synergistic effect of the combined operation could generate the highest concentration of radicals (22 µM) as compared to ultrasonic (15 µM) and ultraviolet (12 µM) irradiation alone. Meanwhile, Mosleh and Rahimi (2017) studied the effect of catalyst on the degradation efficiency of abamectin. Without the presence of $Cu_2(OH)PO_4$-HKUST-1 catalyst, the degradation efficiency was in the range from 4 – 10 % while the degradation efficiency increased to 17 – 99 % after addition of catalyst. This proved that the presence of catalyst could promote the cavitational activity to produce more reactive radicals, which in turn resulted in better degradation performance.

2.4 Titanium Dioxide (TiO_2) as Catalyst

TiO_2 has been used in a wide range of applications such as antireflective coatings, optical filters and catalysts (Nasralla et al., 2013). It has received considerable attention from researchers as the most promising catalyst used in water treatment system. TiO_2 has become the subject of interest due to its ease of availability, low cost, long durability, strong oxidizing power and high chemical stability (Yuan et al., 2016; Lin et al., 2017; Ramandi et al., 2017). TiO_2 may exist in two major crystallographic forms i.e. anatase and rutile. The metastable anatase can be transformed irreversibly to thermodynamically stable rutile phase when undergo thermal treatment. In most of the cases, anatase TiO_2 is more favourable than rutile due to its high catalytic activity (Su et al., 2011; Taherinia et al., 2017). On the other hand, several studies had

proven that rutile TiO_2 favoured the decomposition of terephthalic acid and methylene blue (Yener et al., 2017, Vijayarangamuthu et al., 2018).

2.4.1 Modification of TiO_2

The application of TiO_2 is limited due to the fast recombination of electron-hole pairs and large energy band gap of 3.2 eV. This indicated that TiO_2 could only be activated under UV light (wavelength shorter than 387 nm) and a small range of solar irradiation (Lin et al., 2017; Ramandi et al., 2017). There are several modification techniques on TiO_2 which have been investigated in order to enhance its catalytic activity in terms of structural changes, charge carrier recombination, interfacial transfer of charge carrier and light adsorption. For example, doping and impregnation are two commonly applied techniques. Ramadi et al. (2017) had carried out non-metal dopants such as carbon (C), nitrogen (N) and sulphur (S) on TiO_2. The band gap energy of TiO_2 was successfully reduced from 3.2 to 2.66 eV. Hassani et al. (2016) investigated the sonocatalytic degradation of ciprofloxacin using bare TiO_2 and TiO_2/montmorillonite. Based on the result obtained, the presence of TiO_2/montmorillonite achieved higher degradation efficiency of 65 % than bare TiO_2 (45 %).

Metal doping is the most popular technique among all the modification techniques. Fe is a potential dopant, owing to the similar ionic radius of Fe^{3+} (0.064 nm) to that of Ti^{4+} (0.068 nm), which can be easily incorporated into the crystal structure of TiO_2. Besides, it is expected that the Fe can reduce the energy band gap of TiO_2 due to its lower energy band gap (2.6 eV) (Nasralla

et al., 2013). Sood et al. (2015) found that the anatase peak intensity in XRD pattern reduced with increasing Fe dopant concentration. This suggested that distortion occurred in anatase structure and caused slight decrease in crystallinity. Meanwhile, increasing the Fe dopant concentration could also improve the absorption of light by extending the wavelength to 426 nm. This result was supported by Birben et al. (2017) which that the visible light activity of Fe-doped TiO_2 could narrow the energy band gap to 2.55 eV. This happened due to the formation of Fe energy levels (Fe^{3+}/Fe^{4+}) into the band gap of TiO_2, which reduced the energy required to excite the electrons to the conduction band of TiO_2 (Moradi et al., 2016).

Bhatia and Dhir (2016) investigated the catalytic activity of TiO_2 at various bismuth (Bi) dopant concentrations. It was found that the TiO_2 and 0.25 wt% Bi-TiO_2 achieved 76 % and 89 % of ibuprofen degradation after 6 hours, respectively. This proved that the presence of Bi could promote the charge separation and subsequently enhanced the catalytic activity. They further explained that Bi appeared as a suitable dopant due to their similar radius which enabled Bi^{3+} to diffuse into the crystal lattice of TiO_2 and promote the red shift of absorbance range to enhance the catalytic activity. However, unfavourable effect occurred when dopant concentration increased from 0.25 to 1.0 wt%, which suggested that excessive metals could compete for the entrapment of e^- and resulted in lower production of •OH.

2.4.2 Heat treatment of TiO_2 and Modified TiO_2

Calcination temperature is a critical parameter which affects the physicochemical characteristics of a catalyst. Ganesh et al. (2012) investigated the effect of calcination temperature on structural changes of 5 wt% Fe-doped TiO_2 prepared by co-precipitation method. It was found that increasing the calcination temperature could improve crystallinity and promote phase transformation. When calcination temperature was increased from 400 °C to 600 °C, it was found that poorly crystalline anatase phase was developed into highly crystalline phase, indicated by the increase in peak intensity of XRD pattern. Further increasing the calcination temperature to 700 °C led to the occurrence of phase transformation whereby some of anatase phase was transformed into rutile phase. In contrary, Gareso et al. (2017) found that the phase transformation of 2 wt% Fe-doped TiO_2 occurred at 200 °C and the rutile peak intensity was greatly enhanced with increasing calcination temperature up to 500 °C. This suggested that the phase transformation temperature at which phase transformation occurs may differ from each other, depending on the synthesising techniques and conditions applied.

Besides, the particle sizes of Fe-doped TiO_2 increased with increasing calcination temperature. Subsequently, the surface area of Fe-doped TiO_2 was found to decrease with increasing calcination temperature. According to Nasralla et al. (2013), the particle size of Fe-doped TiO_2 calcined at 800 °C significantly increased as compared to those calcined at 400 °C and 600 °C, probably related to sintering effect and higher growth rate of rutile phase.

Mioduska et al. (2016) studied the effect of calcination temperature on catalytic activity of WO_3/TiO_2 composites. It was found that increasing the calcination temperature could enhance the catalytic activity of WO_3/TiO_2 composites. This was due to the enhancement in crystalline structure of WO_3/TiO_2 composites. As the calcination temperature increased, the amorphous phase was reduced while increasing the formation of anatase and rutile. They further explained that the amorphous structure did not contribute good catalytic activity as it contained imperfections such as defect point which caused recombination of charge carrier.

2.4.3 Characterisations of TiO_2 and Modified TiO_2

Characterisation of catalyst is an important step as it provides first insight of the physical and chemical properties of particles prior to its application in wastewater treatment. The main purpose of catalyst characterisation is to understand and relating the properties to its catalytic performance. Various characterisation techniques, i.e. field emission scanning electron microscopy (FESEM), energy dispersive X-ray microscopy (EDX) and X-ray diffraction (XRD) can be employed to characterise the TiO_2.

FESEM-EDX is employ to observe the surface morphology and elemental composition of TiO_2 and modified TiO_2. EDX mapping is one of the functions of FESEM-EDX to determine the distribution of each element on the surface of TiO_2. XRD is an effective technique to evaluate the crystalline structure of TiO_2 using CuK_α irradiation. It can also use to determine the

crystallite size of TiO_2 and Fe-doped TiO_2 by obtaining the peak intensity data from XRD pattern (Zhang et al., 2017a).

Nitrogen adsorption-desorption measurement analysis is an analytical technique to determine the surface area and porous structure of TiO_2 and modified TiO_2 using Brunauer-Emmett-Teller (BET) and Barrett-Joyner-Halenda (BJH) methods, respectively (Siwinska-Stefanska et al., 2014). Meanwhile, X-ray photoelectron spectroscopy (XPS) is used to evaluate the surface composition and electronic states of TiO_2 and modified TiO_2. The high resolution XPS spectra is corresponded to the electron configuration, i.e. 1s, 2s and 2p. Peak identification is analysed by peak fitting process of an element at specific binding energies, i.e. C 1s peak occurs at 284.6 eV (Cai et al., 2016).

2.5 Parameter Studies

2.5.1 Effect of Energy Source

By comparing the three types of catalytic reaction (sono-, photo and sonophotocatalytic processes), it was often reported that the combined application of sonophotocatalytic process could achieve better degradation performance than their individual processes. Jelic et al. (2013) found that sonophotocatalytic treatment had greatly improved the degradation of carbamazepine from 7 % (photolytic process) to 82 % after 120 minutes. The synergistic effect of combined application might attribute to the enhancement of mass transfer between liquid phase of carbamazepine and solid phase of catalyst. Micheal et al. (2014) reported that sonolytic and photolytic processes

were ineffective to treat ibuprofen (10 %) and diclofenac (21 %), respectively. However, when subjected to combined application, the degradation efficiency of diclofenac and ibuprofen were greatly enhanced to 96 % and 85 % after 2 hours, respectively. The analysis of toxicity was also performed using freshwater species *Daphnia magna* as a control subject. The acute toxicity of the diclofenac and ibuprofen to *Daphnia magna* were monitored and showed that sonophotocatalytic process was able to decrease toxicity to 20 % after 48 hours. Therefore, it proved that combine two different energy sources had a superior performance to enhance the degradation process.

Besides, the photo- and sonophoto-degradation efficiency could be affected by the wavelength of different light sources. Generally, different types of light sources release different wavelengths and energies. The light source that commonly applied are vacuum ultraviolet (185 nm), ultraviolet (254 nm) and visible (400 nm). In the case of direct photolysis, the photon absorption by the EPs is crucial to determine the degradation performance. Strong light absorption occurred from deep UV region to 220 nm and weak absorption from 220 to 460 nm. Eskandarian et al. (2016) studied the direct photolytic degradation of sulfamethoxazole. Based on their study, the degradation efficiencies of sulfamethoxazole were approximately 60 %, 80 % and 100 % under UV-A (315 nm), UV-B (280 nm) and UV-C (100 nm), respectively after 3 hours. On the other hand, Cizmic et al. (2017) reported that UV-C could achieve better performance than UV-A in the degradation of praziquantel (anthelmintic drug). During direct photolysis under UV-C, a complete degradation of praziquantel was achieved after 15 minutes. However, no degradation was observed when subjected to photolysis under UV-A. This

suggested that UV-A was unable to provide sufficient energy to destruct praziquantel. This also indicated that light source with shorter wavelength such as UV-C could provide higher energy and thus, promote the degradation reaction of EPs.

2.5.2 Effect of Initial Concentration of Target Pollutant

The initial concentration of target pollutant could affect the performance of sono-, photo- and sonophoto-degradation significantly. Generally, low initial concentration of target pollutant can achieve higher degradation efficiency in a shorter treatment period. Dai et al. (2012) reported the effect of initial concentration of carbamazepine during photocatalytic degradation. When increasing the dye concentration from 4.2 to 42.3 μM, the degradation efficiency was found to decrease from approximately 70 % to 25 % after 10 minutes irradiation. They mentioned that the decrement in degradation efficiency might probably related to the amount of pollutant being adsorbed and reacted on a fixed number of active sites on catalyst surface.

Meanwhile, Karaca et al. (2016) also reported that increasing the initial concentration of pollutant could decrease the sonocatalytic degradation efficiency. They found that the degradation efficiency of naproxen at concentration of 5 and 20 mg/L were about 90 % and 60 %, respectively. With increasing initial concentration of naproxen, it was expected that larger amount of •OH was required for the degradation process. However, water and dissolved oxygen molecules were hampered to reach the catalyst surface as most of the catalyst surface was occupied by the adsorbed pollutants and, thus

resulted in a low production of •OH on catalyst surface. As a consequence, the degradation efficiency was decreased.

2.5.3 Effect of Catalyst Dosage

The addition of catalyst plays an important role during sono, photo and sonophoto-degradation processes. Generally, increasing the catalyst dosage could lead to a more prominent degradation performance due to the increase in total surface area and therefore enhance the creation of radical species on catalyst surface. Hassani et al. (2015, 2016) carried out sonocatalytic and photocatalytic degradation of ciprofloxacin in the presence of TiO_2/montmorillonite catalyst. The catalyst dosage applied was in the range from 0.05 to 0.4 g/L. Sonocatalytic degradation efficiency of ciprofloxacin increased with increasing catalyst dosage up to 0.2 g/L and remained constant thereafter. At the optimum catalyst dosage of 0.2 g/L, the highest degradation efficiency of 65% was achieved. Meanwhile, photocatalytic degradation of ciprofloxacin achieved the highest degradation efficiency of 61% when the catalyst dosage fix at 0.1 g/L. Beyond that, a decreased in degradation efficiency was observed.

Similar results were also obtained by Huang et al. (2018) in a study of photocatalytic degradation of thiobencarb. They found that excessive dosage of catalyst could cause detrimental effect to the degradation efficiency. By varying the catalyst dosage from 0.25 to 1.0 g/L of MoS_2 catalyst, the degradation efficiency was increased from 60 % to 95 % due to the increased active sites available on the catalyst surface. However, slight decreased in

degradation efficiency to 90 % was observed when increasing catalyst dosage up to 1.5 g/L. This suggested that excessive catalyst dosage might probably cause agglomeration and result in light scattering, reduce active sites of catalyst and increase turbidity of solution (Shah et al., 2018).

2.5.4 Effect of Solution pH

Solution pH is a crucial parameter that affects the availability of radical species, surface charge of catalyst and form of target EPs. The solution pH is highly dependent on the acid strength (pK_a) of target EPs and the zero point charge (pH_{zpc}) of catalyst. Rao et al. (2016) studied on the effect of solution pH on sonochemical degradation of carbmamazepine. Carbamazepine is a non-volatile compounds that has two pK_a values of 2.3 (ketone group) and 13.9 (amino group). There was no significant effect to the degradation of carbamazepine in the solution pH ranged from 4.5 to 11. At solution pH 2, carbamazepine exists in ionic form with high hydrophilicity and solubility in water. Therefore, carbamazepine would accumulate in the bulk solution where lesser amount of •OH was readily available and resulted in a lower degradation efficiency. Contradictory, the sonochemical degradation of ibuprofen (pK_a = 4.7) performed better in solution pH 2.6 than pH 8 (Adityosulindro et al., 2017). Under acidic medium, molecular form of ibuprofen tends to exist in the interfacial region between cavitation bubble and bulk solution, whereby this region has high concentration of •OH and therefore results in a higher pseudo first-order reaction rate of 0.0035 min^{-1}. On the other hand, Yuan et al. (2016) reported the usage of N-doping carbon

nanotubes/TiO_2 (pH_{zpc} = 4.4) in photocatalytic degradation of ibuprofen. The catalyst displayed positive surface charge (Ti-OH_2^+) when solution pH < pH_{zpc} and negative surface charge (TiO^-) when solution pH > pH_{zpc}. In acidic medium, ibuprofen could dissociate to its conjugate base with negative charge. Therefore, the negatively charge ibuprofen preferably adsorbed and reacted on the positively charge catalyst and hence promoted the photodegradation efficiency from 53% to 89%.

2.5.5 Effect of H_2O_2 Amount

The purpose of H_2O_2 addition is to increase the concentration of •OH in the reaction system. It has been reported that H_2O_2 may react with target EPs and intermediate compounds due to their non-selectivity properties. Hassani et al. (2015) had proven the enhancer effect of H_2O_2 in the photocatalytic degradation of ciprofloxacin. The degradation efficiency of ciprofloxacin was found to increase from 61 % to 83 % after addition of 1 mM of H_2O_2. This was due to the higher creation of •OH through Equations (2.6) and (2.8). Besides, H_2O_2 could also generate •OH via reaction (2.26).

Golash and Gogate (2012) reported the effect of H_2O_2 in sonolytic degradation of dichlorvos by varying the H_2O_2 concentration from 10 – 60 ppm. It was found that the degradation efficiency was increased from 50 % to 62.5 % with the addition of 15 ppm H_2O_2. When increasing the H_2O_2 concentration to 35 ppm and 60 ppm, the degradation efficiency were 55 % and 48 %, respectively. This suggested that scavenging action of H_2O_2 occurred when excessive amount of H_2O_2 was added into the system. This

result was in good agreement with the findings obtained by Adityosulindro et al. (2017). They explained that the H_2O_2 could act as a scavenger that could react with •OH to form •OOH with lower oxidation potential (Equation (2.9)).

$$H_2O_2 + e^- \rightarrow \bullet OH + OH^- \quad (2.26)$$

CHAPTER 3

METHODOLOGY

3.1 Materials and Chemicals

The chemicals used are tabulated in Table 3.1. Tetrabutyl orthotitanate and iron (III) nitrate nonahydrate were used as starting materials while ethanol was used as solvent in synthesising TiO_2 and Fe-doped TiO_2. Hydrochloric acid, sodium hydroxide and sulphuric acid were used as pH adjuster. Liquid chromatography grade of methanol was involved in HPLC detection. The target pollutant was paracetamol tablet pills which obtained over-the-counter from pharmacy.

3.2 Instruments

Table 3.2 presents the instruments and their usage in this study. A furnace was used for post-treatment to TiO_2 and Fe-doped TiO_2 particles at various temperatures. Field emission scanning electron microscope, energy dispersive X-ray spectroscope, X-ray diffractometer, surface area analyser and X-ray photoelectron spectroscope were used to characterise the particles. The ultrasonic and UV irradiation sources were obtained from a sonicator and a UV lamp, respectively. Liquid samples collected during degradation process were analysed by HPLC and chemical oxygen demand (COD) colorimeter.

Table 3.1: Chemical reagents involved in the experimental work

Chemical	Purity	Brand	Molecular weight (g/mol)	Purpose of use	Potential hazard
Tetrabutyl orthotitanate, $C_{16}H_{36}O_4Ti$	≥ 98	Merck	340.32	Titanium source	Flammable, eyes irritation, harmful by inhalation
Iron (III) nitrate nonahydrate, $Fe(NO_3)_3 \cdot 9H_2O$	≥ 98	Merck	403.95	Iron source	Flammable, may cause irritation of eyes, skin and respiratory tract
Ethanol, C_2H_5OH	96	Merck	46.07	Solvent	Flammable, may cause eyes irritation and damage to organ
Sulphuric acid, H_2SO_4	98	Merck	98.07	pH adjustment (synthesise TiO_2 and Fe-doped TiO_2)	Corrosive, explosive, may cause severe irritation of eyes, skin and respiratory tract
Hydrochloric acid, HCl	37	Sigma-Aldrich	36.46	pH adjustment	Corrosive, explosive, may cause severe irritation of eyes, skin and respiratory tract
Sodium hydroxide, NaOH	97	Sigma-Aldrich	39.99	pH adjustment	Corrosive, explosive, may cause severe irritation of eyes, skin and respiratory tract
Hydrogen peroxide, H_2O_2	30	Sigma-Aldrich	34.01	Oxidizing agent	Corrosive, explosive, may cause severe irritation of eyes, skin and respiratory tract

Table 3.1: Continued

Methanol, CH_3OH	≥ 99.8	Merck	32.04	Mobile phase in HPLC	Flammable, may cause eyes irritation and damage to organ
Paracetamol, $C_8H_9NO_2$	≥ 90	Dynapharm	151.16	Target pollutant	May cause eyes and skin irritation, allergic skin reaction

*Appropriate personal protective equipment such as gloves, goggle and mask should be wear when handling with the chemical reagents.

Table 3.2: Model and function of instruments used

Instruments	Model	Function
Furnace	Carbolite RHF 15/8	To calcine the prepared TiO_2 and Fe-doped TiO_2
pH meter	Ionix pH tester kit	To check the solution pH
Sonicator	Daihan Scientific WUC-A03H	To provide ultrasonic wave
UV lamp	Analytikjena UVP 3UV-lamp	To provide ultraviolet light
Field emission scanning electron microscope equipped with energy dispersive X-ray spectroscope	JEOL JSM-6710F	To obtain surface morphology and elemental composition of the prepared TiO_2 and Fe-doped TiO_2
X-ray diffractometer	Shimadzu XRD-6000	To obtain phase structure and crystallite size of the TiO_2 and Fe-doped TiO_2
Surface area analyser	Quantachrome Autosorb	To determine the surface area, pore size and pore volume of the prepared TiO_2 and Fe-doped TiO_2
X-ray photoelectron spectroscope	Omicron Multiprobe	To determine the electronic state of surface elements of 3% Fe-doped TiO_2-600
COD colorimeter	DRB200	To determine the remaining amount of organic compounds in the sample solution after the degradation process
HPLC	Shimadzu Prominence Modular HPLC	To measure the remaining paracetamol concentration after the degradation process

3.3 Overall Experimental Flowchart

Figure 3.1 shows the overall experimental activities in this study. The first stage began with the synthesising of TiO_2 and Fe-doped TiO_2. The particles were subjected to characterisation by FESEM-EDX, XRD, XPS and nitrogen adsorption-desorption measurement analysis. This was followed by operating parameter studies in order to investigate the influence of each parameter on the sonophotocatalytic degradation of paracetamol. The operating parameter studies include Fe dopant concentration, calcination temperature, energy source, initial concentration of paracetamol, catalyst dosage, solution pH and H_2O_2 amount. Liquid samples collected were subjected to HPLC and COD analyses. Besides, the reusability of Fe-doped TiO_2 and kinetic study of sonophotocatalytic degradation of paracetamol were also included in this research study.

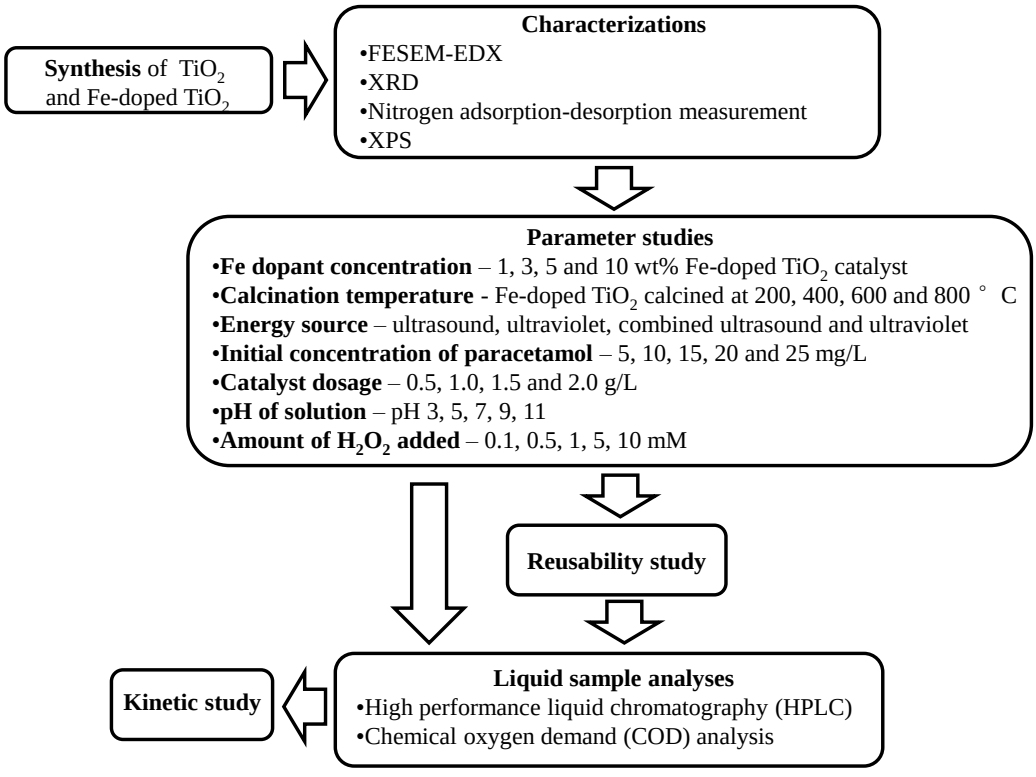

Figure 3.1: Flowchart of overall experiment activities

3.4 Experimental Setup

The batch experiments of sonophotocatalytic degradation of paracetamol using TiO_2 and Fe-doped TiO_2 catalyst were carried out as shown in Figure 3.2. Sonicator was operated at a frequency of 50 kHz and a maximum effective power of 296 W. UV irradiation was obtained from a 8 W UV light that could be operated at various wavelengths (256, 302 and 365 nm). A 100 mL paracetamol solution was prepared at concentration of 5 mg/L. The pH of the solution was adjusted to the desired pH using 1.0 M HCl and 0.1 M NaOH (Appendices A and B). For a typical experiment, 1 g/L Fe-doped TiO_2 was added into paracetamol solution. The mixture was allowed to stir continuously for 30 minutes in order to achieve adsorption-desorption equilibrium of paracetamol on the surface of Fe-doped TiO_2 catalyst. During the degradation reaction, 5 mL of solution was withdrawn at a specified time intervals within 2 hours reaction time. The collected sample solutions were filtered using 0.22 µm syringe filter prior to the HPLC detection to identify the remaining concentration. Various operating parameters such as Fe dopant concentrations (1, 3, 5 and 10 wt% Fe), calcination temperatures (200, 400, 600 and 800 °C), energy sources (ultrasonic irradiation, ultraviolet irradiation, combination of ultrasonic and ultraviolet irradiations), initial concentrations of paracetamol (5, 10, 15, 20 and 25 mg/L), catalyst dosages (0.5, 1.0, 1.5 and 2.0 g/L), solution pH (pH 3, 5, 7, 9 and 11) and H_2O_2 amounts (0.1, 0.5, 1, 5 and 10 mM) were investigated during sonophotocatalytic degradation of paracetamol.

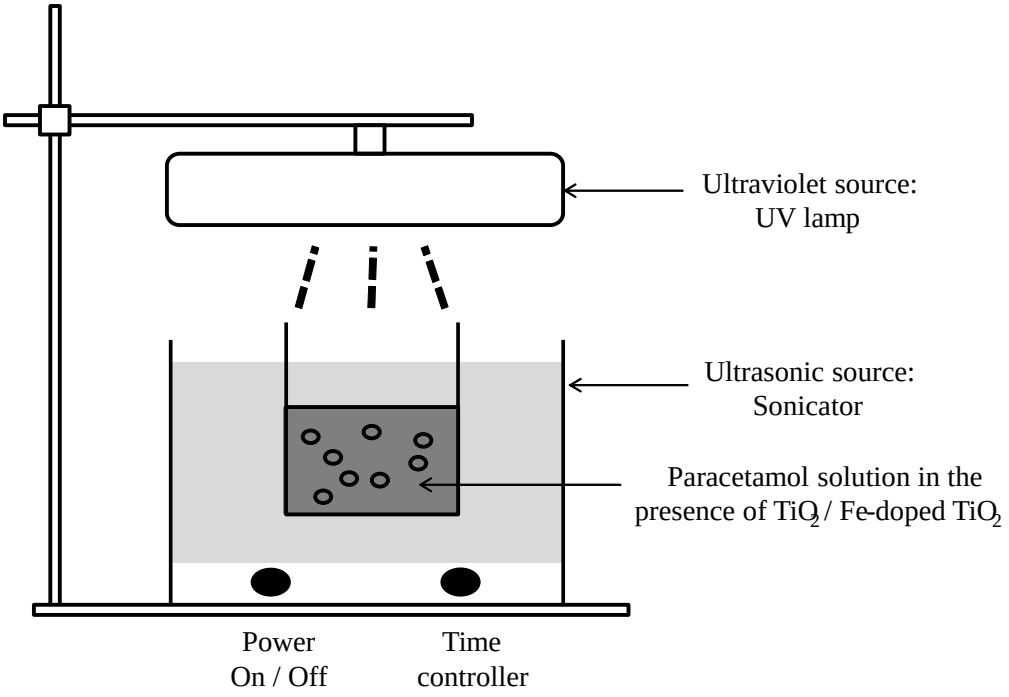

Figure 3.2: Schematic diagram of the experimental setup

3.5 Preparation and Characterisation of TiO_2 and Fe-doped TiO_2 Particles

3.5.1 Synthesis of TiO_2 and Fe-doped TiO_2

A modified sol-gel method was applied to synthesis TiO_2 and Fe-doped TiO_2 (Moradi et al., 2016). $C_{16}H_{36}O_4Ti$ and $Fe(NO_3)_3 \cdot 9H_2O$ were used as titanium and iron sources, respectively. First, 5 mL of $C_{16}H_{36}O_4Ti$ was dissolved in 50 mL of C_2H_5OH solvent under continuous stirring at ambient temperature. The pH of the solution was adjusted using a known amount of H_2SO_4 and a transparent sol was obtained. Meanwhile, appropriate concentration of Fe (1, 3, 5 and 10 wt%) was dissolved in distilled water before introduced into the transparent sol (Appendix C). The mixture was then sonicated in an ultrasonic bath for 10 minutes and further heated in a water bath at 80 °C for 2 hours.

The resulting gel was centrifuged and washed with distilled water. Finally, the resulting gel was dried in an oven at 80 °C for 8 hours and calcined at 400 °C for 2 hours. The Fe-doped TiO_2 with 1, 3, 5 and 10 wt% Fe were denoted as 1% Fe-doped TiO_2-400, 3% Fe-doped TiO_2-400, 5% Fe-doped TiO_2-400 and 10% Fe-doped TiO_2-400, respectively. For the 3% Fe-doped TiO_2 particles with the highest catalytic activity were subjected to calcination at various temperatures (200, 600 and 800 °C) and represented as 3% Fe-doped TiO_2-200, 3% Fe-doped TiO_2-600, 3% Fe-doped TiO_2-800.

3.5.2 Characterisation of TiO_2 and Fe-doped TiO_2 particles

Characterisation of TiO_2 and Fe-doped TiO_2 particles is important to be carried out in order to understand its properties, i.e. surface morphology, elemental composition, crystalline structure and surface area. The surface morphology, elemental composition and elemental mapping of the prepared samples were analysed by FESEM (JEOL JSM-6710F) equipped with an EDX. Prior to the characterisation, the TiO_2 and Fe-doped TiO_2 particles were adhered on the specimen holder using double-sided carbon tape. Sputter coating was carried out to reduce electrostatic distortion. FESEM-EDX was operated at electron accelerating voltages of 4.0 kV and magnification of 100,000 ×.

The phase structure and crystallite size of the TiO_2 and Fe-doped TiO_2 particles could be determined from X-ray diffractometer (Shimadzu XRD-6000) with CuK_α (λ = 0.154 nm) radiation source. The diffraction pattern was recorded in 2θ scans range between 10° and 80° with a scan rate of

2 °/minutes and a scan step of 0.02 °. The phase composition of anatase, rutile and brookite were calculated by Equations (3.1) – (3.3) (Appendix D) (Wahyuningsih et al., 2017). Meanwhile, the Debye-Scherrer equation (Equation (3.4)) was applied to calculate the crystallite size of TiO_2 and Fe-doped TiO_2 particles (Appendix E) (Tabasideh et al., 2017).

$$W_A = \frac{K_A A_A}{K_A A_A + A_R + K_B A_B} \tag{3.1}$$

$$W_R = \frac{A_R}{K_A A_A + A_R + K_B A_B} \tag{3.2}$$

$$W_B = \frac{K_B A_B}{K_A A_A + A_R + K_B A_B} \tag{3.3}$$

where

W_A, W_R, W_B = phase composition of anatase, rutile and brookite, respectively.

A_A, A_R, A_B = peak intensity of anatase, rutile and brookite, respectively.

K_A, K_B = coefficient of anatase (0.886) and brookite (2.721), respectively.

$$\tau = \frac{k\lambda}{\beta \cos\theta} \tag{3.4}$$

where

k = Scherrer constant (0.9)

λ = wavelength of CuK_α radiation (0.154 nm)

β = full-width at half maximum (FWHM in radian)

θ = Bragg angle of prominent peak ($2\theta \approx 25$ ° for anatase and $2\theta \approx 27$ ° for rutile)

The specific surface area was determined by BET method while pore size and pore volume of TiO_2 and Fe-doped TiO_2 particles were determined by BJH methods through nitrogen adsorption-desorption measurement using sorptomatic surface area analyser (Quantachrome Autosorb). Prior to the

analysis, the TiO_2 and Fe-doped TiO_2 particles were dried in an oven at temperature of 80 °C for 2 hours to eliminate the moisture content. After that, the particles were degassed at 200 °C under vacuum for 8 hours. The particles were analysed using liquid nitrogen as coolant at 77 K to obtain a nitrogen adsorption-desorption isotherm.

XPS, a surface analysis technique was carried out to determine the electronic states of surface elements. The XPS spectrum were obtained from Omicron Multiprobe spectrometer using Al K_α (binding energy = 1480 kV) as X-ray irradiation source. All the binding energies were referenced to C 1s peak at 284 eV. The chemical states of an element can be determined by peak identification and peak fitting process.

3.6 Parameter Studies in Sonophotocatalytic Degradation

3.6.1 Effect of Fe Dopant Concentration

The catalytic activity of TiO_2 and Fe-doped TiO_2 in degradation of paracetamol was studied by varying the Fe dopant concentrations (1, 3, 5 and 10 wt%) during the synthesis of Fe-doped TiO_2. The experiment was carried out under initial paracetamol concentration of 5 mg/L with the addition of 1 g/L Fe-doped TiO_2 at different Fe dopant concentrations (1, 3, 5 and 10 wt%) in 100 mL solution. Other parameters, i.e. sonicator power of 296 W, sonicator frequency of 50 kHz, 8 W UV light with wavelength of 302 nm, solution pH of 5 and temperature at 30 °C were kept constant during the experiment. Liquid samples were collected every 10 minutes for the first 30

minutes and every 30 minutes thereafter for a total duration of 2 hours. The catalyst with the highest catalytic activity, i.e. 3% Fe-doped TiO_2-400 was chosen for subsequent studies.

3.6.2 Effect of Calcination Temperature

The effect of calcination temperature on catalytic activity of Fe-doped TiO_2 in degradation of paracetamol was investigated. In each batch of experiment, 1 g/L of the 3% Fe-doped TiO_2 which calcined at different temperatures (200, 400, 600 and 800 °C) was added into a 100 mL of 5 mg/L paracetamol solution. Other parameters, i.e. sonicator power of 296 W, sonicator frequency of 50 kHz, 8 W UV light with wavelength of 302 nm, solution pH of 5 and temperature at 30 °C were kept constant during the experiment. Liquid samples were collected every 10 minutes for the first 30 minutes and every 30 minutes thereafter for a total duration of 2 hours. 3% Fe-doped TiO_2-600 with the best degradation efficiency was chosen for subsequent studies.

3.6.3 Effect of Energy Source

The sonocatalytic, photocatalytic and sonophotocatalytic degradation of paracetamol were carried in order to compare their degradation performance. During sonocatalysis, UV lamp was turned off while sonicator was not used during photocatalysis. Sonophotocatalysis process was carried out with both sonicator and UV lamp were turned on. During sonophotocatalysis, the UV wavelengths (256, 302 and 365 nm) was varied to understand the effect of UV

wavelength on sonophotocatalytic degradation of paracetamol. Other parameters, i.e. sonicator power of 296 W, sonicator frequency of 50 kHz, initial paracetamol concentration of 5 mg/L, 1 g/L of 3% Fe-doped TiO_2-600, solution pH of 5, temperature at 30 °C were kept constant during the experiment. Liquid samples were collected every 10 minutes for the first 30 minutes and every 30 minutes thereafter for a total duration of 2 hours. The sonophotocatalysis at UV wavelength of 302 nm which achieved the best degradation efficiency was chosen for subsequent parameter studies.

3.6.4 Effect of Initial Concentration of Paracetamol

The effect of initial paracetamol concentrations on the sonophotocatalytic degradation efficiency was studied by varying the initial concentrations of paracetamol to 5, 10, 15, 20 and 25 mg/L (Appendix F). Other parameters, i.e. sonicator power of 296 W, sonicator frequency of 50 kHz, 8 W UV light with wavelength of 302 nm, 1 g/L of 3% Fe-doped TiO_2-600, solution pH of 5 and temperature at 30 °C were kept constant during the experiment. Liquid samples were collected every 10 minutes for the first 30 minutes and every 30 minutes thereafter for a total duration of 2 hours. The lowest initial paracetamol concentration of 5 mg/L which achieved the highest degradation efficiency was chosen for subsequent studies.

3.6.5 Effect of Catalyst Dosage

Numerous runs with different catalyst dosages of 0.5, 1.0, 1.5 and 2.0 g/L 3% Fe-doped TiO_2-600 were conducted to study the effect of catalyst dosage on sonophotocatalytic degradation of paracetamol. Other parameters, i.e. sonicator power of 296 W, sonicator frequency of 50 kHz, 8 W UV light with wavelength of 302 nm, initial paracetamol concentration of 5 mg/L, solution pH of 5 and temperature at 30 °C were kept constant during the experiment. Liquid samples were collected every 10 minutes for the first 30 minutes and every 30 minutes thereafter for a total duration of 2 hours. The optimum catalyst dosage, i.e. 1.0 g/L of 3% Fe-doped TiO_2-600 was chosen for subsequent studies.

3.6.6 Effect of Solution pH

The effect of solution pH for sonophotocatalytic degradation of paracetamol was studied by adjusting the 100 mL of 5 mg/L paracetamol solution to pH 3, 5, 7, 9 and 11. Other parameters, i.e. sonicator power of 296 W, sonicator frequency of 50 kHz, 8 W UV light with wavelength of 302 nm, initial paracetamol concentration of 5 mg/L, 1 g/L of 3% Fe-doped TiO_2-600 and temperature at 30 °C were kept constant during the experiment. Liquid samples were collected every 10 minutes for the first 30 minutes and every 30 minutes thereafter for a total duration of 2 hours. The optimal solution pH for the degradation of paracetamol, i.e. pH 5 was chosen and carried forward in the subsequent studies.

3.6.7 Effect of H_2O_2 Amount

The effect of oxidizing H_2O_2 on sonophotocatalytic degradation of paracetamol was investigated by varying the H_2O_2 concentrations to 0.1, 0.5, 1, 5 and 10 mM (Appendix G). Other parameters, i.e. sonicator power of 296 W, sonicator frequency of 50 kHz, 8 W UV light with wavelength of 302 nm, initial paracetamol concentration of 5 mg/L, 1 g/L of 3% Fe-doped TiO_2-600, solution pH of 5 and temperature at 30 °C were kept constant during the experiment. Liquid samples were collected at 5, 10, 20, 30, 60, 90 and 120 minutes. The optimum H_2O_2 concentration, i.e. 0.5 mM was chosen and carried forward to the following experiment.

3.6.8 Reusability Study

The reusability of 3% Fe-doped TiO_2-600 catalyst in degradation of paracetamol was studied by recovering the used catalyst. The used catalyst was rinsed with distilled water for several times and dried in an oven at 80 °C for 8 hours. Subsequently, the used 3% Fe-doped TiO_2-600 catalyst was investigated up to four catalytic cycles of degradation process. Similar conditions as previous experiment, i.e. sonicator power of 296 W, sonicator frequency of 50 kHz, 8 W UV light with wavelength of 302 nm, 100 mL of 5 mg/L paracetamol solution, 1 g/L of 3% Fe-doped TiO_2-600, solution pH of 5, 0.5 mM H_2O_2 and temperature at 30 °C were applied. Liquid samples were collected at 5, 10, 15 and 20 minutes. The degradation efficiencies obtained by using the used catalyst were compared with the activity of fresh catalyst.

3.7 Kinetic Study

In order to predict the degradation rate of paracetamol in a sonophotocatalytic reaction, three kinetic models (pseudo zero-order, pseudo first-order and pseudo second-order reaction kinetics) had been developed and studied. The expressions of three kinetic models were shown in Equations (3.5) – (3.7) (Shibin et al., 2015) (Appendix H).

Pseudo zero-order kinetic:

$$C_t = C_0 - k_0 t \tag{3.5}$$

Pseudo first-order kinetic:

$$\ln C_t = \ln C_0 - k_1 t \tag{3.6}$$

Pseudo second-order kinetic:

$$\frac{1}{C_t} = \frac{1}{C_0} + k_2 t \tag{3.7}$$

where

C_0 = concentration of paracetamol at initial t = 0 min, mg/L

C_t = concentration of paracetamol at a certain reaction time (t), mg/L

k_0 = pseudo zero-order rate constant, mg/L·min

k_1 = pseudo first-order rate constant, min^{-1}

k_2 = pseudo second-order rate constant, L/mg·min

t = reaction time, min

For sonophotocatalytic degradation, synergy index was applied to measure and evaluate the feasibility of combined oxidation processes for the

intensification of paracetamol degradation (Equation (3.8)) (Appendix I) (Mosleh and Rahimi, 2017, Sunasee et al., 2017).

$$Synergy\ index\ = \frac{k_{US+UV+A}}{k_{US+A}+k_{UV+A}} \quad (3.8)$$

where

k_{US+A}, k_{UV+A}, $k_{US+UV+A}$ = rate constant of sono-, photo- and sonophotocatalytic degradation, respectively.

A = catalyst

3.8 Liquid Sample Analysis

The liquid samples collected from each batch of experiment were measured for the remaining concentration of paracetamol in order to study the performance of sonophotocatalytic degradation of paracetamol. The remaining concentration of liquid samples were determined using HPLC system with C18 column (Shim-pack GWS, 250 mm length, 4.6 mm inner diameter) and equipped with a UV detector. The column was maintained at temperature of 30 °C and injected volume of 10 µL was used. The detection wavelength was set at 254 nm. A mobile phase of 70 % deionized water and 30 % chromatography grade methanol were flowing through the column at flowrate of 1 mL/min. The degree of degradation of paracetamol was calculated using Equation (3.9).

$$Degradation\ efficiency\ (\%) = \frac{C_0 - C_t}{C_0} \times 100\% \quad (3.9)$$

where

C_0 = concentration of paracetamol at initial t = 0 min, mg/L

C_t = concentration of paracetamol at a certain reaction time (t), mg/L

COD determination was conducted based on the standard method of potassium dichromate oxidation. 2 mL liquid sample was added into the COD vials which contained potassium dichromate and heated at 150 °C for 2 hours. After that, the COD level was measured using a COD colorimeter.

CHAPTER 4

RESULTS AND DISCUSSION

4.1 Characterisation of TiO_2 and Fe-doped TiO_2

4.1.1 FESEM-EDX Analysis

FESEM was utilized to investigate the surface morphology of bare TiO_2 and Fe-doped TiO_2 particles. Figure 4.1 shows FESEM images of bare TiO_2, Fe-doped TiO_2 at various Fe concentrations and calcination temperatures. All the samples were composed of nano-sized particles in spherical shape. Figure 4.1 (a) shows that bare TiO_2 possessed homogeneous distribution and uniform size (ranged from 15 nm to 25 nm) of spherical shape particles. According to Figure 4.1 (b) – (e), different loadings of Fe did not change the spherical shape of particles. However, agglomerated particles could be easily detected when increasing the Fe dopant concentrations on TiO_2 particles. This implied that Fe dopant could promote agglomeration of particles. Moradi et al. (2016) found that the degree of agglomeration increased with the concentration of Fe dopants.

On the other hand, Figure 4.1 (f) – (h) shows the FESEM images of 3% Fe-doped TiO_2 calcined at various temperatures. It was found that the particle sizes were increased when increasing the calcination temperature from 200 °C

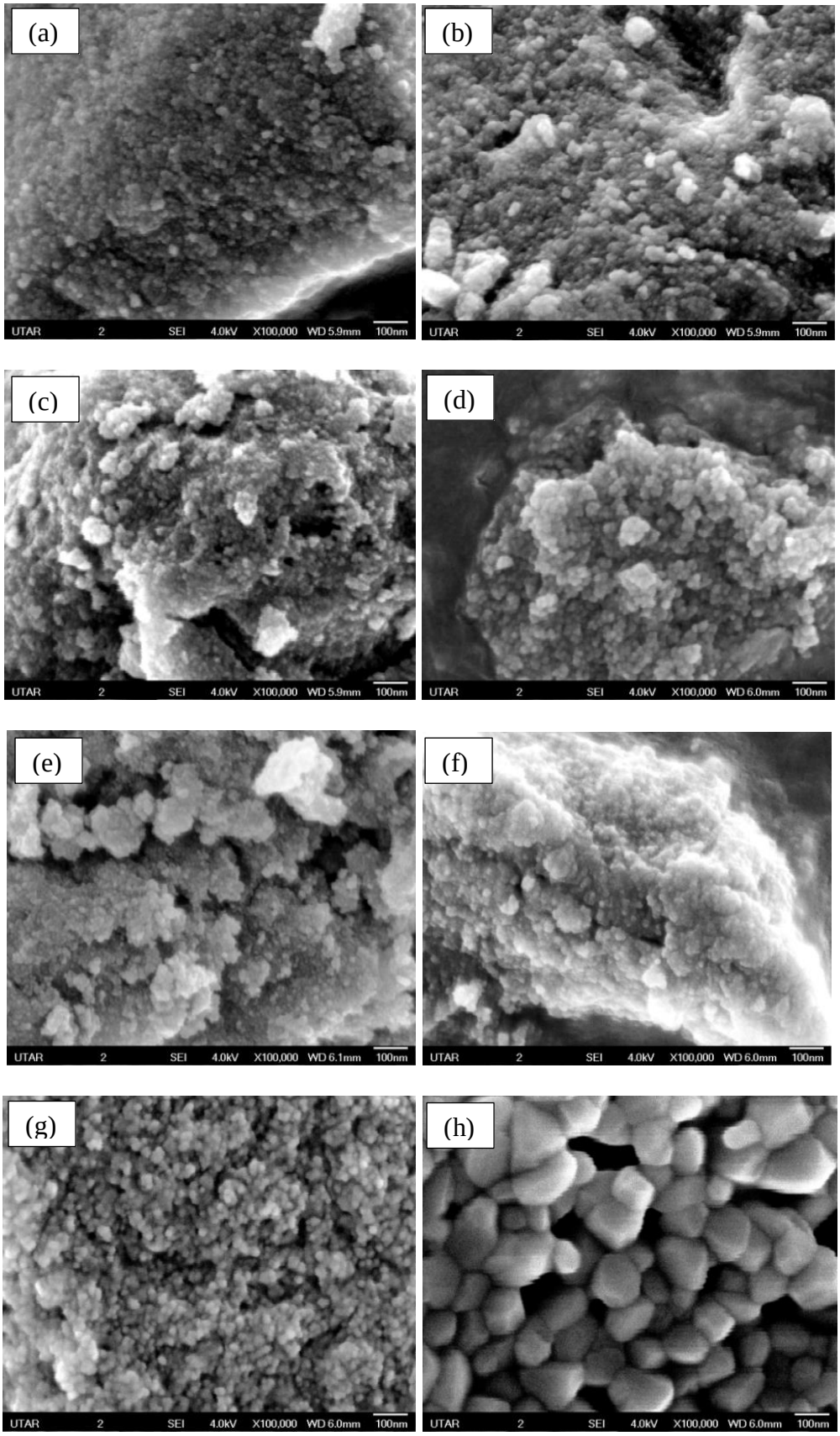

Figure 4.1: FESEM images of (a) bare TiO_2-400, (b) 1% Fe-doped TiO_2-400, (c) 3% Fe-doped TiO_2-400, (d) 5% Fe-doped TiO_2-400, (e) 10% Fe-doped TiO_2-400, (f) 3% Fe-doped TiO_2-200, (g) 3% Fe-doped TiO_2-600 and (h) 3% Fe-doped TiO_2-800

to 800 °C. 3% Fe-doped TiO_2-800 possessed the largest particle sizes ranged from 80 nm to 180 nm. This proved that high calcination temperature could promote the growth in particle size. Agglomeration tend to occur when the particles moved closer to each other and formed larger particles after water content had being dehydrated due to the sintering effect (Ogi et al., 2017).

The elemental composition of bare TiO_2 and Fe-doped TiO_2 particles were analysed by EDX and the results are summarised in Table 4.1. It is observed that the weight percentage of Fe increased with increasing Fe dopant concentration and the detected iron amount was in agreement with the calculated doping contents. This confirmed the successful doping of Fe on TiO_2 particles. The atomic composition of 3% Fe-doped TiO_2-600 was composed of 64.12 % O and 29.95 % Ti, which was similar to the theoretical stoichiometry ratio of O:Ti = 2:1. The presence of suphur (S) element could be ascribed to the usage of H_2SO_4 as pH adjuster during the Fe-doped TiO_2 synthesising process. From the EDX mapping illustrated in Figure 4.2, it was observed that Fe element on TiO_2 was well distributed. This suggested the good interaction between Fe and TiO_2 during the synthesising process via sol-gel method.

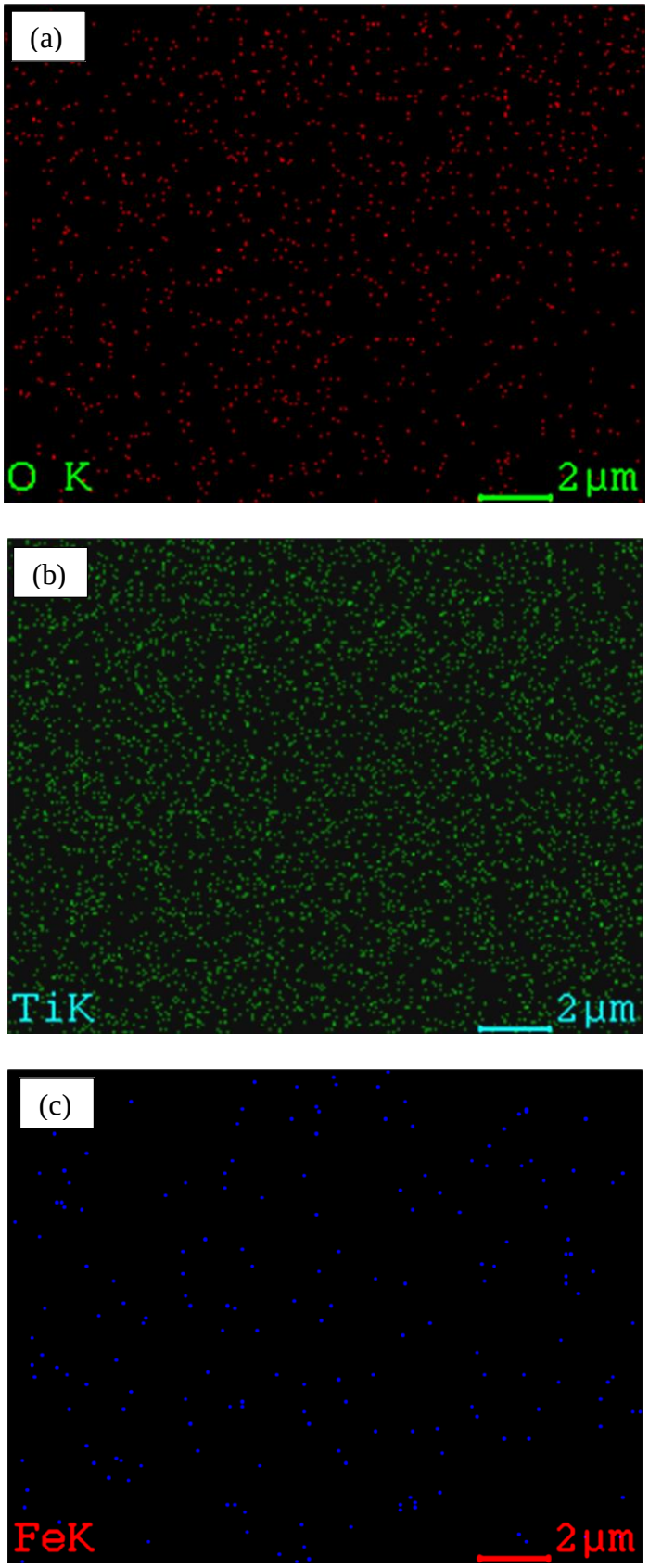

Figure 4.2: Elemental mapping of (a) O, (b) Ti and (c) Fe of 3% Fe-doped TiO_2-600

Table 4.1: The atomic and weight percentage of bare TiO_2 and Fe-doped TiO_2 through EDX analysis

Sample	Atomic (%)				Weight (%)			
	Ti	O	Fe	S	Ti	O	Fe	S
Bare TiO_2-400	32.34	64.18	-	3.48	57.52	38.33	-	4.15
1% Fe-doped TiO_2-400	30.34	64.66	0.67	4.33	54.95	39.02	0.82	5.21
3% Fe-doped TiO_2-400	29.95	64.12	1.34	4.59	52.50	39.23	2.75	5.52
5% Fe-doped TiO_2-400	29.87	62.96	2.41	4.76	52.18	37.29	4.93	5.60
10% Fe-doped TiO_2-400	26.93	63.48	4.00	5.59	48.19	37.34	9.05	5.42
3% Fe-doped TiO_2-200	28.43	65.70	1.29	4.58	51.74	39.94	2.74	5.58
3% Fe-doped TiO_2-600	32.94	63.42	1.27	2.37	57.39	36.91	2.74	2.96
3% Fe-doped TiO_2-800	30.20	66.36	1.28	2.16	54.01	40.24	2.72	3.03

4.1.2 XRD Analysis

XRD analysis was conducted to examine the crystallinity of bare TiO_2 and Fe-doped TiO_2 particles at various Fe dopant concentrations as shown in Figure 4.3. Figure 4.3 reveals that all diffraction peaks of bare TiO_2 and Fe-doped TiO_2 particles could be indexed to anatase phase. The peaks were observed at 2θ = 25.24 °, 38.02 °, 47.84 °, 53.94 ° and 64.00 °, which correspond to the (1 0 1), (0 0 4), (2 0 0), (1 0 5) and (2 0 4) tetragonal crystal planes of anatase TiO_2, respectively. It is well accepted that the intensity of diffraction peaks represents the degree of crystallinity of particles. As shown in Figure 4.3 (b) – (e), the peak intensity of Fe-doped TiO_2 decreased as compared to the bare TiO_2-400 (Figure 4.3 (a)) and the peak intensity significantly reduced with increasing Fe dopant concentration. Meanwhile, the peak broadening and decreased in crystallinity with increasing Fe dopant concentrations suggested that changes in crystallinity of anatase structure occurred due to the accommodation of Fe^{3+} ions into crystal lattice of TiO_2, in which resulting in structural distortion (Ibrahim and Sreekantan, 2014, Yang et al., 2017).

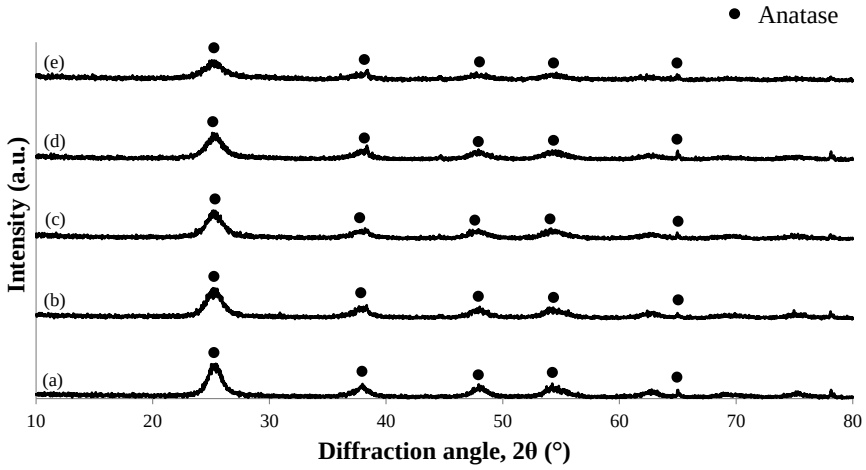

Figure 4.3: XRD pattern of (a) bare TiO_2-400, (b) 1% Fe-doped TiO_2-400, (c) 3% Fe-doped TiO_2-400, (d) 5% Fe-doped TiO_2-400 and (e) 10% Fe-doped TiO_2-400

Figure 4.4 illustrates the XRD patterns of 3% Fe-doped TiO_2 calcined at various temperatures. It was observed that the transformation of pure anatase to mixture of anatase-rutile phases was occurred at 600 °C. This was indicated by the presence of rutile diffraction peaks at $2\theta = 62.60°$ and 70.16° as shown in Figure 4.4 (c). This implied that the temperature of phase transformation from anatase to rutile began at calcination temperature of 600 °C. When the calcination temperature increased from 600 °C to 800 °C, the intensity of rutile increased sharply, suggesting the significant phase transformation to rutile and enhancement in crystallinity (Yan et al., 2017). Several diffraction peaks at 2θ = 27.40°, 36.02°, 39.20°, 41.20°, 44.00°, 54.28°, 56.60°, 62.72°, 64.02°, 69.76° and 76.52° were obviously spotted, which corresponded to the reflections from the (1 1 0), (1 0 1), (2 0 0), (1 1 1), (2 1 0), (2 1 1), (2 2 0), (0 0 2), (3 1 0), (1 1 2) and (2 0 2) planes of rutile phase, respectively. Besides, 3% Fe-doped TiO_2-800 particles showed a minority anatase peaks and a new diffraction peak detected at $2\theta = 32.44°$ was attributed to the brookite phase.

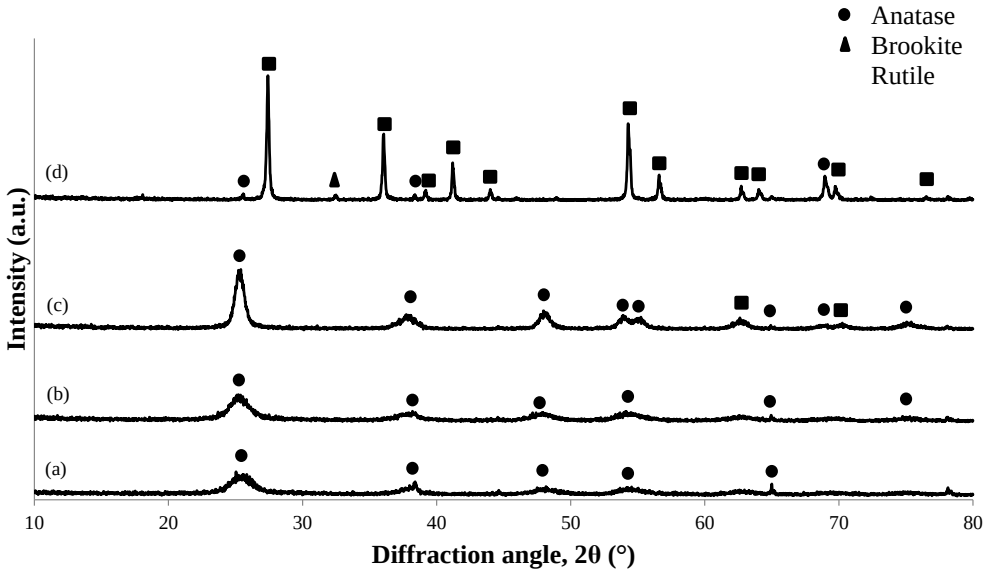

Figure 4.4: XRD pattern of (a) 3% Fe-doped TiO_2-200, (b) 3% Fe-doped TiO_2-400, (c) 3% Fe-doped TiO_2-600 and (d) 3% Fe-doped TiO_2-800

The result obtained was in good agreement with those reported by Kusdianto et al. (2018), in which the phase transformation temperature of Ag-TiO_2 (500 °C) was lower than the bare TiO_2 (900 °C). They suggested that the existence of metal ions could induce the occurrence of crystallisation and therefore, shift the phase transformation to a lower temperature. It is noteworthy that no diffraction peaks of Fe or Fe compounds were detected, even in the sample with the highest Fe dopant concentration at 10 wt%. This was probably attributed to the low Fe dopant amount used which was under detection limit of XRD analysis (Tabasideh et al., 2017). Besides, it was anticipated that Fe^{3+} (0.064 nm) entered into the substitutional sites of the TiO_2 crystal lattice by replacing the Ti^{4+} (0.068 nm) due to their similar radii (Sood et al., 2015).

Table 4.2 shows the calculated crystallite size of bare TiO_2 and Fe-doped TiO_2 particles. It was found that the crystallite size of Fe-doped TiO_2 at various Fe dopant concentrations decreased as compared to bare TiO_2 from 5.98 nm to 4.79 nm. As mentioned earlier, Fe^{3+} with smaller ionic radius as compared to Ti^{4+} could enter into the crystal lattice of TiO_2 by substitutional mode and thus, restrained the crystallite growth of TiO_2 (Wen et al., 2012). Meanwhile, the average crystallite size of 3% Fe-doped TiO_2 at various calcination temperatures increased from 4.47 nm to 43.02 nm. In the early stage of calcination from 200 °C to 600 °C, it was found that the crystallite size of 3% Fe-doped TiO_2 increased slowly, probably related to the presence of hydroxyl groups which restrained the rapid growth in crystallite size (Gaber et al., 2014). Above 600 °C, the crystallite size increased significantly

which could be attributed to the sintering effect and fast growth rate of rutile phase (Nasralla et al., 2013).

Table 4.2: Crystallite size of bare TiO_2 and Fe-doped TiO_2 particles

Sample	Phase composition (%)			Crystallite size (nm)
	Anatase	Rutile	Brookite	
Bare TiO_2-400	100	-	-	5.98
1% Fe-doped TiO_2-400	100	-	-	5.02
3% Fe-doped TiO_2-400	100	-	-	5.02
5% Fe-doped TiO_2-400	100	-	-	5.02
10% Fe-doped TiO_2-400	100	-	-	4.79
3% Fe-doped TiO_2-200	100	-	-	4.47
3% Fe-doped TiO_2-600	92.88	7.12	-	9.69
3% Fe-doped TiO_2-800	1.82	87.01	11.17	43.02

4.1.3 Nitrogen Adsorption-Desorption Measurement

The surface area, pore size and pore volume of the bare TiO_2 and Fe-doped TiO_2 are summarised in Table 4.3. It can be observed that increasing Fe dopant concentration and calcination temperature significantly reduced the surface area of particle. The BET surface area of bare TiO_2-400 was 152.08 m^2/g and reduced to 61.52 m^2/g when the Fe dopant concentration increased up to 10 wt%. Babic et al. (2016) claimed that increased the Fe dopant concentration could induce the particle aggregation, in which resulting in decreased surface area. A slight decrement in pore size and pore volume with increasing Fe dopant concentration were observed. This results obtained was consistent with the study by Siwinska-Stefanska et al. (2014). It was suggested

that a small portion of the Fe dopants had deposited into the porous structure of TiO_2 and led to decrement in pore size and pore volume.

Table 4.3: Surface area, pore size and pore volume of the bare TiO_2 and Fe-doped TiO_2 particles

Sample	Surface area (m^2/g)	Pore size (nm)	Pore volume (cm^3/g)
Bare TiO_2-400	152.08	3.61	0.137
1% Fe-doped TiO_2-400	143.82	2.95	0.106
3% Fe-doped TiO_2-400	131.94	2.76	0.091
5% Fe-doped TiO_2-400	122.16	2.74	0.084
10% Fe-doped TiO_2-400	61.52	4.54	0.070
3% Fe-doped TiO_2-200	180.46	1.96	0.089
3% Fe-doped TiO_2-600	51.69	9.74	0.126
3% Fe-doped TiO_2-800	19.96	10.51	0.052

On the other hand, the surface area of Fe-doped TiO_2 particles was further reduced from 180.46 to 19.96 m^2/g as the calcination temperature increased from 200 to 800 °C. Lin et al. (2018) reported that increasing the calcination temperature not only decreased to the surface area but also affected the pore size and pore volume of the Fe-doped TiO_2 catalyst. As it can be seen from Table 4.3, the pore size increased and the pore volume decreased with increasing calcination temperature. Gaber et al. (2014) claimed that the decreased in surface area and pore volume were attributed by the sintering effect, which caused increment in the particle size and degree of agglomeration. Meanwhile, rupturing of the porous structure which occurred at high calcination temperature could lead to increment in pore size from 1.96 nm to 10.51 nm (Mohd Yusoff and Abdullah, 2018). Thus, this minimised the porosity and reduced the surface area of the sample. Besides, the reduction in

surface area might relate to the phase transformation from anatase to rutile phase as reported by Pang et al. (2010). Interestingly, 3% Fe-doped TiO_2-600 possessed pore volume of 0.126 cm^3/g which implied that the chemisorbed water molecules were being eliminated from the pores under an appropriate temperature and therefore led to larger pore volume (Gaber et al., 2014).

Figure 4.5 illustrates the nitrogen adsorption-desorption isotherm of 3% Fe-doped TiO_2-600. According to the IUPAC classification (Sing, 1985), it was classified as the standard type IV isotherm with a H2 hysteresis loop. This suggested that capillary condensation took place in 'ink-bottle' shaped mesoporous structure at high relative pressure of $0.6 < P/P_0 < 0.8$ (Mohd Yusoff and Abdullah, 2018). The increase in adsorption volume of nitrogen was indicated by the height of hysteresis loop. The pore size distribution was in the range of 5 – 60 nm with maximum peak at approximately 9 nm.

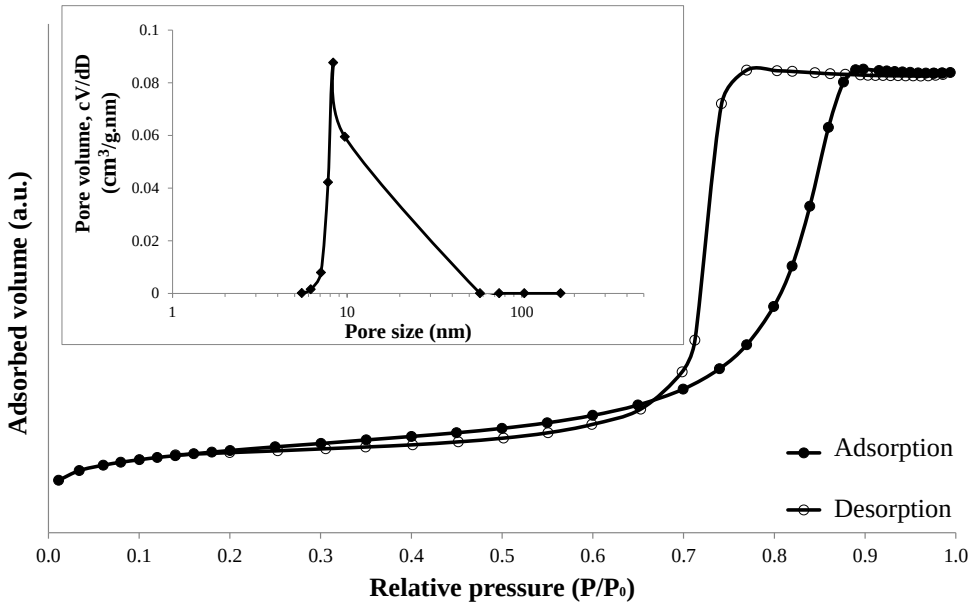

Figure 4.5: Nitrogen adsorption-desorption isotherm and pore size distribution (inset figure) on the surface of 3% Fe-doped TiO_2-600.

4.1.4 XPS analysis

XPS analysis was carried out to examine the chemical state of Fe dopant in the TiO_2. Figure 4.6 illustrates the high resolution XPS spectra of Ti 2p, O 1s and Fe 2p of 3% Fe-doped TiO_2-600. A Ti 2p spectra was shown in Figure 4.6 (a). It can be observed that there were two peaks existed at 464 eV and 458 eV, which were attributed to Ti^{4+} $2p_{1/2}$ and Ti^{4+} $2p_{3/2}$ (Moradi et al., 2018). The high resolution scan of O 1s can be deconvoluted into two peaks at binding energy of 530.2 eV and 532.1 eV as shown in Figure 4.6 (b). The peak at 530.2 eV could be assigned to TiO_2 while another peak at 532.1 eV was attributed to oxygen from the chemisorbed water (Pang and Abdullah, 2013). The Fe $2p_{3/2}$ binding energy for 3% Fe-doped TiO_2-600 was found at 711.6 eV with narrow width, suggested that the Fe existed as Fe^{3+} ion (Moradi et al., 2018). This indicated the successful incorporation of Fe^{3+} into TiO_2 lattice to form Fe-O-Ti bond.

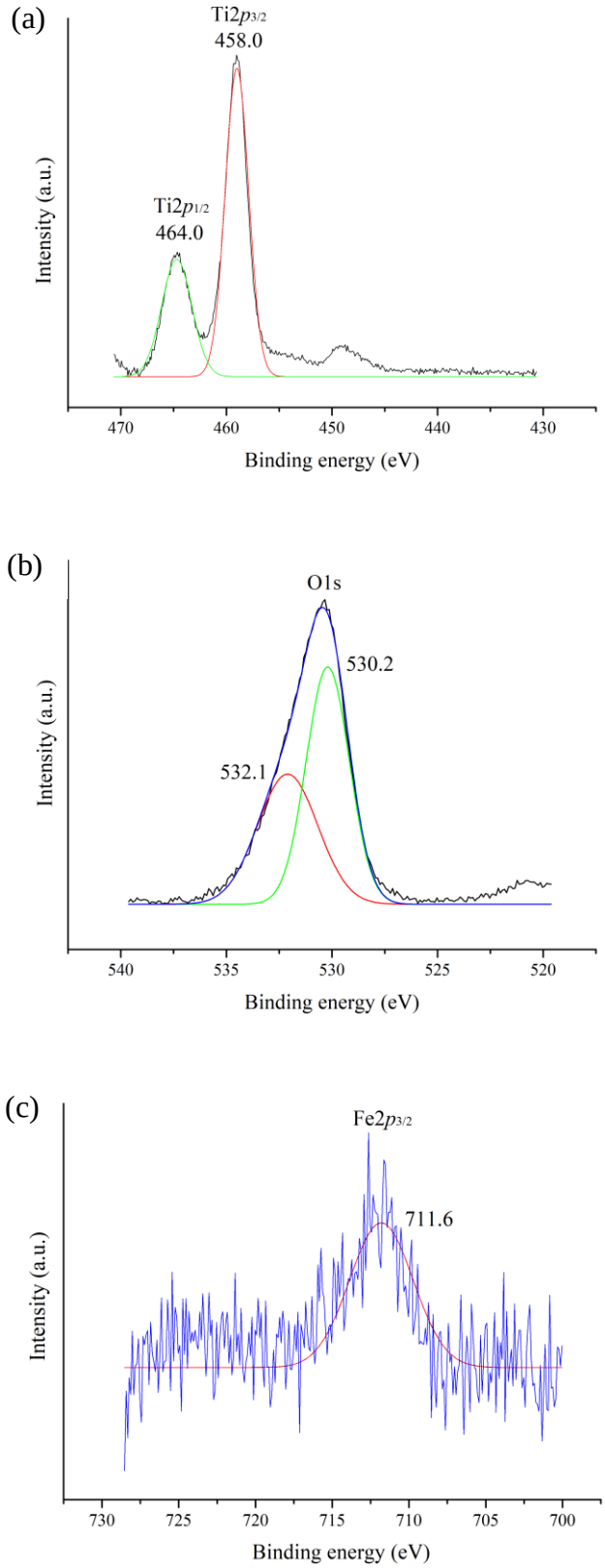

Figure 4.6: XPS spectra of (a) Ti 2p, (b) O 1s and (c) Fe 2p for 3% Fe-doped TiO_2-600

4.2 Parameter Studies

4.2.1 Effect of Fe Dopant Concentration

Figure 4.7 illustrates the sonophotocatalytic degradation efficiency of paracetamol using bare TiO_2 and Fe doped TiO_2 at different Fe concentrations. It was found that the Fe-doped TiO_2 catalyst provided a better performance in paracetamol degradation as compared to bare TiO_2. The highest degradation of 70 % was observed by using 3% Fe-doped TiO_2-400 after 2 hours. Further increasing the Fe dopant concentration above 3 wt% was found to cause detrimental effect on the sonophotocatalytic activity of TiO_2, i.e. degradation efficiency was dropped to 56 % when 10% Fe-doped TiO_2-400 was applied.

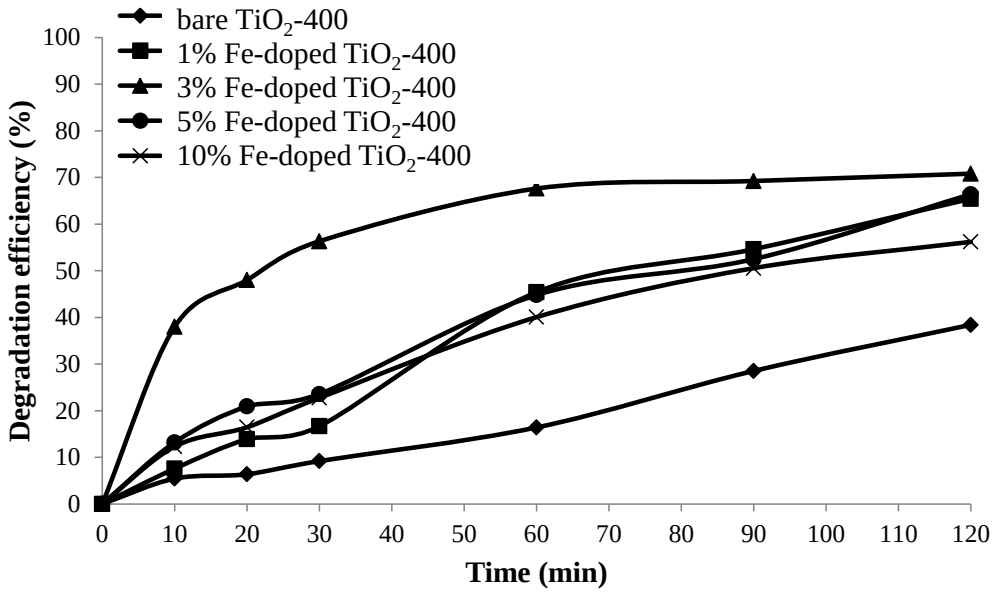

Figure 4.7: Degradation efficiency of paracetamol for bare TiO_2 and Fe-doped TiO_2 with various Fe dopant concentrations (sonicator power = 296 W, sonicator frequency = 50 kHz, UV wavelength = 302 nm, initial concentration of paracetamol = 5 mg/L, catalyst dosage = 1.0 g/L, solution pH = pH 5, temperature = 30 °C)

It was reported that increasing the concentration of Fe dopant could narrow the band gap energy and subsequently, enhanced the optical absorption

by extending the absorption edge of Fe-doped TiO_2 due to the introduction of energy level (Fe^{3+}/Fe^{4+}) of Fe (Moradi et al., 2016). Besides, increasing the Fe dopant concentration could increase the amount of effective heterojunction, which promoted the separation of electron-hole pairs and transferred them to the catalyst surface for degradation reaction (Yan et al., 2017). In addition, Fe^{3+} doping was able to prolong the lifetime of e^- and h^+ by trapping the electron and hole to form Fe^{2+} and Fe^{4+}, respectively (Equations (4.1) – (4.2)). Subsequently, Fe^{2+} and Fe^{4+} would revert back to Fe^{3+} by releasing e^- and h^+, respectively (Equations (4.3) – (4.4)) (Tabasideh et al., 2017).

$$Fe^{3+} + e^- \rightarrow Fe^{2+} \quad (4.1)$$

$$Fe^{3+} + h^+ \rightarrow Fe^{4+} \quad (4.2)$$

$$Fe^{2+} + O_2 \rightarrow Fe^{3+} + O_2^- \quad (4.3)$$

$$Fe^{4+} + OH^- \rightarrow Fe^{3+} + \bullet OH \quad (4.4)$$

However, excessive concentration of Fe dopant on TiO_2 could drastically affect its catalytic activity. High Fe dopant concentration could induce creation of defective sites within the crystal lattice (Sood et al., 2015). The defective sites could reduce the distance between trapping sites of e^- and h^+ (Wetchakun et al., 2008). Consequently, it served as a recombination center to increase the recombination possibility of electron-hole pairs. It also reduced the chances for electron-hole pairs to reach the catalyst surface and initiated the catalytic reaction. Eventually, it would shortened the lifetime of e^- and h^+ generated and subsequently lowered the degradation efficiency (Sui et al., 2018). In this case, 3 wt% of Fe was considered as the optimum doping concentration for TiO_2 particle.

4.2.2 Effect of Calcination Temperature

The 3% Fe-doped TiO_2 calcined at various temperatures were subjected to sonophotocatalytic degradation of paracetamol. As shown in Figure 4.8, the ascending order of the paracetamol degradation efficiency was: 3% Fe-doped TiO_2-200 < 3% Fe-doped TiO_2-800 < 3% Fe-doped TiO_2-400 < 3% Fe-doped TiO_2-600. It was found that the sonophotocatalytic degradation efficiency in the presence of Fe-doped TiO_2 gradually increased with increasing calcination temperature until it reached the optimum calcination temperature of 600 °C. Further increment of the calcination temperature to 800 °C resulted in detrimental effect on the degradation of paracetamol.

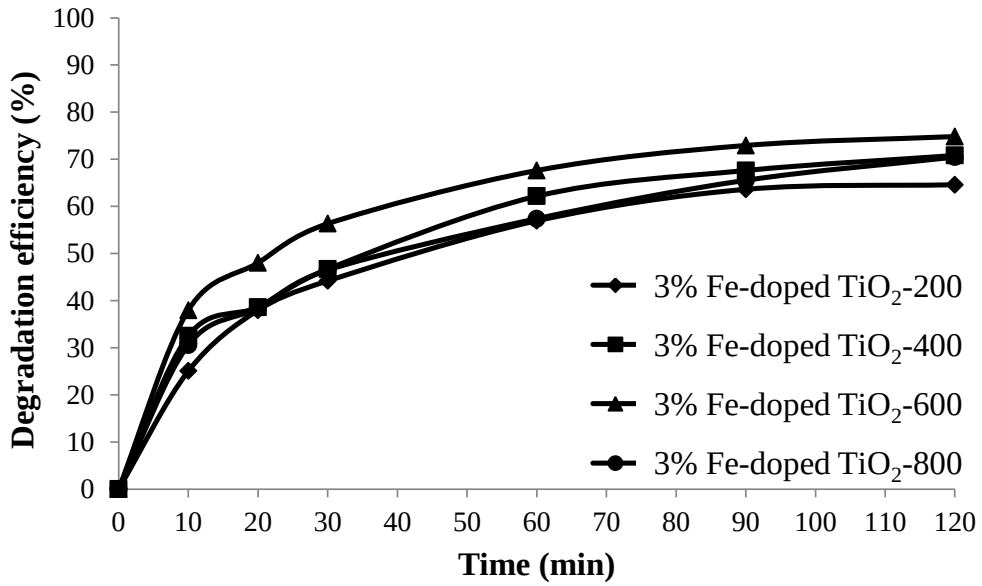

Figure 4.8: Degradation efficiency of paracetamol for various calcined Fe-doped TiO_2 (sonicator power = 296 W, sonicator frequency = 50 kHz, UV wavelength = 302 nm, initial concentration of paracetamol = 5 mg/L, catalyst dosage = 1.0 g/L, solution pH = pH 5, temperature = 30 °C)

It was interesting to highlight that 3% Fe-doped TiO_2-200 with the largest surface area (Table 4.3) did not facilitate the degradation of paracetamol efficiently. This was consistent with the study conducted by Zhu

et al. (2007) and Ye et al. (2012). They mentioned that surface area was not the main contributor to the degradation process, the enhanced crystallinity and appropriate phase composition could also affect its catalytic activity.

It was found that the 3% Fe-doped TiO_2-600 exhibited the highest degradation efficiency of 74.81 % within 2 hours owing to its rugged surface, high crystallinity and mixed phase structure. According to Figure 4.1 (g), 3% Fe-doped TiO_2-600 possessed a rugged surface, which could be beneficial to the mass transfer of paracetamol onto catalyst surface to enhance the degradation efficiency. The crystallinity of the catalyst could be enhanced by increasing the calcination temperature. The migration ability of electrons and holes were dependent on the structural properties of catalyst. The highly crystallined catalyst has a perfect structure and few defects, whereby it facilitates the migration of e^- and h^+ to a further distance within the perfect structure while the defects act as recombination centres for electron-hole pairs (Kusdianto et al., 2018). Therefore, a highly crystallined structure could provide a better separation efficiency of electron-hole pairs and consequently accelerates the catalytic activity.

Besides, the superior catalytic activity for mixed anatase-rutile phases could be explained by the formation of anatase and rutile phases heterojunction, which facilitated the separation of electron-hole pairs and charge transferred at the interface of both phases (Kordouli et al., 2015). As the conduction band of anatase was more negative than rutile, the generated electrons were more likely to transfer from anatase to rutile, while the holes were transferred from rutile and anatase (Li et al., 2015; Kusdianto et al., 2018). This hindered the recombination rate of the e^- and h^+ and thus extended

their lifetime and improved the catalytic activity. However, 3% Fe-doped TiO_2-800 which composed of mixed phase structure exhibited a lower catalytic performance than 3% Fe-doped TiO_2-600, possibly related to the high rutile content (87 %) which had lower catalytic activity than anatase (Kusdianto et al., 2018).

4.2.3 Effect of Energy Source

In order to investigate the effect of energy sources and the synergy effect provided by both ultrasonic and ultraviolet irradiation, three types of catalysis reaction (sono-, photo- and sonophotocatalytic degradation) were performed separately. The results are shown in Figure 4.9. The ascending order of the paracetamol degradation was: photocatalysis < sonocatalysis < sonophotocatalysis.

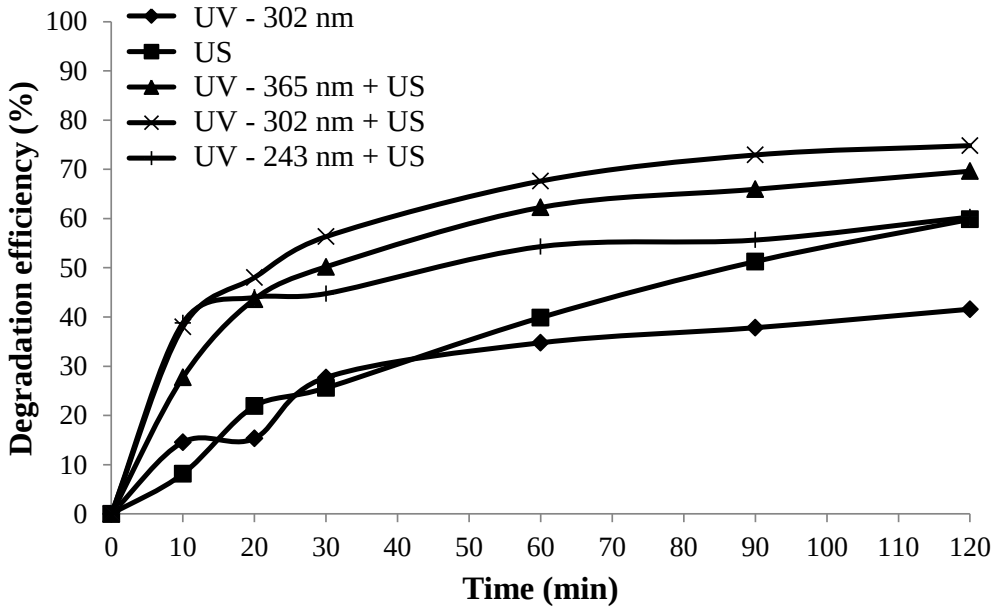

Figure 4.9: Effect of energy source to the degradation efficiency of paracetamol (sonicator power = 296 W, sonicator frequency = 50 kHz, initial concentration of paracetamol = 5 mg/L, catalyst dosage = 1.0 g/L of 3% Fe-doped TiO_2, solution pH = pH 5, temperature = 30 °C)

The sonocatalysis showed better degradation performance than photocatalysis which revealed that paracetamol was more likely to be degraded by ultrasound waves. Paracetamol exists in non-ionic form, in which the hydrophobic characteristic of paracetamol decomposes in the liquid-gas interface region where high concentration of •OH is available (Villaroel et al., 2014). On the other hand, photocatalysis of paracetamol degraded rapidly in first 30 minutes and slowed down thereafter. This implied that the blockage of paracetamol on the catalyst active sites led to the deactivation of catalyst and scattered the penetration of UV light in water medium.

The highest degradation was achieved by sonophotocatalysis (74.81 %) under UV light irradiation at 302 nm. The combined irradiation was able to provide a higher degradation efficiency due to their synergy effect to generate reactive radical species simultaneously. High concentration of radical species in the system could enhance the degradation efficiency of paracetamol. The unique properties of ultrasound include continuous cleaning of the catalyst surface, fragmentation of catalyst into smaller size particles with larger surface area and enhance the mass transfer of paracetamol to catalyst surface (Ziylan-Yavas and Ince, 2016). The incorporation of UV light could help to enhance the light absorption and excite the catalyst effectively. Subsequently, the separation of electron-hole pairs would occur and induce the formation of radical species which were responsible for the degradation of paracetamol.

Figure 4.9 also reveals the influence of UV wavelength on the sonophotocatalytic degradation of paracetamol in the presence of Fe-doped TiO_2 catalyst. Most of the researchers claimed that UV-C (254 nm) had better degradation performance than UV-A (365 nm) and UV-B (302 nm)

(Eskandarian et al., 2016; Cizmic et al., 2017). This was due to the light photons provided by shorter wavelength of UV-C exhibited higher excitation energy. As a consequence, it could activate the catalyst surface effectively and accelerate the degradation efficiency. In contrast, in this study, the highest degradation of 74.81 % was achieved in sonophotocatalysis using UV-B. This result was consistent with study conducted by Zhang et al. (2008), Chen et al. (2017) and Gupta et al. (2017). Zhang et al. (2008) revealed that the photocatalytic degradation of pyrene in the presence of TiO_2 achieved the highest degradation at UV irradiation of 310 nm, followed by 365 and 254 nm. They reported that the application of UV-C was not able to achieve the highest degradation performance consistently. Other parameter effects such as crystallinity of catalyst might also affected the catalytic performance. Therefore, in this study, sonophotocatalytic degradation under UV light irradiation at 302 nm was chosen for the subsequent parameter studies.

4.2.4 Effect of Initial Concentration of Paracetamol

Figure 4.10 illustrates the sonophotocatalytic degradation of paracetamol by varying the initial concentration of paracetamol from 5 to 25 mg/L. A decreasing trend in degradation performance could be observed with increasing initial concentration of paracetamol. The highest degradation of 74.81 % was achieved at the lowest initial paracetamol concentration of 5 mg/L. The degradation efficiency decreased to 41.30 % when the initial concentration was increased to 10 mg/L. When the initial concentration was

increased up to 25 mg/L, the degradation efficiency was found to further decrease to 13.09 %.

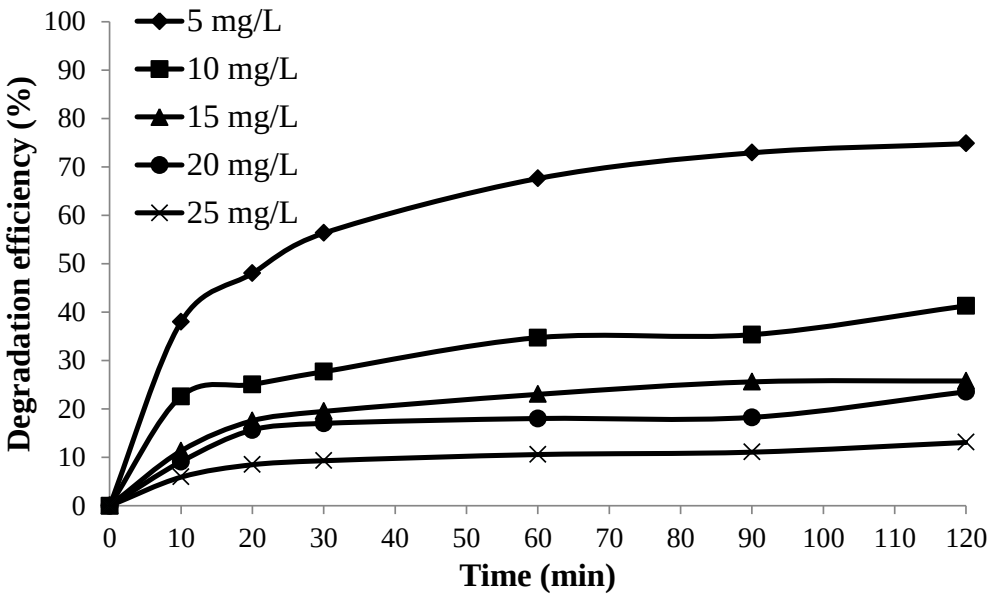

Figure 4.10: Effect of initial concentration on sonophotocatalytic degradation of paracetamol (sonicator power = 296 W, sonicator frequency = 50 kHz, UV wavelength = 302 nm, catalyst dosage = 1.0 g/L of 3% Fe-doped TiO_2-600, solution pH = pH 5, temperature = 30 °C)

High initial concentration of paracetamol indicated high competitions of paracetamol to be attached on Fe-doped TiO_2 active sites. It was found that the number of active sites of catalyst remained the same at a fixed catalyst dosage (Dukkanci, 2017). As the concentration of paracetamol was increased, there were more paracetamol molecules being adsorbed on the catalyst surface to occupy a larger number of active sites. The accumulation of paracetamol molecules could hinder the migration of water and dissolved gas molecules towards catalyst surface (Tabasideh et al., 2017). Subsequently, this situation could decrease the creation of radical species on catalyst surface and led to a decrement in degradation efficiency.

Besides, high concentration of paracetamol could inhibit the light transmission in water medium due to the increment of turbidity. Lesser

amount of photons was available to activate the Fe-doped TiO_2 catalyst surface and generate electron-hole pairs. This could reduce the number of radical species generated within the system and resulted in diminution in degradation efficiency (Lin et al., 2016). Therefore, in this study, the lowest paracetamol concentration of 5 mg/L was chosen as the optimum initial concentration for the subsequent parameter studies.

4.2.5 Effect of Catalyst Dosage

The effect of 3% Fe-doped TiO_2-600 catalyst dosage in sonophotocatalytic degradation of paracetamol was investigated and the results are presented in Figure 4.11. It was found that the degradation of paracetamol increased significantly in the absence of catalyst up to 1.0 g/L of catalyst dosage. The degradation efficiency was increased from 38 % to 75 %. However, further increment of the catalyst dosage to 1.5 and 2.0 g/L resulted in decrement in degradation efficiency to 71 % and 53 %, respectively.

The degradation efficiency of paracetamol increased with increasing catalyst dosage up to 1.0 g/L. The increment in degradation efficiency was probably due to the increased number of active sites and nucleation sites which led to more effective interaction between target pollutants and radical species on catalyst surface (Dukkanci, 2017).

Further increasing the catalyst dosage beyond the optimum amount would result in negative impact to paracetamol degradation. This was probably due to the agglomeration of catalyst and increment in solution turbidity (Lazar et al., 2012). With the aids of ultrasound, it could constantly

deagglomerated the catalyst and therefore increased the exposure of catalyst surface to ultrasound and UV light. However, the increment in solution turbidity could not be resolved effectively and resulted in light scattering in which the penetration of light through the paracetamol-containing solution was reduced. Therefore, catalyst dosage of 1.0 g/L was chosen as the optimum for the subsequent studies.

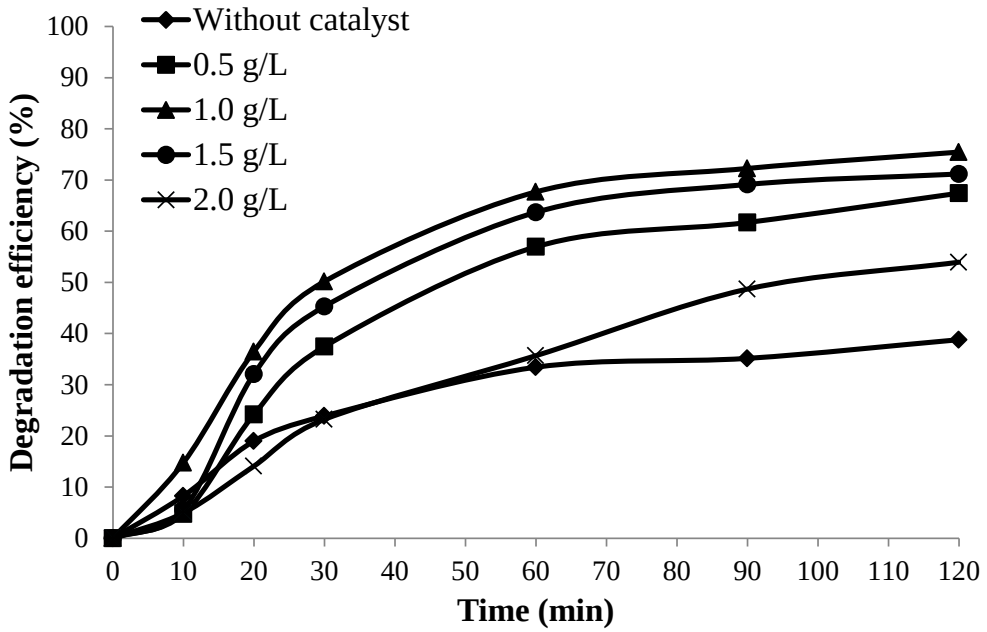

Figure 4.11: Effect of catalyst dosage on sonophotocatalytic degradation of paracetamol (sonicator power = 296 W, sonicator frequency = 50 kHz, UV wavelength = 302 nm, initial concentration of paracetamol = 5 mg/L, solution pH = pH 5, temperature = 30 °C)

4.2.6 Effect of Solution pH

It has been reported that the solution pH is a crucial parameter during sonophotocatalytic degradation, in which the solution pH can affect the surface charge of catalyst, ionisation state of paracetamol and concentration of •OH (Jallouli et al., 2017). Thus, the effect of solution pH on sonophotocatalytic degradation of paracetamol with the presence of 3% Fe-

doped TiO_2-600 catalyst was investigated and illustrates in Figure 4.12. It was found that acidic aqueous medium favoured the paracetamol degradation than that in neutral and alkaline medium. For example, approximately 75 % of paracetamol was successfully degraded in 2 hours at solution pH 5.

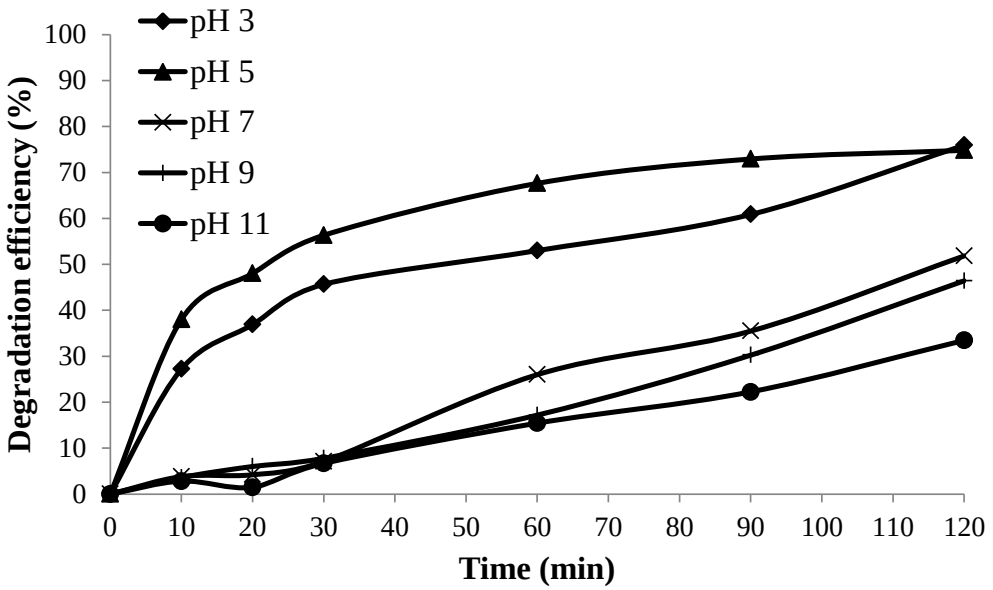

Figure 4.12: Effect of solution pH on sonophotocatalytic degradation of paracetamol (sonicator power = 296 W, sonicator frequency = 50 kHz, UV wavelength = 302 nm, initial concentration of paracetamol = 5 mg/L, catalyst dosage = 1.0 g/L of 3% Fe-doped TiO_2-600, temperature = 30 °C)

Paracetamol is a polar compound due to the variation of electronegativity between atoms and it has no lines of symmetry. It could not enter into the cavitation bubble and therefore, the degradation was most probably occurred through •OH attacks at the bubble interface or bulk solution (Villaroel et al., 2014). In acidic medium, when the pH is less than acid dissociation constant (pK_a) = 9.5, paracetamol exists as non-ionic form. Under this condition, its hydrophobicity is favoured and will accumulate at the interface of cavitation bubble, where there are high concentration of •OH available to degrade the paracetamol. Besides, acidic condition also favors the electrostatic interaction of paracetamol on the positively charged Fe-doped

TiO_2 surface (zero point charge of TiO_2, pH_{zpc} = 6.3). This can enhance the degradation reaction between generated radical species and adsorbed paracetamol on catalyst surface. Zhang et al. (2017a) and Tabasideh et al. (2017) also suggested that acidic medium could perform better degradation of paracetamol and diazinon, respectively.

The lowest degradation efficiency of paracetamol (33 %) was achieved at pH 11. As the solution pH increased, the hydrophobicity of paracetamol decreased as its hydroxyl group was ionised. The degradation reaction took place at the bulk solution where the •OH concentration was much lower than at interface and therefore contributed to a lower degradation efficiency. At pH 11, both paracetamol and catalyst surface were negatively charged due to surface ionisation. Under these circumstances, paracetamol molecules were not adsorbed effectively onto the catalyst surface due to the electrostatic repulsion, resulting in a lower degradation efficiency (Jallouli et al., 2017). Besides, a significant recombination of •OH occurred at solution pH 11 as shown in Equations (4.5) and (4.6) (Tan et al., 2014; Villaroel et al., 2014). This led to a reduction of •OH concentration in the reaction system. However, several researchers had reported that higher photocatalytic degradation of paracetamol was achieved under alkaline medium (Lin et al., 2016). Lin et al. (2016) found that there were more hydroxide groups (-OH) available on catalyst surface to facilitate the formation of •OH at high solution pH (e.g., pH 9), in which consequently enhanced the degradation efficiency of paracetamol. Hence, in this study, the solution pH 5 was chosen as the optimum solution pH for the subsequent parameter studies.

$$\bullet OH + OOH^- \rightarrow H_2O + O_2^- \quad (4.5)$$

$$\bullet OH + OOH^- \rightarrow \bullet OOH + OH^- \quad (4.6)$$

4.2.7 Effect of H_2O_2 Amount

The addition of H_2O_2 is one of the methods to increase the concentration of •OH in the reaction system. The reactions with H_2O_2 were not only limited to paracetamol but also within themselves and other intermediate compounds available in the system due to their non-selectivity and competing reactions might take place. Figure 4.13 shows the sonophotocatalytic degradation of paracetamol under different amount of H_2O_2 (0.1 – 10 mM). It could be clearly observe that the addition of H_2O_2 especially 0.5 mM could enhance the paracetamol degradation significantly. However, further increasing the amount of H_2O_2 did not bring significant improvement to the degradation.

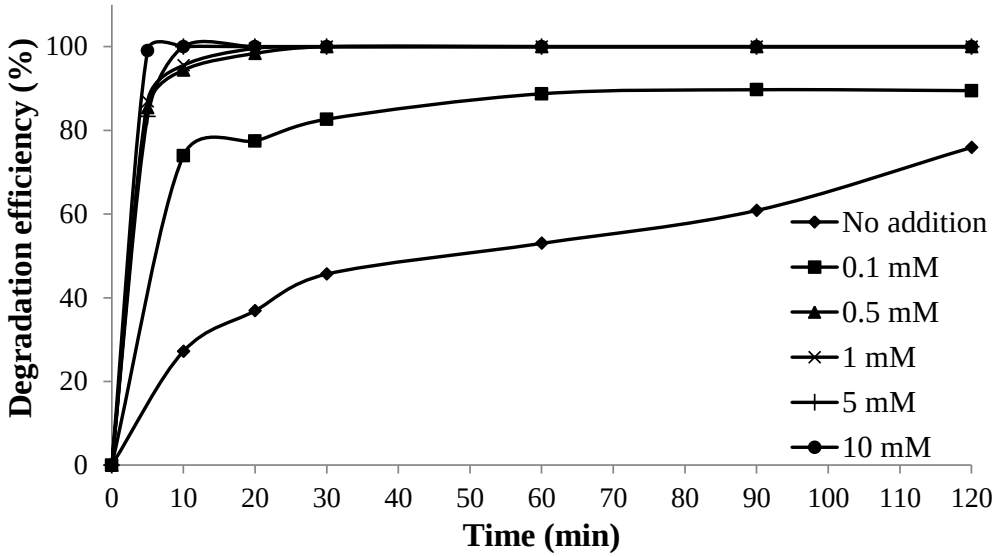

Figure 4.13: Effect of H_2O_2 amount on sonophotocatalytic degradation of paracetamol (sonicator power = 296 W, sonicator frequency = 50 kHz, UV wavelength = 302 nm, initial concentration of paracetamol = 5 mg/L, catalyst dosage = 1.0 g/L of 3% Fe-doped TiO_2-600, solution pH = pH 5, temperature = 30 °C)

The addition of H_2O_2 was expected to improve the degradation as it could decompose to form •OH and thus increased the concentration of •OH

within the reaction system (Duran et al., 2013; Tan et al., 2014). As mentioned by Tan et al. (2014), the amount of H_2O_2 added to the reaction system played an important role in degradation reaction. They recorded that the degradation efficiency increased with increasing the amount of H_2O_2 up to 30 mM. Beyond 30 mM, the degradation efficiency was found to decrease due to the scavenging effect of H_2O_2 oxidant. This was supported by Xiong and Hu (2017) which mentioned that excessive amount of H_2O_2 would act as a radical scavenger, competing with the paracetamol for the active sites on the catalyst surface and therefore brought scavenging effect to the overall degradation efficiency. However, in this study, the scavenging effect of H_2O_2 was not being observed, which suggested that it was yet to achieve the maximum concentration of H_2O_2 amount.

4.3 Reusability Study

The evaluation on catalyst reusability is important to consider for its practical usage in commercialize wastewater treatment in terms of economic feasibility and environmental safety. In order to assess the reusability of 3% Fe-doped TiO_2-600 catalyst, four experiment cycles were performed under similar reaction conditions for 20 minutes. Figure 4.14 presents the comparison of degradation efficiency achieved by fresh and spent 3% Fe-doped TiO_2-600 for four consecutive cycles. The degradation efficiencies for fresh 3% Fe-doped TiO_2-600 were reduced from 98 % to 97 %, 96 %, 92 % and 83 % after four catalytic cycles. These results implied that 3% Fe-doped TiO_2-600 had excellent catalytic activity during sonophotocatalytic degradation of

paracetamol due to the insignificant reduction of catalytic activity in each catalytic cycle. The spent 3% Fe-doped TiO_2-600 experienced slight reduction of catalytic activity might cause by catalyst loss during the catalyst recovery.

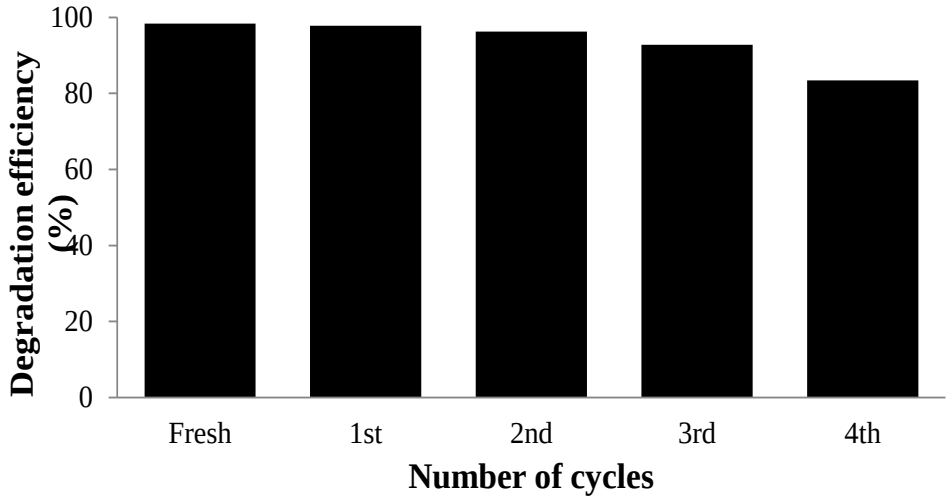

Figure 4.14: Degradation efficiency of fresh and spent 3% Fe-doped TiO_2-600 catalyst in sonophotocatalytic degradation of paracetamol (sonicator power = 296 W, sonicator frequency = 50 kHz, UV wavelength = 302 nm, initial concentration of paracetamol = 5 mg/L, catalyst dosage = 1.0 g/L of 3% Fe-doped TiO_2-600, solution pH = pH 5, H_2O_2 amount = 0.5 mM, temperature = 30 °C)

4.4 Kinetic Study

In order to determine the reaction order for sonophotocatalytic degradation, kinetic studies were carried out based on the rate of disappereance of paracetamol. Pseudo zero-, first- and second-order reaction kinetic graphs were studied by comparing the sono-, photo- and sonophotocatalytic degradation of paracetamol (Appendix H).

Figure 4.15 shows that the sono-, photo- and sonophotocatalytic degradation of paracetamol were satisfactory fitted to the pseudo first-order reaction kinetics with high regression constant (R^2 > 0.90). The pseudo first-order rate constant (k_1) was determined by the slope of the straight lines. Table

4.4 shows that the sonophotocatalytic degradation of paracetamol achieved the highest k_1 of 0.0142 min^{-1}. The synergy index was employed to evaluate the feasibility of combined oxidation processes for the intensification of paracetamol degradation. The calculated synergy index was 1.09, which was larger than 1 and this indicated a positive synergistic effect of the combined processes to the degradation of paracetamol (Wu et al., 2016; Mosleh and Rahimi, 2017; Sunasee et al., 2017).

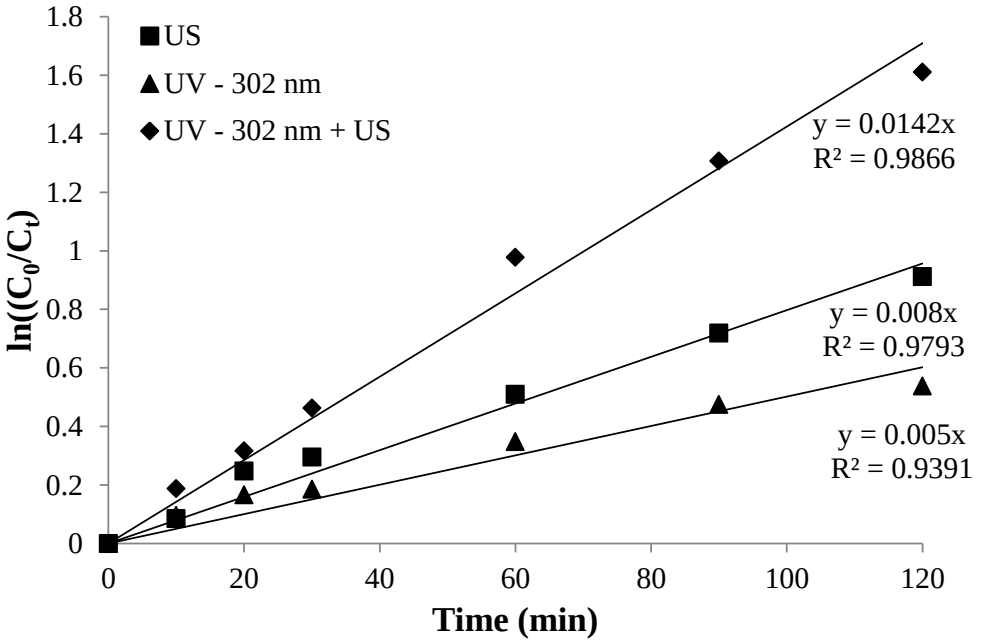

Figure 4.15: Pseudo first-order reaction kinetics graph for sono-, photo- and sonophoto-degradation of paracetamol (sonicator power = 296 W, sonicator frequency = 50 kHz, UV wavelength = 302 nm, initial concentration of paracetamol = 5 mg/L, catalyst dosage = 1.0 g/L of 3% Fe-doped TiO_2-600, solution pH = pH 5, temperature = 30 °C)

Table 4.4: Apparent rate constant and regression constants for sono-, photo- and sonophoto-degradation of paracetamol

Applications	Pseudo first-order rate constant, k_1 (min^{-1})	Regression constant, R^2
US	0.008	0.9793
UV – 302 nm	0.005	0.9391
UV – 302 nm + US	0.0142	0.9866

4.5 COD Analysis

The COD test was conducted to determine the remaining amount of organic compounds in the sample solution. The COD removal by the sonophotocatalytic degradation of paracetamol under optimised conditions (296 W and 50 kHz of sonicator, 8 W UV light with wavelength of 302 nm, 1.0 g/L of 3 wt% Fe-doped TiO_2-600 catalyst, 5 mg/L of paracetamol, solution pH of 5 and 0.5 mM of H_2O_2) was investigated and the result is presented in Figure 4.16.

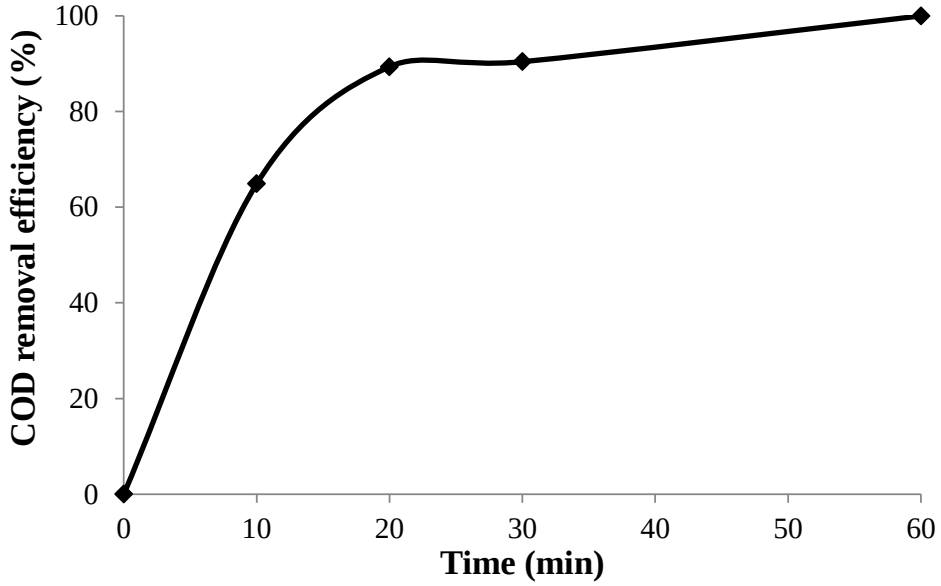

Figure 4.16: COD removal efficiency by sonophotocatalytic degradation of paracetamol under optimized conditions (sonicator power = 296 W, sonicator frequency = 50 kHz, UV wavelength = 302 nm, initial concentration of paracetamol = 5 mg/L, catalyst dosage = 1.0 g/L 3% Fe-doped TiO_2-600, solution pH = pH 5, H_2O_2 amount = 0.5 mM, temperature = 30 °C)

The initial COD reading of the solution before sonophotocatalytic degradation was 94 mg/L. It experienced a rapid COD reduction in the first 20 minutes. It was found that the COD removal efficiencies were 89 % and 100 % after 20 minutes and 60 minutes. This suggested that longer application period was required to achieve a complete oxidation of paracetamol. This also

suggested that 3 wt% Fe-doped TiO_2-600 could potentially act as a catalyst in sonophotocatalytic degradation of paracetamol to degrade the paracetamol in water and wastewater.

CHAPTER 5

CONCLUSIONS AND RECOMMENDATIONS

5.1 Conclusions

TiO_2 and a series of Fe-doped TiO_2 particles at different Fe dopant concentrations (1, 3, 5 and 10 wt%) and calcination temperatures (200, 400, 600 and 800 °C) were successfully synthesised through sol-gel method. The prepared particles were subjected to various types of characterisations. FESEM and XRD results revealed that the particles tend to be agglomerated and the crystallinity decreased when increasing the Fe dopant concentration. EDX results confirmed that the presence of Fe element was in accordance with the doping concentrations of 1, 3, 5 and 10 wt%. Surface area, pore size and pore volume were reduced when the Fe dopant concentration was increased. XPS analysis confirmed that Fe existed as Fe^{3+} ion which indicating the successful incorporation of Fe^{3+} into crystal lattice of TiO_2. Meanwhile, FESEM results showed that the particle sizes of Fe-doped TiO_2 increased when increasing the calcination temperature. XRD results revealed that phase transformation from anatase to rutile phase occurred at 600 °C. Beside, a reduction in BET surface area was observed due to the sintering effect.

In order to identify the optimum experimental conditions for sonophotocatalytic degradation of paracetamol, a series of batch experiments were carried out by varying the Fe dopant concentrations on TiO_2 (1, 3, 5 and

10 wt% Fe), calcination temperatures (200, 400, 600 and 800 °C of Fe-doped TiO_2), energy sources (ultrasonic irradiation, ultraviolet irradiation and combined irradiations), initial concentrations of paracetamol (5, 10, 15, 20 and 25 mg/L), catalyst dosages (0.5, 1.0, 1.5, 2.0 g/L), solution pH (pH 3, 5, 7, 9 and 11) and H_2O_2 amounts (0.1, 0.5, 1, 5 and 10 mM). Sonophotocatalytic degradation of paracetamol achieved 100 % after 30 minutes when utilizing 296 W and 50 kHz of sonicator, UV wavelength of 302 nm, 5 mg/L paracetamol, 1 g/L 3% Fe-doped TiO_2-600, solution pH 5 and 0.5 mM H_2O_2. Besides, it was found that 100 % COD reduction was achieved after 1 hour of sonophotocatalytic degradation of paracetamol under optimised conditions.

The reusability of 3% Fe-doped TiO_2-600 was conducted for four catalytic cycles. It was found that the spent 3% Fe-doped TiO_2-600 exhibited a slight decrease in catalytic activity (83 %) as compared to fresh 3% Fe-doped TiO_2-600 (98 %) after four cycles. This suggested that 3% Fe-doped TiO_2-600 exhibited good reusability and stability for sonophotocatalytic degradation of paracetamol. The kinetic study showed that the sonophotocatalytic degradation of paracetamol can be interpreted well with pseudo first-order reaction kinetic model with high R^2 values. It had achieved the highest k_1 of 0.0142 min^{-1}. The synergy index for sonophotocatalytic degradation of paracetamol was 1.09, indicated a positive synergistic effect of the combined processes. Therefore, this proved that sonophotocatalytic degradation process in the presence of Fe-doped TiO_2 is a potential solution on pharmaceutical compounds.

5.2 Recommendations

In this research study, synthetic wastewater was used. It is suggested to utilize real wastewater such as wastewater collected from pharmaceutical factory. This is because the real wastewater matrix is more complex due to the presence of organic and inorganic matters. Several studies had shown that the presence of humic acid, sulphate and nitrate in wastewater could significantly affect the degradation rate (Chu et al., 2017, Kumar and Pandey, 2017). Thus, more detailed studies are needed to understand their synergistic and antagonistic effect on the degradation process. This will be important to develop a reliable protocol on sonophotocatalytic degradation.

Besides, lab scale and batch mode experiments were carried out for sonophotocatalytic degradation of paracetamol. However, this might not be applicable for industrial setting. Thus, in order to industrialize the application of sonophotocatalytic degradation, comprehensive studies on scale up process and continuous operation mode are required.

Lastly, it is suggested to identify the potential intermediate products formed during the sonophotocatalytic degradation of paracetamol using liquid chromatography coupled with a mass spectrometry detector (LC-MS). It is expected that the identification of intermediate products can be performed by comparing the generated mass spectrum of detected intermediates with the mass spectra of standard chemical which could be obtained commercially (Hisaindee et al., 2013). This would be important to understand the oxidation process on cleavage of paracetamol molecules prior to the mineralisation.

REFERENCES

Abedi, N., Nabi, A., Mangoli, E. and Talebi, A. R., 2017. Short and long term effects of different doses of paracetamol on sperm parameters and DNA integrity in mice. *Middle East Fertility Society Journal,* 22**,** 323-328.

Acero, J. L., Benitez, F. J., Real, F. J. and Garcia, C., 2009. Removal of phenyl-urea herbicides in natural waters by UF membranes: Permeate flux, analysis of resistances and rejection coefficients. *Separation and Purification Technology,* 65**,** 322-330.

Adewu-Yi, Y. G., 2005. Sonochemistry in environmental remediation. 2. Heterogeneous sonophotocatalytic oxidation processes for the treatment of pollutants in water. *Environmental Science and Technology,* 39**,** 8557-8570.

Adityosulindro, S., Barthe, L., Gonzalez-Labrada, K., Haza, U. J. J., Delmas, H. and Julcour, C., 2017. Sonolysis and sono-Fenton oxidation for removal of ibuprofen in (waste)water. *Ultrasonics Sonochemistry,* 39**,** 889-896.

Ahmed, M. B., Zhou, J. L., Ngo, H. H., Guo, W., Thomaidis, N. S. and Xu, J., 2017. Progress in the biological and chemical treatment technologies for emerging contaminant removal from wastewater: A critical review. *Journal of Hazardous Materials,* 323**,** 274-298.

Altmann, J., Ruhl, A. S., Zietaschmann, F. and Jekel, M., 2014. Direct comparison of ozonation and adsorption onto powdered activated carbon for micropollutant removal in advanced wastewater treatment. *Water Research,* 55**,** 185-193.

Arora, P. K., Srivastava, A. and Singh, V. P., 2014. Novel degradation pathway of 4-chloro-2-aminophenol via 4-chlorocatechol in Burkholderia sp. RKJ 800. *Environmental Science and Pollution Research,* 21**,** 2298-2304.

Babic, B., Zarubica, A., Arsic, T. M., Pantic, J., Jokic, B., Abazovic, N. and Matovic, B., 2016. Iron doped anatase for application in photocatalysis. *Journal of the European Ceramic Society,* 36, 2991-2996.

Baccar, R., Sarra, M., Bouzid, J., Feki, M. and Blanquez, P., 2012. Removal of pharmaceutical compounds by activated carbon prepared from agricultural by-product. *Chemical Engineering Journal,* 211**,** 310-317.

Barik, A. J. and Gogate, P. R., 2016. Degradation of 4-chloro 2-aminophenol using combined strategies based on ultrasound, photolysis and ozone. *Ultrasonics Sonochemistry,* 28**,** 90-99.

Beier, S., Koster, S., Veltmann, K., Schroder, H. F. and Pinnekamp, J., 2010. Treatment of hospital wastewater effluent by nanofiltration and reverse osmosis. *Water Science and Technology,* 61**,** 1691-1698.

Bhatia, V. and Dhir, A., 2016. Transition metal doped TiO_2 mediated photocatalytic degradation of anti-inflammatory drug under solar irradiations. *Journal of Environmental Chemical Engineering,* 4**,** 1267-1273.

Bilgin Simsek, E., 2017. Solvothermal synthesized boron doped TiO_2 catalysts: Photocatalytic degradation of endocrine disrupting compounds and pharmaceuticals under visible light irradiation. *Applied Catalysis B: Environmental,* 200**,** 309-322.

Birben, N. C., Uyguner-Demirel, C. S., Kavurmaci, S. S., Gurkan, Y. Y., Turkten, N., Cinar, Z. and Bekbolet, M., 2017. Application of Fe-doped TiO_2 specimens for the solar photocatalytic degradation of humic acid. *Catalysis Today,* 281**,** 78-84.

Boix, C., Ibanez, M., Sancho, J. V., Parsons, J. R., Voogt, P. and Hernandez, F., 2016. Biotransformation of pharmaceuticals in surface water and during waste water treatment: Identification and occurrence of transformation products. *Journal of Hazardous Materials,* 302**,** 175-187.

Burrows, H. D., Caniel, M., Santaballa, J. A. and Steenken, S., 2002. Reaction pathways and mechanisms of photodegradation of pesticides. *Journal of Photochemistry and Photobiology B: Biology,* 67**,** 71-108.

Cai, J., Xin, W., Liu, G., Lin, D. and Zhu, D., 2016. Effect of calcination temperature on structural properties and photocatalytic activity of Mn-C-codoped TiO_2. *Materials Research,* 19**,** 401-407.

Chen, W.-L., Cheng, J.-Y. and Lin, X.-Q., 2018. Systematic screening and identification of the chlorinated transformation products of aromatic pharmaceuticals and personal care products using high-resolution mass spectrometry. *Science of The Total Environment,* 637**,** 253-263.

Chen, X., Nielsen, J. L., Furgal, K., Liu, Y. Lolas, I. B. and Bester, K., 2011. Biodegradation of triclosan and formation of methyl-triclosan in activated sludge under aerobic conditions. *Chemosphere,* 84**,** 452-456.

Chen, Y., Zhang, X., Mao, L. and Yang, Z., 2017. Dependence of kinetics and pathway of acetaminophen photocatalytic degradation on irradiation photon energy and TiO_2 crystalline. *Chemical Engineering Journal,* 330, 1091-1099.

Chong, M. N., Jin, B., Chow, C. W. K. and Saint, C., 2010. Recent developments in photocatalytic water treatment technology: A review. *Water Research,* 44**,** 2997-3027.

Chu, K. H., Al-Hamadani, Y. A. J., Park, C. M., Lee, G. Jang, M. Jang, A., Her, N., Son, A. and Yoon, Y., 2017. Ultrasonic treatment of endocrine disrupting compounds, pharmaceuticals, and personal care products in water: A review. *Chemical Engineering Journal,* 327**,** 629-647.

Cizmic, M., Ljubas, D., Curkovic, L., Skoric, I. and Babic, S., 2017. Kinetics and degradation pathways of photolytic and photocatalytic oxidation of the anthelmintic drug praziquantel. *Journal of Hazardous Materials,* 323**,** 500-512.

Cruz-Morato, C., Lucas, D., Llorca, M., Rodriguez-Mozaz, S., Gorga, M., Petrovic, M., Barcelo, D., Vicent, T., Sarra, M. and Marco-Urrea, E., 2014. Hospital wastewater treatment by fungal bioreactor: Removal efficiency for pharmaceuticals and endocrine disruptor compounds. *Science of the Total Environment,* 493**,** 365-376.

Dai, C.-M., Zhou, X.-F., Zhang, Y.-L., Duan, Y.-P., Xiang, Z.-M. and Zhang, T. C., 2012. Comparative study of the degradation of carbamazepine in water by advanced oxidation processes. *Environmental technology,* 33**,** 1101-1109.

Deng, S. Chen, Y., Wang, D., Shi, T., Wu, X., Ma, X., Li, X., Hua, R., Tang, X. and Li, Q. X., 2015. Rapid biodegradation of organophosphorus pesticides by Stenotrophomonas sp: G1. *Journal of Hazardous Materials,* 297**,** 17-24.

Dukkanci, M., 2017. A Parametric Study on the Heterogeneous Photo-Fenton-Like Oxidation of Bisphenol-A over an Fe/TiO_2 Catalyst under Visible Light. *Politeknik Dergisi,* 20, 25-36.

Duran, A., Monteagudo, J. M., Sanmartin, I. and Garcia-Diaz, A., 2013. Sonophotocatalytic mineralization of antipyrine in aqueous solution. *Applied Catalysis B: Environmental,* 138-139**,** 318-325.

Duran-Alvarez, J. C., Avella, E., Ramirez-Zamora, R. M. and Zanella, R., 2016. Photocatalytic degradation of ciprofloxacin using mono- and bi-metallic nanoparticles supported on TiO_2 under UV-C and simulated sunlight. *Catalysis Today,* 266**,** 175-187.

Ebele, A. J., Abou-Elwafa Abdallah, M. and Harrad, S., 2017. Pharmaceuticals and personal care products (PPCPs) in the freshwater aquatic environment. *Emerging Contaminants,* 3**,** 1-16.

El-Shafey, E.-S. I., Al-Lawati, H. and Al-Sumri, A. S., 2012. Ciprofloxacin adsorption from aqueous solution onto chemically prepared carbon from date palm leaflets. *Journal of Environmental Sciences,* 24**,** 1579-1586.

El-Shahawi, M. S., Hamza, A., Bashammakh, A. S. and Al-Saggaf, W. T., 2010. An overview on the accumulation, distribution, transformations, toxicity and analytical methods for the monitoring of persistent organic pollutants. *Talanta,* 80**,** 1587-1597.

Eren, Z., 2012. Ultrasound as a basic and auxiliary process for dye remediation: A review. *Journal of Environmental Management,* 104**,** 127-141.

Eskandarian, M. R., Choi, H., Fazli, M. and Rasoulifard, M. H., 2016. Effect of UV-LED wavelengths on direct photolytic and TiO_2 photocatalytic degradation of emerging contaminants in water. *Chemical Engineering Journal,* 300**,** 414-422.

Fan, G., Wang, B., Liu, C. and Li, D., 2017. Prenatal paracetamol use and asthma in childhood: A systematic review and meta-analysis. *Allergologia et immunopathologia,* 45**,** 528-533.

Fujishima, A. and Rao, T. N., 1997. Recent advances in heterogeneous TiO_2 photocatalysis. *Proceedings of the Indian Academy of Sciences: Chemical Sciences,* 109**,** 471-486.

Gaber, A., Abdel--Rahim, M. A., Abdel-Latief, A. Y. and Abdel--Salam, M. N., 2014. Influence of calcination temperature on the structure and porosity of nanocrystalline SnO_2 synthesized by a conventional precipitation method. *International Journal of Electrochemical Science,* 9, 81-95.

Ganesh, I., Kumar, P. P., Gupta, A. K., Sekhar, P. S. C., Radha, K., Padmanabham, G. and Sundararajan, G., 2012. Preparation and characterization of Fe-doped TiO_2 powders for solar light response and photocatalytic applications. *Processing and application of ceramics,* 6**,** 21-36.

Gareso, P. L., Sampe, N., Palentek, V. and Taba, P., 2017. Influence of annealing on Fe-doped TiO_2 powders using co-precipitation technique. *AIP Publishing,* 1801, 1-5.

Geissen, V., Mol, H., Klumpp, E., Umlauf, G., Nadal, M., van der Ploeg, M., van dee Zee, S. E. A. T. M. and Ritsema, C. J., 2015. Emerging pollutants in the environment: A challenge for water resource management. *International Soil and Water Conservation Research,* 3**,** 57-65.

Golash, N. and Gogate, P. R., 2012. Degradation of dichlorvos containing wastewaters using sonochemical reactors. *Ultrasonics Sonochemistry,* 19**,** 1051-1060.

Gole, V. L. and Alhat, A., 2017. Treatment of malachite green dye using combined oxidation techniques based on different irradiation. *Korean Journal of Chemical Engineering,* 34**,** 1393-1399.

Gole, V. L., Priya, A. and Danao, S. P., 2017. Decolorization of brilliant green dye using immersed lamp sonophotocatalytic reactor. *Applied Water Science,* 7**,** 4237-4245.

Gupta, V. K., Saravanan, R., Agarwal, S., Gracia, F., Khan, M. M., Qin, J. and Mangalaraja, R. V., 2017. Degradation of azo dyes under different wavelengths of UV light with chitosan-SnO_2 nanocomposites. *Journal of Molecular Liquids,* 232, 423-430.

Gupte, G. L., 2016. Management of paracetamol overdose. *Paediatrics and Child Health,* 26**,** 459-463.

Hassani, A., Khataee, A. and Karaca, S., 2015. Photocatalytic degradation of ciprofloxacin by synthesized TiO_2 nanoparticles on montmorillonite: Effect of operation parameters and artificial neural network modeling. *Journal of Molecular Catalysis A: Chemical,* 409**,** 149-161.

Hassani, A., Khataee, A., Karaca, S., Karaca, C. and Gholami, P., 2016. Sonocatalytic degradation of ciprofloxacin using synthesized TiO_2 nanoparticles on montmorillonite. *Ultrasonics Sonochemistry,* 35**,** 251-262.

Heo, J., Flora, J. R. V., Her, N., Park, Y.-G., Cho, J., Son, A. and Yoon, Y., 2012. Removal of bisphenol A and 17β-estradiol in single walled carbon nanotubes–ultrafiltration (SWNTs–UF) membrane systems. *Separation and Purification Technology,* 90**,** 39-52.

Hisaindee, S., Meetani, M. and Rauf, M., 2013. Application of LC-MS to the analysis of advanced oxidation process (AOP) degradation of dye products and reaction mechanisms. *TrAC Trends in Analytical Chemistry*, 49, 31-44.

Huang, S., Chen, C., Tsai, H., Shaya, J. and Lu, C., 2018. Photocatalytic degradation of thiobencarb by a visible light-driven MoS_2 photocatalyst. *Separation and Purification Technology,* 197**,** 147-155.

Hughes, S. R., Kay, P. and Brown, L. E. 2013. Global Synthesis and Critical Evaluation of Pharmaceutical Data Sets Collected from River Systems. *Environmental Science and Technology*, 47**,** 661-677.

Ibrahim, S. A. and Sreekantan, S. 2014. Fe-TiO_2 nanoparticles by hydrothermal treatment with photocatalytic activity enhancement. *Advanced Materials Research*,1024, 39-43.

Jallouli, N., Elghhiji, K., Trabelsi, H. and Ksibi, M., 2017. Photocatalytic degradation of paracetamol on TiO_2 nanoparticles and TiO_2/cellulosic fiber under UV and sunlight irradiation. *Arabian Journal of Chemistry,* 10, 3640-3645.

Jelic, A., Michael, I., Archilleos, A., Hapeshi, E., Lambropoulou, D., Perez, S., Petrovic, M., Fatta-Kassinos, D. and Barcelo, D., 2013. Transformation products and reaction pathways of carbamazepine during photocatalytic and sonophotocatalytic treatment. *Journal of Hazardous Materials,* 263**,** 177-186.

Johnson, K. M., Anil Kumar, M. R., Ponmurugan, P. and Mythili Gananamangai, B., 2010. Ultraviolet radiation and its germicidal effect in drinking water purification. *Journal of Phytology*, 2, 15-19.

Joseph, C. G., Li Puma, G., Bono, A. and Krishnaiah, D., 2009. Sonophotocatalysis in advanced oxidation process: A short review. *Ultrasonics Sonochemistry,* 16**,** 583-589.

Kapelewska, J., Kotowska, U., Karpinska, J., Kowalczuk, D., Arciszewska, A. and Swirydo, A., 2018. Occurrence, removal, mass loading and environmental risk assessment of emerging organic contaminants in leachates, groundwaters and wastewaters. *Microchemical Journal,* 137**,** 292-301.

Karaca, M., Kiransan, M., Karaca, S., Khataee, A. and Karimi, A., 2016. Sonocatalytic removal of naproxen by synthesized zinc oxide nanoparticles on montmorillonite. *Ultrasonics Sonochemistry,* 31**,** 250-256.

Khaled, S. A., Alexander, M. R., Wildman, R. D., Wallace, M. J., Sharpe, S., Yoo, J. and Roberts, C. J., 2018. 3D extrusion printing of high drug loading immediate release paracetamol tablets. *International Journal of Pharmaceutics,* 538**,** 223-230.

Khokhawala, I. M. and Gogate, P. R., 2010. Degradation of phenol using a combination of ultrasonic and UV irradiations at pilot scale operation. *Ultrasonics Sonochemistry,* 17**,** 833-838.

Kordouli, E., Dracopoulos, V., Vaimakis, T., Bourikas, K., Lycourghiotis, A. and Kordulis, C., 2015. Comparative study of phase transition and textural changes upon calcination of two commercial titania samples: A pure anatase and a mixed anatase-rutile. *Journal of Solid State Chemistry,* 232, 42-49.

Kumar, A. and Pandey, G., 2017. A review on the factors affecting the photocatalytic degradation of hazardous materials. *Material Science and Engineering International Journal,* 1**,** 1-10.

Kusdianto, K., Jiang, D., Kubo, M. and Shimada, M., 2018. Effect of annealing temperature on the photocatalytic activity of Ag–TiO_2 nanocomposite films by one-step gas-phase deposition. *Materials Research Bulletin,* 97, 497-505.

Lazar, M. A., Varghese, S. and Nair, S. S., 2012. Photocatalytic water treatment by titanium dioxide: recent updates. *Catalysts,* 2, 572-601.

Leong, S., Razmjou, A., Wang, K., Hapgood, K., Zhang, X. and Wang, H., 2014. TiO_2 based photocatalytic membranes: A review. *Journal of Membrane Science,* 472**,** 167-184.

Lester, Y., Sharpless, C. M., Mamane, H. and Linden, K. G., 2013. Production of photo-oxidants by dissolved organic matter during UV water treatment. *Environmental Science and Technology,* 47**,** 11726-11733.

Li, H., Shen, X., Liu, Y., Wang, L., Lei, J. and Zhang, J., 2015. Facile phase control for hydrothermal synthesis of anatase-rutile TiO_2 with enhanced photocatalytic activity. *Journal of Alloys and Compounds,* 646, 380-386.

Lim, M., Son, Y. and Khim, J., 2014. The effects of hydrogen peroxide on the sonochemical degradation of phenol and bisphenol A. *Ultrasonics Sonochemistry,* 21**,** 1976-1981.

Lin, J. C. T., De Luna, M. D. G., Aranzamendez, G. L. and Lu, M. C., 2016. Degradations of acetaminophen via a $K_2S_2O_8$-doped TiO_2 photocatalyst under visible light irradiation. *Chemosphere,* 155, 388-394.

Lin, J. C.-T., Sopajaree, K., Jitjanesuwan, T. and Lu, M.-C., 2018. Application of visible light on copper-doped titanium dioxide catalyzing degradation of chlorophenols. *Separation and Purification Technology,* 191, 233-243.

Lin, L., Wang, H. and Xu, P., 2017. Immobilized TiO_2-reduced graphene oxide nanocomposites on optical fibers as high performance photocatalysts for degradation of pharmaceuticals. *Chemical Engineering Journal,* 310, 389-398.

Mahvi, A. H., 2009. Application of ultrasonic technology for water and wastewater treatment. *Iranian Journal of Public Health,* 38**,** 1-17.

Mansour, D. et al., 2014. Improvement of the activated sludge treatment by its combination with electro Fenton for the mineralization of sulfamethazine. *International Biodeterioration and Biodegradation,* 88**,** 29-36.

Marco-Urrea, E., Perez-Trujillo, M., Vicent, T. and Caminal, G., 2009. Ability of white-rot fungi to remove selected pharmaceuticals and identification of degradation products of ibuprofen by Trametes versicolor. *Chemosphere,* 74**,** 765-772.

Meffe, R. and De Bustamante, I., 2014. Emerging organic contaminants in surface water and groundwater: A first overview of the situation in Italy. *Science of the Total Environment,* 481**,** 280-295.

Michael, I., Archilleos, A., Lambropoulou, D., Torrens, O., Perez, S., Petrovic, M., Barcelo, D. and Fatta-Kassinos, D., 2014. Proposed transformation pathway and evolution profile of diclofenac and ibuprofen transformation products during (sono)photocatalysis. *Applied Catalysis B: Environmental,* 147**,** 1015-1027.

Mioduska, J., Zielinska-Jurek, A., Janczarek, M. and Hupka, J., 2016. The effect of calcination temperature on structure and photocatalytic properties of WO_3/TiO_2 nanocomposites. *Journal of Nanomaterials,* 2016, 1-8.

Miraji, H., Othman, O. C., Ngassapa, F. N. and Mureithi, E. W., 2016. Research trends in emerging contaminants on the aquatic environments of Tanzania. *Scientifica,* 2016.

Mohd Yusoff, M. H. and Abdullah, A. Z. 2018. Effect of calcination temperature on the physicochemical and catalytic properties of SZSBA-15 catalyst in the production of monopalmitin. *Chemical Engineering Communications,* 205**,** 506-518.

Moradi, H., Eeshaghi, A., Hosseini, S. R. and Ghani, K., 2016. Fabrication of Fe-doped TiO_2 nanoparticles and investigation of photocatalytic decolorization of reactive red 198 under visible light irradiation. *Ultrasonics Sonochemistry,* 32**,** 314-319.

Moradi, V., Jun, M. B. G., Blackburn, A. and Herring, R. A., 2018. Significant improvement in visible light photocatalytic activity of Fe doped TiO_2 using an acid treatment process. *Applied Surface Science,* 427**,** 791-799.

Mosleh, S. and Rahimi, M. R., 2017. Intensification of abamectin pesticide degradation using the combination of ultrasonic cavitation and visible-light driven photocatalytic process: Synergistic effect and optimization study. *Ultrasonics Sonochemistry,* 35**,** 449-457.

Murgolo, S. Yargeau, V., Gerbasi, R., Visentin, F., Habra, N. E., Ricco, G., Lacchetti, I., Carere, M., Curri, M. L. and Mascolo, G., 2017. A new supported TiO_2 film deposited on stainless steel for the photocatalytic degradation of contaminants of emerging concern. *Chemical Engineering Journal,* 318**,** 103-111.

Na, S., Jinhua, C., Cui, M. and Khim, J., 2012. Sonophotolytic diethyl phthalate (DEP) degradation with UVC or VUV irradiation. *Ultrasonics Sonochemistry,* 19**,** 1094-1098.

Naidu, R., Arias Espana, V. A., Liu, Y. and Jit, J., 2016. Emerging contaminants in the environment: Risk-based analysis for better management. *Chemosphere,* 154**,** 350-357.

Nasralla, N., Yeganeh, M., Astuti, Y., Piticharoenphun, S., Shahtahmasebi, N., Kompany, A., Karimipour, M., Mendis, B. G., Poolton, N. R. J. and Siller, L., 2013. Structural and spectroscopic study of Fe-doped TiO_2 nanoparticles prepared by sol–gel method. *Scientia Iranica,* 20**,** 1018-1022.

Norvill, Z. N., Shilton, A. and Guieysse, B., 2016. Emerging contaminant degradation and removal in algal wastewater treatment ponds: Identifying the research gaps. *Journal of Hazardous Materials,* 313**,** 291-309.

Ogi, T., Zulhijah, R., Iwaki, T. and Okuyama, K., 2017. Recent progress in nanoparticle dispersion using bead mill. *KONA Powder and Particle Journal,* 2017, 3-23.

Ou, H. S., Ye, J.-S., Ma, S., Wei, C.-H., Gao, N.-Y. and He, J.-Z., 2016. Degradation of ciprofloxacin by UV and UV/H_2O_2 via multiple-wavelength ultraviolet light-emitting diodes: Effectiveness, intermediates and antibacterial activity. *Chemical Engineering Journal,* 289**,** 391-401.

Pal, A., He, Y., Jekel, M., Reinhard, M. and Gin, K. Y. H., 2014. Emerging contaminants of public health significance as water quality indicator compounds in the urban water cycle. *Environment International,* 71**,** 46-62.

Pang, Y. L. and Abdullah, A. Z., 2013. Effect of carbon and nitrogen co-doping on characteristics and sonocatalytic activity of TiO_2 nanotubes catalyst for degradation of Rhodamine B in water. *Chemical Engineering Journal,* 214**,** 129-138.

Pang, Y. L., Abdullah, A. Z. and Bhatia, S., 2010. Effect of annealing temperature on the characteristics, sonocatalytic activity and reusability of nanotubes TiO_2 in the degradation of Rhodamine B. *Applied Catalysis B: Environmental,* 100**,** 393-402.

Pang, Y. L., Abdullah, A. Z. and Bhatia, S.,2011a. Review on sonochemical methods in the presence of catalysts and chemical additives for treatment of organic pollutants in wastewater. *Desalination,* 277**,** 1-14.

Pang, Y. L., Bhatia, S. and Abdullah, A. Z., 2011b. Process behavior of TiO_2 nanotube-enhanced sonocatalytic degradation of Rhodamine B in aqueous solution. *Separation and Purification Technology,* 77**,** 331-338.

Park, B., Cho, E., Son, Y. and Khim, J., 2014. Distribution of electrical energy consumption for the efficient degradation control of THMs mixture in sonophotolytic process. *Ultrasonics Sonochemistry,* 21**,** 1982-1987.

Petrie, B., Barden, R. and Kasprzyk-Hordern, B., 2015. A review on emerging contaminants in wastewaters and the environment: Current knowledge, understudied areas and recommendations for future monitoring. *Water Research,* 72**,** 3-27.

Ramandi, S., Entezari, M. H. and Ghows, N., 2017. Sono-synthesis of solar light responsive S–N–C–tri doped TiO_2 photo-catalyst under optimized conditions for degradation and mineralization of Diclofenac. *Ultrasonics Sonochemistry,* 38**,** 234-245.

Rao, Y., Yang, H., Xue, D., Guo, Y., Qi, F. and Ma, J., 2016. Sonolytic and sonophotolytic degradation of Carbamazepine: Kinetic and mechanisms. *Ultrasonics Sonochemistry,* 32**,** 371-379.

Remucal, C. K., 2014. The role of indirect photochemical degradation in the environmental fate of pesticides: A review. *Environmental Sciences: Processes and Impacts,* 16**,** 628-653.

Richards, W. T. and Loomis, A. L., 1927. The chemical effects of high frequency sound waves I. A preliminary survey. *Journal of the American Chemical Society,* 49**,** 3086-3100.

Rivera-Utrilla, J., Sanchez-Polo, M., Ferro-Garcia, M. A., Prados-Joya, G. and Ocampo-Perez, R., 2013. Pharmaceuticals as emerging contaminants and their removal from water. A review. *Chemosphere,* 93**,** 1268-1287.

Rizzo, L., Fiorentino, A., Grassi, M., Attanasio, D. and Guida, M., 2015. Advanced treatment of urban wastewater by sand filtration and graphene adsorption for wastewater reuse: Effect on a mixture of pharmaceuticals and toxicity. *Journal of Environmental Chemical Engineering,* 3**,** 122-128.

Rodriguez-Narvaez, , O. M., Peralta-Hernandez, J. M., Goonetilleke, A. and Bandala, E. R., 2017. Treatment technologies for emerging contaminants in water: A review. *Chemical Engineering Journal,* 323**,** 361-380.

Rubio-Clemente, A., Torres-Palma, R. A. and Penuela, G. A., 2014. Removal of polycyclic aromatic hydrocarbons in aqueous environment by chemical treatments: A review. *Science of the Total Environment,* 478**,** 201-225.

Sangion, A. and Gramatica, P., 2016. PBT assessment and prioritization of contaminants of emerging concern: Pharmaceuticals. *Environmental Research,* 147**,** 297-306.

Santos, M. S. F., Alves, A. and Madeira, L. M., 2016. Chemical and photochemical degradation of polybrominated diphenyl ethers in liquid systems - A review. *Water Research,* 88**,** 39-59.

Sauve, S. and Desrosiers, M., 2014. A review of what is an emerging contaminant. *Chemistry Central Journal,* 8**,** 15.

Shah, J., Jan, M. R. and Khitab, F., 2018. Sonophotocatalytic degradation of textile dyes over Cu impregnated ZnO catalyst in aqueous solution. *Process Safety and Environmental Protection,* 116**,** 149-158.

Sharma, V., Vinoth Kumar, R., Pakshirajan, K. and Pugazhenthi, G., 2017. Integrated adsorption-membrane filtration process for antibiotic removal from aqueous solution. *Powder Technology,* 321**,** 259-269.

Sheng, C., Nnanna, A. G. A., Liu, Y. and Vargo, J. D., 2016. Removal of trace pharmaceuticals from water using coagulation and powdered activated carbon as pretreatment to ultrafiltration membrane system. *Science of the Total Environment,* 550**,** 1075-1083.

Shibin, O. M., Yesodharan, S. and Yesodharan, E. P., 2015. Sunlight induced photocatalytic degradation of herbicide diquat in water in presence of ZnO. *Journal of Environmental Chemical Engineering,* 3**,** 1107-1116.

Siddique, S., Kubwabo, C. and Harris, S. A., 2016. A review of the role of emerging environmental contaminants in the development of breast cancer in women. *Emerging Contaminants,* 2**,** 204-219.

Sing, K. S. W., 1985. Reporting physisorption data for gas/solid systems with special reference to the determination of surface area and porosity. *Pure and applied chemistry,* 57, 603-619.

Siwinska-Stefanska, K., Paukszta, D., Piasecki, A. and Jesionowski, T., 2014. Synthesis and physicochemical characteristics of titanium dioxide doped with selected metals. *Physicochemical Problems of Mineral Processing,* 50, 265-276.

Sood, S., Umar, A., Mehta, S. K. and Kansal, S. K. 2015. Highly effective Fe-doped TiO_2 nanoparticles photocatalysts for visible-light driven photocatalytic degradation of toxic organic compounds. *Journal of Colloid and Interface Science,* 450**,** 213-223.

Sophia A, C. and Lima, E. C. 2018. Removal of emerging contaminants from the environment by adsorption. *Ecotoxicology and Environmental Safety,* 150**,** 1-17.

Su, C., Chen, H.-S., Chen, J.-L., Yang, T.-S., Hsu, N.-M. and Li, W.-R., 2011. Preparation and characterization of pure rutile TiO_2 nanoparticles for photocatalytic study and thin films for dye-sensitized solar cells. *Journal of Nanomaterials,* 2011, 1-8.

Suhring, R., Moller, A., Freese, M., Pohlmann, J. D., Wolschke, H., Sturm, R., Xie, Z., Hanel, R. and Ebinghaus, R., 2013. Brominated flame retardants and dechloranes in eels from German Rivers. *Chemosphere,* 90**,** 118-124.

Suhring, R., Byer, J., Freese, M., Pohlann, J. D., Wolschke, H., Moller, A., Hodson, P. V., Alaee, M., Hanel, R. and Ebinghaus, R., 2014. Brominated flame retardants and dechloranes in European and American eels from glass to silver life stages. *Chemosphere,* 116**,** 104-111.

Suhring, R., Freese, M., Schneider, M., Schubert, S. Pohlamm, J. D., Alaee, M., Wolschke, H., Hanel, R. Ebinghaus, R. and Marohn, L., 2015. Maternal transfer of emerging brominated and chlorinated flame retardants in European eels. *Science of the Total Environment,* 530**,** 209-218.

Sui, Y., Liu, Q., Jiang, T. and Guo, Y., 2018. Synthesis of nano-TiO_2 photocatalysts with tunable Fe doping concentration from Ti-bearing tailings. *Applied Surface Science,* 428, 1149-1158.

Sunasee, S., Wong, K. T., Lee, G., Pichiah, S., Ibrahim, S., Park, C., Kim, N. C., Yoon, Y. and Jang, M., 2017. Titanium dioxide-based sonophotocatalytic mineralization of bisphenol A and its intermediates. *Environmental Science and Pollution Research,* 24, 15488-15499.

Tabasideh, S., Maleki, A., Shahmoradi, B., Ghahremani, E. and McKay, G. 2017. Sonophotocatalytic degradation of diazinon in aqueous solution using iron-doped TiO_2 nanoparticles. *Separation and Purification Technology,* 189**,** 186-192.

Taherinia, M., Nasiri, M., Abedini, E. and Pouretedal, H. R., 2017. The effect of solvent of titanium precursor in the sol-gel process on the activity of TiO_2 nanoparticles for H_2 production. *Iranian Journal of Hydrogen & Fuel Cell,* 4**,** 139-151.

Tan, C., Gao, N., Zhou, S., Xiao, Y. and Zhuang, Z., 2014. Kinetic study of acetaminophen degradation by UV-based advanced oxidation processes. *Chemical Engineering Journal,* 253**,** 229-236.

Taneja, P., Sharma, S., Umar, A., Mehta, S. K., Ibhadon, A. O. and Kansal, S. K., 2018. Visible-light driven photocatalytic degradation of brilliant green dye based on cobalt tungstate ($CoWO_4$) nanoparticles. *Materials Chemistry and Physics,* 211**,** 335-342.

Thi, V. H. T. and Lee, B. K., 2017. Effective photocatalytic degradation of paracetamol using La-doped ZnO photocatalyst under visible light irradiation. *Materials Research Bulletin,* 96, 171-182.

Thompson, L. H. and Doraiswamy, L. K., 1999. Sonochemistry: Science and engineering. *Industrial and Engineering Chemistry Research,* 38**,** 1215-1249.

Tijani, J. O., Fatoba, O. O., Babajide, O. O. and Petrik, L. F., 2016. Pharmaceuticals, endocrine disruptors, personal care products, nanomaterials and perfluorinated pollutants: a review. *Environmental Chemistry Letters,* 14**,** 27-49.

Vandermeersch, G., Lourenco, H. M., Alvarez-Munoz, D., Cunha, S., Diogene, J., Cano-Sancho, G., Sloth, J. J., Kwadijk, C., Barcelo, D., Allegaert, W., Bekaert, K., Fernandes, J. O., Marques, A. and Robbems, J., 2015. Environmental contaminants of emerging concern in seafood – European database on contaminant levels. *Environmental Research,* 143, 29-45.

Vieno, N., Hallgren, P., Wallberg, P., Pyhala, M. and Zandaryaa, S., 2017. *Pharmaceuticals in the aquatic environment of the Baltic Sea region: a status report*, UNESCO Publishing.

Vijayarangamuthu, K., Youn, J.-S., Park, C.-M. and Jeon, K.-J., 2018. Facile synthesis of core–shell-structured rutile TiO_2 with enhanced photocatalytic properties. *Catalysis Today*.

Villaroel, E., Silva-Agredo, J., Petrier, C., Taborda, G. and Torres-Palma, R. A. 2014. Ultrasonic degradation of acetaminophen in water: Effect of sonochemical parameters and water matrix. *Ultrasonics Sonochemistry,* 21, 1763-1769.

Wahyuningsih, S., Ramelan, A. H., Saputri, L. N. M. Z., 2017. A study on structure/phase transformation of TiO_2 nanorods at various annealing temperatures. *IOP Conference Series: Earth and Environmental Science,* 75**,** 1-6.

Wang, Y., Roddick, F. A. and Fan, L., 2017. Direct and indirect photolysis of seven micropollutants in secondary effluent from a wastewater lagoon. *Chemosphere,* 185**,** 297-308.

Wang, Y., Zhao, D., Ma, W., Chen, C. and Zhao, J., 2008. Enhanced sonocatalytic degradation of azo dyes by Au/TiO_2. *Environmental Science and Technology,* 42**,** 6173-6178.

Wen, L., Liu, B., Zhao, X., Nakata, K., Murakami, T. and Fujishima, A., 2012. Synthesis, Characterization, and Photocatalysis of Fe-Doped: A Combined Experimental and Theoretical Study. *International Journal of Photoenergy,* 2012, 1-10.

Wetchakun, N., Pirakitikulr, P., Chiang, K. and Phanichphant, S., 2008. Visible light-active nano-sized Fe-doped TiO_2 photocatalysts and their characterization. *IEEE International Nanoelectronics Conference*, 836-841.

Wu, C., Xu, L., Bian, K., Chen, X. and He, F., 2016. Synergetic degradation of benzotriazole by ultraviolet and ultrasound irradiation. *Desalination and Water Treatment,* 57, 17955-17962.

Xiong, P. and Hu, J., 2017. Decomposition of acetaminophen (Ace) using TiO_2/UVA/LED system. *Catalysis Today,* 282, 48-56.

Xu, L. J., Chu, W. and Graham, N., 2013. Sonophotolytic degradation of dimethyl phthalate without catalyst: Analysis of the synergistic effect and modeling. *Water Research,* 47**,** 1996-2004.

Yan, T., Wu, T., Zhang, Y., Sun, M., Wang, X., Wei, Q. and Du, B., 2017. Fabrication of In_2S_3/Zn_2GeO_4 composite photocatalyst for degradation of acetaminophen under visible light. *Journal of Colloid and Interface Science,* 506, 197-206.

Yang, Y., Yu, Y., Wang, J., Zheng, W. and Cao, Y., 2017. Doping and transformation mechanisms of Fe^{3+} ions in Fe-doped TiO_2. *CrystEngComm,* 19, 1100-1105.

Yao, Y. Gao, B., Chen, H., Jiang, L., Inyang, M., Zimmerman, A. R., Cao, X., Yang, L., Xue, Y. and Li, H., 2012. Adsorption of sulfamethoxazole on biochar and its impact on reclaimed water irrigation. *Journal of Hazardous Materials,* 209**,** 408-413.

Ye, M., Chen, Z., Zhang, T. and Shao, W., 2012. Effect of calcination temperature on the catalytic activity of nanosized TiO_2 for ozonation of trace 4-chloronitrobenzene. *Water Science and Technology,* 66**,** 479-486.

Yener, H. B., Yilmaz, M., Deliismail, O., Ozkan, S. F. and Helvaci, S. S., 2017. Clinoptilolite supported rutile TiO_2 composites: Synthesis, characterization, and photocatalytic activity on the degradation of terephthalic acid. *Separation and Purification Technology,* 173**,** 17-26.

Yousif, E. and Haddad, R., 2013. Photodegradation and photostabilization of polymers, especially polystyrene: Review. *SpringerPlus,* 2, 1-32.

Yuan, C., Hung, C.-H., Li, H.-W. and Chang, W.-H., 2016. Photodegradation of ibuprofen by TiO_2 co-doping with urea and functionalized CNT irradiated with visible light – Effect of doping content and pH. *Chemosphere,* 155**,** 471-478.

Zangeneh, H., Zinatizadeh, A. A. L., Habibi, M., Akia, M. and Hasnain Isa, M., 2015. Photocatalytic oxidation of organic dyes and pollutants in wastewater using different modified titanium dioxides: A comparative review. *Journal of Industrial and Engineering Chemistry,* 26**,** 1-36.

Zhang, L., Li, P., Gong, Z. and Li, X., 2008. Photocatalytic degradation of polycyclic aromatic hydrocarbons on soil surfaces using TiO_2 under UV light. *Journal of Hazardous Materials,* 158, 478-484.

Zhang, Y., Fan, J., Yang, B. and Ma, L., 2017a. Synergistic effect of ferrous ion and copper oxide on the oxidative degradation of aqueous acetaminophen at acid conditions: A mechanism investigation. *Chemical Engineering Journal,* 326, 612-619.

Zhang, Y., Zhu, H., Szewzyk, U. and Geissen, S. U. 2017b. Enhanced removal of sulfamethoxazole with manganese-adapted aerobic biomass. *International Biodeterioration & Biodegradation,* 116**,** 171-174.

Zhu, J., Ren, J., Huo, Y., Bian, Z. and Li, H., 2007. Nanocrystalline Fe/TiO_2 visible photocatalyst with a mesoporous structure prepared via a nonhydrolytic sol−gel route. *The Journal of Physical Chemistry C,* 111**,** 18965-18969.

Ziylan-Yavas, A. and Ince, N. H., 2016. Enhanced photo-degradation of paracetamol on n-platinum-loaded TiO_2: The effect of ultrasound and •OH/hole scavengers. *Chemosphere,* 162, 324-332.

Zoschke, K., Bornick, H. and Worch, E. 2014., Vacuum-UV radiation at 185 nm in water treatment – A review. *Water Research,* 52**,** 131-145.

Zur, J., Wojcieszynska, D., Hupert-Kocurek, K., Marchlewicz, A. and Guzik, U., 2018. Paracetamol-toxicity and microbial utilization. Pseudomonas moorei KB4 as a case study for exploring degradation pathway. *Chemosphere,* 206**,** 192-202.

APPENDICES

APPENDIX A: Preparation of 1 M HCl

To prepare 100 mL of 1 M HCl from 37 % HCl solution, the volume required was calculated.

Molecular weight = 36.46 g/mol

Specific density = 1.19 g/mol

Mass of HCl needed $= 1 \frac{\text{mol}}{\text{L}} \times \frac{36.46\ \text{g}}{\text{mol}} \times 0.1\ \text{L}$

$= 3.646.\text{g of HCl}$

1 g of 37 % HCl consists of 0.37 g of HCl.

x g of 37 % HCl consists of 3.646 g of HCl.

By using the relation in ratio,

Mass of 37% HCl required, $x = \frac{1}{0.37} \times 3.646\ \text{g}$

$= 9.85\ \text{g of 37\% HCl}$

Volume of 37% HCl required $= 9.85\ \text{g} \times \frac{\text{mL}}{1.19\ \text{g}}$

$= 8.27\ \text{mL of 37\% HCl}$

Therefore, in order to prepare 1 M HCl, 8.27 mL of 37% HCl was required and top-up to 100 mL using distilled water.

APPENDIX B: Preparation of 0.1 M NaOH

To prepare 100 mL of 0.1 M NaOH from 97 % NaOH powder, the mass required was calculated.

Molecular weight = 40 g/mol

Mass of NaOH powder required = $0.1 \frac{\text{mol}}{\text{L}} \times \frac{40\ \text{g}}{\text{mol}} \times 0.1\ \text{L} \times \frac{100}{97}$

= 0.41 g of NaOH powder.

Therefore, 0.1 M NaOH could be obtained by dissolving 0.41 g of NaOH powder in 100 mL distilled water.

APPENDIX C: Preparation of Fe-doped TiO_2 Particles

The material balance for synthesizing of TiO_2:

$$Ti(OC_4H_9)_4 + 2\ H_2O \rightarrow TiO_2 + 4\ C_4H_9OH$$

Molecular weight of TiO_2 = 79.87 g/mol

Molecular weight of $Ti(OC_4H_9)_4$ = 340.32 g/mol

Molecular weight of $Fe(NO_3)_3 \cdot 9H_2O$ = 404.06 g/mol

To calculate the mass of TiO_2 produced,

Moles of $Ti(OC_4H_9)_4$ used $= 5\ mL \times 1 \frac{g}{mL} \times \frac{mol}{340.32\ g}$

$= 0.015$ mol

Mass of TiO_2 produced $= 0.015\ mol \times \frac{79.87\ g}{mol}$

$= 1.198$ g

To calculate the Fe needed in order to prepare 1% Fe-doped TiO_2,

Mass ratio of Ti to Fe = 99 : 1

By using the mass ratio of Ti to Fe,

Mass of Fe required $= \frac{1}{99} \times 1.198$ g

$= 0.012$ g

Molecular weight ratio of Fe to $Fe(NO_3)_3 \cdot 9H_2O$ = 55.85 : 404.06

By using the molecular weight ratio of Fe to $Fe(NO_3)_3 \cdot 9H_2O$,

Mass of $Fe(NO_3)_3 \cdot 9H_2O$ required = $\frac{404.06}{55.85} \times 0.012$ g

= 0.087 g

Therefore, in order to prepare 1% Fe-doped TiO_2, 0.087 g of $Fe(NO_3)_3 \cdot 9H_2O$ was weighted and added to TiO_2.

Table C1: Amount of $Fe(NO_3)_3 \cdot 9H_2O$ required to prepare Fe-doped TiO_2 with various Fe dopant concentrations (1, 3, 5 and 10 wt%)

Fe (wt%)	Amount of $Fe(NO_3)_3 \cdot 9H_2O$ required (g)
1	0.087
3	0.268
5	0.962
10	2.170

APPENDIX D: Calculation of Phase Composition

The phase composition of anatase, rutile and brookite of Fe-doped TiO_2 were calculated using the following equations.

$$W_A = \frac{K_A A_A}{K_A A_A + A_R + K_B A_B}$$

$$W_R = \frac{A_R}{K_A A_A + A_R + K_B A_B}$$

$$W_B = \frac{K_B A_B}{K_A A_A + A_R + K_B A_B}$$

where

W_A, W_R, W_B = phase composition of anatase, rutile and brookite, respectively.

A_A, A_R, A_B = peak intensity of anatase, rutile and brookite, respectively.

K_A, K_B = coefficient of anatase (0.886) and brookite (2.721), respectively.

Taking 3% Fe-doped TiO_2-800 as an example, the peak data obtained from XRD pattern were recorded as following:

A_A, A_R, A_B = 16, 678 and 32, respectively.

$$\mathrm{W_A} = \frac{(0.886)(16)}{(0.886)(16) + 678 + (2.721)(32)} \times 100\ \%$$

$$= 1.82\ \%$$

$$\mathrm{W_R} = \frac{(678)}{(0.886)(16) + 678 + (2.721)(32)} \times 100\ \%$$

$$= 87.01\ \%$$

$$W_B = \frac{(2.721)(32)}{(0.886)(16) + 678 + (2.721)(32)} \times 100\ \%$$

$= 11.17\ \%$

APPENDIX E: Calculation of Crystalline Size

The crystalline size of Fe-doped TiO_2 was calculated using Debye-Scherrer equation.

$$\tau = \frac{k\lambda}{\beta \cos\theta}$$

where

k = Scherrer constant, 0.9

λ = wavelength of CuK_α radiation, 0.154 nm

β = full-width at half maximum, FWHM in radian

θ = Bragg angle of prominent peak ($2\theta \approx 25$ ° for anatase and $2\theta \approx 27$ ° for rutile)

Taking 3% Fe-doped TiO_2-800 as an example, the peak data obtained from XRD pattern were recorded as following:

β = 0.19 ° = 0.0033 rad

2θ = 37.39 °

$$\tau = \frac{(0.9)(0.154)}{(0.0033)\cos\frac{37.29}{2}}$$

= 43.02 nm

APPENDIX F: Preparation of Paracetamol Solution

In order to prepare a stock solution, a tablet of 500 mg paracetamol was dissolved in 100 mL distilled water, produced paracetamol stock solution at concentration of 5000 mg/L. 100 mL of paracetamol dilution solutions were prepared, in the ranged between 5 to 25 mg/L (Table A1) by:

$$C_1V_1 = C_2V_2$$

where

C_1, C_2 = concentration of stock solution and dilution solution, mg/L

V_1, V_2 = volume of stock solution and dilution solution, mL

To prepare 100 mL of 5 mg/L paracetamol solution, the volume of stock solution required was calculated as following:

$$\left(5000\frac{mg}{L}\right)(V_1) = (5\frac{mg}{L})(100\ mL)$$

$$V_1 = 0.1\ mL$$

Therefore, in order to prepare 5 mg/L paracetamol solution, 0.1 mL of stock solution was pipetted and top-up with 99.9 mL of distilled water.

Table F1: Preparation of dilution solutions from stock solution

Concentration required (mg/L)	Volume from stock solution required (mL)	Volume of distilled water required for top-up (mL)
5	0.1	99.9
10	0.2	99.8
15	0.3	99.7
20	0.4	99.6
25	0.5	99.5

APPENDIX G: Preparation of H_2O_2 Solution

To prepare various molarity of H_2O_2, the volume required from 30 % H_2O_2 assay solution was calculated.

Molecular weight = 34.01 g/mol

Specific density = 1.11 g/mL

To prepare 0.1 mM H_2O_2 solution,

Mass of H_2O_2 required = $\frac{0.1 \text{ mmol}}{\text{L}} \times \frac{34.01 \text{ g}}{\text{mol}} \times 0.1 \text{ L} \times \frac{1\ mol}{1000\ mmol}$

= 0.00034 g

1 g of 30 % H_2O_2 assay solution contains 0.30 g of H_2O_2 and 0.70 g of H_2O.

x g of 30 % H_2O_2 assay solution contains 0.00034 g of H_2O_2.

By using the relation in ratio, $x = \frac{1}{0.30} \times 0.00034\ g$

= 0.00113 g of 30 % H_2O_2 assay solution

Volume of 30 % H_2O_2 assay solution = $0.001134 \text{ g} \times \frac{\text{mL}}{1.11 \text{ g}}$

= 0.00102 mL

= 1.0 µL

Therefore, in order to prepare 0.1 mM H_2O_2 solution, 1.0 µL of 30 % H_2O_2 assay solution was required.

Table G1: Volume required from 30 % H_2O_2 assay solution in preparation of H_2O_2 at various molarities

Molarity (mM)	Volume required from 30 % H_2O_2 assay solution (µL)
0.1	1.0
0.5	5.1
1.0	10.2
5.0	51.0
10.0	102.1

APPENDIX H: Reaction Kinetic Plots

Pseudo zero-order reaction:

$$C_t = C_0 - k_0 t$$

A plot of C_t againt t is shown in Figure H1.

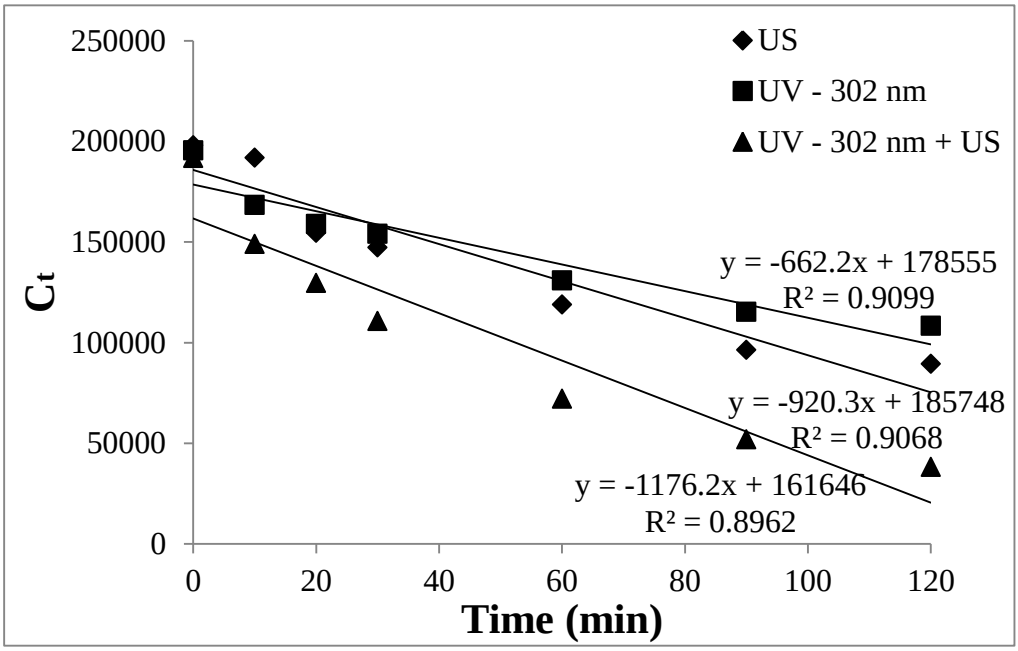

Figure H1: Pseudo zero-order reaction kinetics graph for sono-, photo- and sonophoto-degradation of paracetamol (sonicator frequency = 50 kHz, UV wavelength = 302 nm, initial concentration of paracetamol = 5 mg/L, catalyst dosage = 1.0 g/L 3% Fe-doped TiO_2-600, solution pH = pH 5, temperature = 30 °C)

Pseudo second-order reaction:

$$\frac{1}{C_t} = \frac{1}{C_0} + k_2 t$$

A plot of $\frac{1}{C_t}$ against *t* is shown in Figure H2.

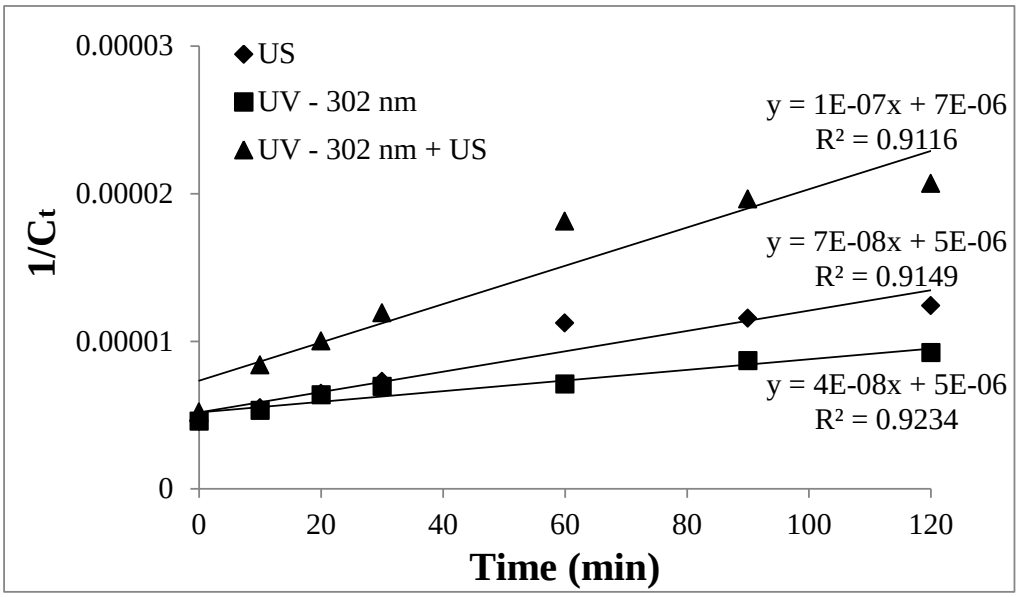

Figure H2: Pseudo second-order reaction kinetics graph for sono-, photo- and sonophoto-degradation of paracetamol (sonicator frequency = 50 kHz, UV wavelength = 302 nm, initial concentration of paracetamol = 5 mg/L, catalyst dosage = 1.0 g/L 3% Fe-doped TiO_2-600, solution pH = pH 5, temperature = 30 °C)

Appendix I: Calculation of Synergy Index

For sonophotocatalytic degradation, synergy index is calculated as following:

$$Synergy\ index\ = \frac{k_{US+UV+A}}{k_{US+A}+k_{UV+A}}$$

where

k_{US+A}, k_{UV+A}, $k_{US+UV+A}$ = rate constant of sono-, photo- and sonophotocatalytic degradation, respectively.

A = catalyst

Taking the k_{US+A}, k_{UV+A}, $k_{US+UV+A}$ = 0.008 min^{-1}, 0.005 min^{-1} and 0.0142 min^{-1}, respectively.

$$Synergy\ index\ = \frac{0.0142}{0.008+0.005}$$

$$= 1.09$$

LIST OF PUBLICATION

Paper type	Title	Status
Review paper	A comprehensive review on state-of-the-art photo-, sono-, and sonophotocatalytic treatments to degrade emerging contaminants	Published on International Journal of Environmental Science and Technology
Conference paper	Influence of calcination temperature on the characteristic and sonophotocatalytic activities of Fe-doped TiO_2 particles	Published on AIP Conference Proceedings